University of Alberta

Characterizing the Transport of Process-Affected Water Contained in Oil Sands Tailings Ponds into the underlying Pleistocene clay till in Northern Alberta's Athabasca Oil Sands region: A Field Study

by

Mostafa Abolfazlzadehdoshanbehbazari

A thesis submitted to the Faculty of Graduate Studies and Research
in partial fulfillment of the requirements for the degree of

Master of Science
in
Geoenvironmental Engineering

Civil and Environmental Engineering

Fall 2011
Edmonton, Alberta

Dedication

To my parents, Sari Pourjabar and Ghaffar Abolfazlzadeh, who dedicated their lives to teach their students not only their subjects but also lessons in the human love for freedom.

My father (first person on the right) and his primary school students in a small village, Gilan Province, Iran; 1970.

Abstract

A small scale Infiltration Pond was constructed to characterize the transport of oil sands process affected (PA) water contained in Suncor's South Tailings Pond (STP) to the Wood Creek Sand Channel (WCSC) through a 5-8 m thick glacial clay till.

The extent of PA water infiltration was determined by extracting pore water samples from the clay till, analyzing their isotopic ($\delta^{18}O$), major ions, and metals composition over a two year time period. As conservative tracers, $\delta^{18}O$ and chloride concentration trends indicated the water penetration line at approximately 0.9 m, while major ion and metal mobility lagged this line. Uptake of Mo, Pb, sodium and sulphate and release of Ba, Sr, calcium and magnesium suggest that adsorption and ion exchange reactions are the foremost attenuation processes controlling inorganic solutes transport. In addition, a correlation coefficient of 0.96 between diffusion analytical models and field measurements for tracers, provided evidence of a diffusion-dominated system.

Acknowledgement

Firstly, it is with utmost gratitude that I thank my supervisor Dr. Ania C. Ulrich who exercised confidence in me with her constant vision, patient guidance, enthusiastic encouragement and technical and financial support during all phases of my graduate studies.

I would also like to thank my M.Sc. committees, Dr. Carl Mendoza and Dr. Ward Wilson who critically reviewed this thesis, and for their thoughtful advice and comments. Furthermore, invaluable assistance and technical support from Dr. Carl Mendoza for the modeling chapter of this thesis is appreciated.

The financial support provided by the University of Alberta, the Natural Science and Engineering Research Council (NSERC), and Suncor Energy Inc. is gratefully acknowledged.

I am grateful for the cooperation received from Alberta Innovates Technology Futures and the University of Waterloo for isotopic analysis and Suncor Energy Inc. for providing facilities for field work. Particularly, I would like to thank Dr. Jean S. Birks and I owe much to Michael C. Moncur of Alberta Innovates Technology Futures who provided invaluable encouragements and help during the field work and sampling.

I would also like to thank my former M.Sc. supervisor at Tehran University, Dr. Saied Gitipour, who had big contributions to the native soil physical properties tests when he was involved in this project as a visiting professor at the University of Alberta. Thanks for his generous advice and suggestions on this study.

The interest and support of the technicians within both Geotechnical and Environmental Engineering laboratories of the University of Alberta: Steve Gamble, Christine Hereygers, Jela Burkus and Elena A. Dlusskaya is appreciated.

Special thanks are extended to my friends, outstanding graduate students and researchers in Geo-environmental Engineering group of the University of Alberta, who provided valuable direction, advice and review on my study. Particularly, the author is indebted to Alexander Holden and Dr. Macoura Kone for their invaluable help in both laboratory and field work. I would also like to thank my former group mate Abimbola A. Ojekanmi for Infiltration Pond start up and conducting double ring infiltrometer tests. I am also grateful for the help and advice from my dear friend, Babak Khamsehi, for thesis presentation.

Finally, I would like to thank my wife, Dr. Mehrnaz Salehi, for her love, continued patience, moral support and considerations during my graduate studies.

Table of Contents

List of Tables:

List of Figures:

Chapter 1: Introduction

1-1 Background

In the last twenty years, the demand for crude oil in highly industrial countries like Canada has been increasing. Besides, a quick look at our daily life shows how we are continuing to rely on energy from oil and gas for our homes, cars and different applications. Although Middle East countries were the main source of crude oil, political issues in recent decades made governments of some countries find alternative sources of oil such as oil sands [1,2].

Canada is one of the eight countries with major accumulations of oil sands [3,4]. The Canadian Athabasca oil sands deposit with 178 billion barrels estimated recoverable oil places Canada as the second largest oil resource in the world after Saudi Arabia. Around 50,000 km^2 of this area is covered by shallow deposits which give the opportunity for surface mining to extract oil sands [5]. Syncrude Canada Ltd. and Suncor Energy Inc. are the largest Alberta oil sands companies conducting oil sands mining and extraction in the north-eastern part of the province. These companies use different surface mining techniques to excavate oil sands and then send them to upgrading facilities to extract bitumen form oil sand ores. Furthermore, steam assisted gravity drainage (SAGD) is a commonly used in situ technology in the case of deep oil sands sources which are not suitable for surface mining [6-8].

1-2 Environmental Impact of Oil Sands Extraction

Oil sand companies have some major environmental challenges. By using current technology, Clark caustic hot water extraction method, 2-4.5 m^3 of water is used

to produce 1m^3 of crude oil [9,10]. This amount of process-affected (PA) water is accompanied by other residual parts of oil sands ore and from oil sands operation waste water. In fact, large quantities of water, sand, silt, clay and left over bitumen (9-12%) as well as high concentrations of dissolved ions and chemicals are the result of oil sand operations to separate bitumen using hot water [11]. This slurry waste is called oil sands tailings which is toxic to many aquatic organisms. Under "zero discharge policies" oil sands operators cannot release PA water into the environment. As a result, manmade tailings ponds are constructed to contain and settle the tailings. In order to reduce the volume of fresh water needed, a portion of PA water is recycled to oil sands operation for ore processing, although large and growing volume of PA water is contained in tailings ponds. As of 2008, the volume of fine tailings (PA water, silt, clay) is reported at 720 million m^3 [12]. Moreover, the National Energy Board estimated that by 2020 the volume of tailings only produced by Suncor and Syncrude will exceed one billion m^3 [13]. The potential risk of tailings ponds recharge to groundwater is identified as one of the most important hazards associated with tailings ponds [14]. Without proper protection, oil sand tailings contaminants enter the soil underlying tailings ponds, surface water and subsequently to the groundwater resources and may find a pathway to downstream outlets such as rivers. The risk of leaks from oil sand tailings impoundments is a major threat due to its toxicity to both humans and animals [7].

Suncor Energy Inc.'s oil sands mining operation is located approximately 30 km north of Fort McMurray, Alberta. Due to expanding its oil sands production,

Suncor developed the 2300 ha South Tailings Pond (STP). It has a tailings and PA water storage capacity of 336 Mm^3. Tailings placement in STP started from June 2006. STP was built over a 5-8 m thick glacial till because of its low permeability. The glacial till overlies the Wood Creek Sand Channel (WCSC) which is a buried glaciofluvial channel with typically 1000 m to 1500 m width and a 30 m thick highly permeable sand [15]. Since a significant portion (around 50% of) STP overlies the WCSC, it poses a potential preferential flow pathway for PA water to migrate from the STP impoundment to Mclean Creek which discharges to the Athabasca River. This scenario poses a big environmental challenge for Suncor Energy Inc. [15]. On the other hand, the PA water plume investigation in STP provides a unique opportunity to track and examine PA water chemistry passing through the clay till and sandy aquifer and interacting with groundwater, microorganisms as well as field and laboratory evaluation of soil geochemistry on PA water impacted soils.

1-3 Motivation

In 2004, Golder Associates Ltd. investigated and modeled the STP, showing that PA water will infiltrate through the clay till layer and subsequently leach into the WCSC [16]. In response Suncor established hydraulic containment of the WCSC through the following mechanisms: (1) A line of pumping wells was installed at the northwest corner of STP to prevent migration of PA water and return it to the pond; and (2) Construction of a bentonite cut-off wall across a branch of the WCSC located under west dyke of STP. Although this modelling study showed

the likelihood of PA water infiltration into the WCSC, the extent of this pollution and interactions such as biological and chemical reactions between soil particles, groundwater aquifers and PA water in both clay till and WCSC is still poorly understood [16].

To date, most research on environmental issues in the Athabasca Oil Sands region has focused on PA water organic pollutants and particularly naphthenic acids. Research on biological degradation [17], adsorption behavior [18] and tracking NAs from impoundment to subsurface [19] are available in the literature. However, there are only a handful of studies looking at the major ions and trace metals in PA water. Mackinnon et al. [20] monitored PA water for trace metals, major ions and NAs concentration passing through fluvial sand and Oiffer et al. [21] completed a field scale investigation on the fate and transport of NAs and arsenic within a shallow sand aquifer. With growing awareness about the groundwater pollution and significant knowledge gap regarding the interaction of trace metals and major ions of PA water and native sediments in the Athabasca Oil Sands region, a collaborative research program was initiated between the University of Alberta, University of Waterloo, University of British Columbia and Suncor Energy Inc. The objective of the collaboration is to examine PA water fate and migration within the clay till as well as the WCSC and ultimately to provide remediation strategies for the contaminated WCSC. Undoubtedly, the knowledge of biological and geochemical interactions between different soil layers and PA water has a big role both in contaminant transport investigation and in exploring any remediation strategy in future.

1-4 Objectives

Based on preliminary investigations and groundwater monitoring, PA water infiltration from STP into the WCSC aquifer is probable and may contain components that are environmentally hazardous, such as heavy metals and/or organic pollutants. It is also hypothesized that heavy metals and major anions and cations in process affected water can be used as an indicator to track the PA water seepage through the clay till and WCSC.

Therefore, the main objective of this study is to better characterize the transport and impact of PA water into the clay till layer in order to develop a predictive flow model for PA water infiltration. In fact, by conducting a detailed field scale investigation, the cardinal purpose of this research is to use major ions, cations and trace elements as an indicator of PA water seepage through the clay till layer. To do this field study, on the South Eastern portion of WCSC, a 10m x 10m Infiltration pond was constructed. This pond served as a small scale model of the STP.

Coupling the results of this research with isotopic analysis on PA water in STP and pore water at different depths allows use to better understand geochemical processes in the soil layers and groundwater.

The detailed objectives of this study are as follows:

1- To characterize the native soils underlying a constructed infiltration pond with boreholes, soil physical tests and permeability analysis (e.g double ring infiltrometer).

2- To determine the pore water chemistry underlying the infiltration pond at two time points: (i) prior to filling with process-affected water and (ii) two years after filling. Pore water will be analyzed for metals, cations and anions, pH, alkalinity and isotopes (^{2}H, ^{18}O). The pore water chemistry at different depths underlying the pond and over time will indicate PA water seepage.

3- To create a predictive flow model of PA water seepage based on results attained from objectives 1 and 2.

1-5 Outline of thesis

This thesis is divided into 6 chapters presenting different aspects of the study. Chapter 2 is a literature review discussing previous academic endeavors related to the similar areas. Chapter 3 is centred on the native soil physical and hydraulic properties, while Chapter 4 is focused on isotopic analysis and geochemistry properties of soil samples pore water and PA water samples from Infiltration Pond which addresses objective number 2. The third objective is explored in chapter 5 which reports one-dimensional analytical models developed for the soil systems underlying the infiltration pond. Chapter 6 presents final conclusions, engineering significance of the work and future recommendations.

1-6 References

(1) Williams B. Heavy hydrocarbons playing key role in peak-oil debate, future energy supply. Oil Gas J 2003; 101(29): 20-27.

(2) Mikula RJ, Munoz VA, Omotoso O. Water Use in Bitumen Production: Tailings Management in Surface Mined Oil Sands National Energy Board Canada's oil sands: a supply and market outlook to 2015, National Energy Board: Calgary, 2000; 2008.

(3) Chalaturnyk RJ, Scott JD, Özüm B. Management of oil sands tailings. Petrol Sci Technol; 2002; 20(9-10): 1025-1046.

(4) Greene DL, Hopson JL, Li J. Have we run out of oil yet? Oil peaking analysis from an optimist's perspective. Energy Policy; 2006; 34(5): 515-531.

(5) Government of Alberta. Fact Sheets. Oil Sands Discovery Centre; 2008.

(6) Syncrude Canada Ltd.
Syncrude Factbook (4th Edition). Syncrude Canada Ltd
Government and Public Affairs Department. Fort McMurray, Alberta, Canada; 2003.

(7) Suncor Energy Inc. Report on Sustainability. Available at: http://www.suncor.com/doc.aspx?id=114; 2007.

(8) Tompkins TG. Natural Gradient Tracer Tests to Investigate the Fate and Migration of Oil Sands Process-Affected Water in the Wood Creek Sand Channel. Ontario, Canada: University of Waterloo; 2009.

(9) Griffiths M, Taylor A, Woynillowicz D, Pembina Institute for Appropriate Development, Canada. Environment Canada, Walter & Duncan Gordon Foundation. Troubled waters, troubling trends : technology and policy options to reduce water use in oil and oil sands development in Alberta. 1st ed. Drayton Valley, Alta.: Pembina Institute; 2006.

(10) Kasperski KL. Review of research on aqueous extraction of bitumen from mined oil sands. Unpublished report. Canmet Energy Technology Centre, Natural Resources Canada, Devon, Alta.; 2003.

(11) Clemente JS, Fedorak PM. A review of the occurrence, analyses, toxicity, and biodegradation of naphthenic acids. Chemosphere; 2005; 60(5): 585-600.

(12) Energy Resources Conservation Board (ERCB). Alberta's Oil Sands: Strengthening regulatory requirements, in: 2008 Year in Review. Available at: http://yearinreview.ercb.ca/pdfs/Albertas_Oil_Sands.pdf; 2009.

(13) National Energy Board. Canada's oil sands: opportunities and challenges to 2015. Calgary, Alta.: National Energy Board; 2004.

(14) MacKinnon MD, Retallack JT. Preliminary characterization and detoxification of tailings pond water at the Syncrude Canada Ltd Oil Sands Plant; 1981: 185–210.

(15) Klohn Crippen Consultants Ltd. Millenium Mine Design of the South Tailings Pond – Final Report. Report submitted to Suncor Energy, Inc.; November 2004.

(16) Hall T. Water quality modelling report for the Suncor south tailings pond project; 2004; Golder Associates Ltd: 51.

(17) Peters LE, MacKinnon M, Van Meer T, van den Heuvel MR, Dixon DG. Effects of oil sands process-affected waters and naphthenic acids on yellow perch (Perca flavescens) and Japanese medaka (Orizias latipes) embryonic development. Chemosphere 2007; 67(11): 2177-2183.

(18) Janfada A, Headley J, Peru K, Barbour S. A laboratory evaluation of the sorption of oil sands naphthenic acids on organic rich soils. J Environ Sci Health Part A Toxic Hazard Subst Environ Eng.; 2006; 41(6): 985-997.

(19) Gervais FJM. Fate and Transport of Naphthenic Acids in a Glacial Aquifer. Ontario, Canada: University of Waterloo; 2004.

(20) Thomson NR, editor. Indicators for assessing transport of oil sands process-affected waters. Bringing Groundwater Quality Research to the Watershed Scale, Proceedings of GQ2004 ,The 4th International Groundwater Quality Conference; 2004.

(21) Oiffer AAL, Barker JF, Gervais FM, Mayer KU, Ptacek CJ, Rudolph DL. A detailed field-based evaluation of naphthenic acid mobility in groundwater. J Contam Hydrol; 2009; 108(3-4): 89-106.

Chapter 2: Literature Review

2-1 Introduction:

Groundwater is a major source of drinking water. Increasing trends in sub soil and groundwater contamination have lead scientists and engineers from different disciplines to describe water flow and solute transport through soil. Investigations on the non-reactive and reactive solutes transport through different types of soils in saturated and unsaturated conditions result in a wide range of terminology and research findings. For the theories behind non-reactive and reactive transport the reader is referred to comprehensive review articles by Feyen et al. [1] and Phillips [2], respectively. Due to the wide breadth of research on solute transport, this chapter focuses on a review of literature on solute transport through clay till soil layers.

2-2 Solute and water transport

To understand and manage soil and groundwater pollution, in recent decades, lots of research has been conducted on solute transport focusing on both theoretical simulations (comprehensive reviews may be found in [3,4]) and experimental investigations [5-8].

The water and solute flux physical description using mathematical models in literature can be seen in three categories: (1) mass transport models [9-11], (2) mixing cell models [12-15] and (3) preferential flow models in heterogeneous soils [16-18]. In the case of chemical reactive transport, different aspects of complicated chemical reactions are theoretically modeled. For example, cation exchange reactions [19-21], adsorption [22] precipitation and dissolution

[21,23,24], redox reactions [24] and biodegradation [16,25,26] have been comprehensively evaluated.

Beside the theoretical models, field scale studies showed that solute transport through soil is highly affected by soil-water system properties [27] including: surface and subsurface boundary conditions, hydraulic and transport properties [28,29] and spatial heterogeneity [30] . The laboratory experiments cannot measure these features [31] and field scale experiments are required (e.g. [32-34]). In fact, the theories developed based on the laboratory scale experiments are generally not applicable for field scale experiments. These complexities in field scale transport reveal the necessity for validating the theoretical models with field scale experiments [35]. Furthermore, complexities of solute transport in the field scale due to physicochemical and biological processes, like adsorption/ desorption and biodegradation were evaluated in different studies [5,28,29,34].

Parallel studies where verification of theoretical models with actual field data, to evaluate the physical and chemical heterogeneities in soil achieved major progress in this field of study [31, 36,37]. For example, Fredericia [38], and Nilsson et al. [39] showed that the measured hydraulic conductivity from large scale field tests and laboratory column tests could be up to two orders of magnitude different.

2-3 Tracers used for tracking the infiltration in field studies

Over the past few decades, scientists have employed different methods including non-invasive optical imaging methods (e.g. [40,41]) and tracer testing to study porous media properties and the processes occurring within them both in reactive and non-reactive seepage of solutes. Due to the complexities involved in solute transport phenomena and lack of subsurface information, tracer tests have a crucial role in the design of reliable transport models [42]. Naturally occurring isotopic and chemical tracers are two commonly used tracers. The conservative (tracer) properties of Cl^- [12,43] and $\delta^{18}O$ and $\delta^{2}H$ of pore water are established and proven in numerous studies including solute transport mechanisms, hydraulic conductivity, groundwater flow and geologic studies [43-45] .

2-4 Clay till properties

Clay till layers have been used to contain industrial waste water (ponds) and to store waste due to their natural low hydraulic conductivity, about 10^{-10} m/s [41,49]. In this capacity, in the last twenty years, contaminant transport through clay till layers has been extensively investigated. Some studies (e.g. [42-44]) have established that due to extremely low flow velocity ($<10^{-3}$ m/year), molecular diffusion is the dominant process governing the solute transport through clay till. The highly reactive properties and heterogeneous nature of clay tills makes it difficult to model and characterize solute transport. Field studies to verify the models seem to be essential.

Hendry et al. [50] identified that “cation exchange reactions” are the major attenuation process in the clay till layer. Timms et al. [51] studied the long-term migration of dissolved $Ca^{2+,}$ Na^{+}, Mg^{2+}, Sr^{2+}, and K^{+} impacted by cation exchange reactions over a 20 m depth of clay till aquitard and showed diffusion dominant transport of solutes. The cations (Sr^{2+} and K^{+}) were delayed in downward migration because of cation exchange reactions.

In situ and laboratory tests to measure effective diffusion on clay till conducted by Hendry et al. [27] using $\delta^{2}H$ as a tracer resulted in an effective diffusion coefficient (D*) values of $2.5\text{-}3.5\times10^{-10}$ m^2/s and 4×10^{-10} m^2/s, respectively. A second study on clay till by Hendry et al. [42], showed vertical profiles of $\delta^{2}H$ and $\delta^{18}O$ indicating diffusion dominant transport in the system. In this study, high heterogeneity of soil resulted in subtle deviations between field data and one dimensional diffusion trends.

2-5 Previous relevant research in the Athabasca oil sands region

Oil sands tailings management is beset with environmental and geotechnical challenges. Concerns about soil and groundwater pollution in the Athabasca region have resulted in different studies focused on tailings PA water toxicity, its seepage through dyke and groundwater remediation.

2-6 PA water chemistry and toxicity

Based on numerous studies conducted on PA water (e.g. [52-55]) it is alkaline, slightly brackish, with acute toxic properties to aquatic biota due to elevated levels of organic acids as a by-product of the bitumen extraction process and contains considerable amounts of reactive chemical components. Residual bitumen, naphthenic acids (NAs), humic and fulvic acids, asphaltenes, benzene, polycyclic aromatic hydrocarbons (PAHs), creosols, phenols, phthalates, and toluene are the detected organic compounds of typical PA water [52,53,56-58]. Among these organic compounds, naphthenic acids with the typical concentration of 50-70 mg/L in PA water are classified as the most toxic organic and the main reason for PA water toxicity [59-61].

Elevated levels of calcium, magnesium, bicarbonate, sodium, chloride, ammonia and sulphate, in comparison to local surface waters, are by products of the bitumen extraction processes resulting in high total dissolved solids (TDS) (typical concentration of 1900-2221 mg/L) concentration in PA water [52-54]. Al, As, Cd, Cr, Cu, Fe, Pb, Mo, Ti, V, and Zn are the common trace metals in PA water reported in different studies [53,56,62,63]. From a toxicity prospective, As, Cd, Cr, Cu, Ni, Pb, and Zn are classified as priority pollutants by USEPA's Clean Water Act [59] .

In a comprehensive review paper by Allen [59] it is concluded that, due to their high concentration in comparison to environmental guidelines, NAs, bitumen, ammonia, sulphate, chloride, aromatic hydrocarbons, and trace metals are

chemicals of environmental concern in oil sands processing. Therefore, a better understanding of their fate and transport into the environment is necessary.

2-7 Fate and transport of PA water compounds

To date, most of the available environmental investigations associated with oil sand tailings PA water in the Athabasca river region are focused on the organic compounds of PA water, particularly NAs [64-68]. Details of the fate and transport of NAs including adsorption and biodegradation mechanisms have been evaluated in some laboratory and field studies. For example, the adsorption capacity of organic-rich Fort McMurray soil for NAs were measured by Peng et al. [64] and Janfada et al. [65] using a laboratory batch sorption method. To characterize the naphthenic acids attenuation processes (adsorption and biodegradation) during PA water seepage through clay till, in 2004, Gervais and Barker conducted a field study [66] . These field studies completed by, Oiffer et al. [67] and Tompkins [68] focused on NAs transport and natural attenuation through the glaciofluvial sand channel underlying the clay till layer. In both studies, the trace metals mobilization were evaluated but only through the sand channel aquifer.

More recently, Holden et al. [69] conducted a detailed laboratory batch sorption experiment on clay till samples in the vicinity of the South Tailing Pond to evaluate the release and attenuation of ions as PA water infiltrates the clay till. The results from this study indicate (1) a high level of sodium adsorption on the clay till particles, corresponding with a Ca^{2+} and Mg^{2+} release into pore water (as

a result of exchange with Na), (2) conservative behaviour of Cl^- and (3) a notable increase in the sulphate concentration due to the dissolution of pre-existing sulphate salts from the clay till particles. Likewise, in another study, Holden et al. [70] examined the mitigation or release of trace elements from clay till particles using radial diffusion cells. The findings of this research revealed the mitigation or uptake of Mo and Zn from the PA water by clay till particles and in contrast the release of Si, Pb, Sr and Ba from clay particles to pore water. As reported by Holden in both studies, at the time of publication, those were the first detailed laboratory experiments characterizing the Athabasca clay till soil for attenuation and release of inorganic species.

The most recent relevant study, was conducted by Gibson et al. [71], where a suite of isotopic and geochemical tracers were used for labelling PA water from oil sands operations and tracking it through the surface and subsurface bodies of water. The authors found that, due to evaporation during oil sands extraction processes, $\delta^{18}O$ and $\delta^{2}H$ are enriched in PA water which can make it distinguishable from other natural bodies of water. Moreover, it is stated that major-, minor- and trace element geochemistry, and organic composition can be used indicators to distinguish PA water from natural surface water in that area. Gibson et al. [71] concluded that evidence did not support PA water seepage into the Athabasca River.

2-8 Conclusion of studies conducted on PA water infiltration into clay till

To date there have been few laboratory studies describing the fate and transport of inorganic compounds found in PA water through the clay till layer, but none of them has explored a field scale study. Previous findings by researchers have emphasized the need to conduct field studies to verify laboratory results as well as solute transport models. As a result, in this research a field based evaluation is conducted on the stable isotopes and inorganic compounds of PA water migration through the clay till. To complement the field efforts, experimental evaluations on the effect of PA water seepage on pore water chemistry, could improve our understanding of the physicochemical reactions between PA water and clay till particles as well as indicating the dominant solute transport mechanism.

2-9 References

(1) Feyen J, Jacques D, Timmerman A, Vanderborght J. Modelling water flow and solute transport in heterogeneous soils: A review of recent approaches. J Agric Eng Res; 1998; 70(3): 231-256.

(2) Phillips IR, Black AS. Predicting exchangeable cation distributions in soil by using exchange coefficients and solution activity ratios. Aust J Soil Res; 1991; 29(3): 403-414.

(3) Dagan G, Neuman S. Subsurface flow and transport: a stochastic approach. : Cambridge University Press; 1997.

(4) Sardin M, Schweich D, Leij F, van Genuchten MTh. Modelling the nonequilibrium transport of linearly interacting solutes in porous media: a review. Water Resour Res; 1991; 27: 2287–307.

(5) Butters GL, Jury WA. Field scale transport of bromide in an unsaturated soil 2. Dispersion modeling. Water Resour Res; 1989; 25(7): 1583-1589.

(6) Heuvelman WJ, McInnes K. Solute travel time distributions in soil: A field study. Soil Sci; 1999; 164(1): 2-9.

(7) Kim DJ, Feyen J. Comparison of flux and resident concentrations in macroporous field soils. Soil Sci; 2000; 165(8): 616-623.

(8) Zhang R, Yang J, Ye Z. Solute transport through the vadose zone: A field study and stochastic analyses. Soil Sci; 1996; 161(5): 270-277.

(9) Larsson MH, Jarvis NJ. Evaluation of a dual-porosity model to predict field-scale solute transport in a macroporous soil. J Hydrol; 1999; 215(1-4): 153-171.

(10) Allinson G, Turoczy NJ, Kelsall Y, Allinson M, Stagnitti F, Lloyd-Smith J, et al. Mobility of the constituents of chromated copper arsenate in a shallow sandy soil. New Zealand J Agric Res; 2000; 43(1): 149-156.

(11) De Rooij GH, Stagnitti F. Spatial variability of solute leaching: Experimental validation of a quantitative parameterization. Soil Sci Soc Am J; 2000; 64(2): 499-504.

(12) Harrington GA, Walker GR, Love AJ, Narayan KA. A compartmental mixing-cell approach for the quantitative assessment of groundwater dynamics in the Otway Basin, South Australia. J Hydrol; 1999; 214(1-4): 49-63.

(13) Grochulska J, Kladivko EJ. A two-region model of preferential flow of chemicals using a transfer function approach. J Environ Qual; 1994; 23(3): 498-507.

(14) Bidwell VJ. State-space mixing cell model of unsteady solute transport in unsaturated soil. Environ Model Softw; 1999; 14(2-3): 161-169.

(15) Travis CC, Etnier EL. A survey of sorption relationships for reactive solutes in soil. J Environ Qual; 1981; 10(1): 8-17.

(16) Prommer H, Barry DA, Davis GB. A one-dimensional reactive multi-component transport model for biodegradation of petroleum hydrocarbons in groundwater. Environ Model Softw; 1999; 14(2-3): 213-223.

(17) Stagnitti F, Allinson G, Morita M, Nishikawa M, Il H, Hirata T. Temporal moments analysis of preferential solute transport in soils. Environ Model Assess; 2000; 5(4): 229-236.

(18) Brusseau ML, Rao PSC. Modeling solute transport in structured soils: a review. Geoderma; 1990; 46(1-3): 169-192.

(19) Valocchi AJ. Effect of radial flow on deviations from local equilibrium during sorbing solute transport through homogeneous soils. Water Resour Res; 1986; 22(12): 1693-1701.

(20) Valocchi AJ. Validity of the local equilibrium assumption for modeling sorbing solute transport through homogeneous soils. Water Resour Res; 1985; 21(6): 808-820.

(21) Lichtner PC. Continuum model for simultaneous chemical reactions and mass transport in hydrothermal systems. Geochim Cosmochim Acta; 1985; 49(3): 779-800.

(22) Gwo JP, Jardine PM, Wilson GV, Yeh GT. A multiple-pore-region concept to modeling mass transfer in subsurface media. J Hydrol; 1995; 164(1-4): 217-237.

(23) Zysset A, Stauffer F, Dracos T. Modeling of chemically reactive groundwater transport. Water Resour Res; 1994; 30(7): 2217-2228.

(24) Bryant SL, Schechter RS, Lake LW. Interactions of precipitation/dissolution waves and ion exchange in flow through permeable media. AICHE J; 1986; 32(5): 751-764.

(25) Barker JF, Patrick GC, Major D. Natural attenuation of aromatic hydrocarbons in a shallow sand aquifer. Ground Water Monitoring Review; 1987; 7(1): 64-71.

(26) Barbaro JR, Barker JF, Lemon LA, Mayfield CI. Biotransformation of BTEX under anaerobic, denitrifying conditions: Field and laboratory observations. J Contam Hydrol; 1992; 11(3-4): 245-272.

(27) Hendry MJ, Barbour SL, Boldt-Leppin BEJ, Reifferscheid LJ, Wassenaar LI. A comparision of laboratory and field based determinations of molecular diffusion coefficients in a low permeability geologic medium. Environ Sci Technol; 2009; 43(17): 6730-6736.

(28) Van De Pol RM, Wierenga PJ, Nielsen DR. Solute movement in a field soil. Soil Sci Soc Am; J 1977; 41(1): 10-13.

(29) Biggar JW, Nielsen DR. Spatial variability of the leaching characteristics of a field soil. Water Resour Res; 1976; 12(1): 78-84.

(30) Stephens DB, Heermann S. Dependence of anisotropy on saturation in a stratified sand. Water Resour Res; 1988; 24(5): 770-778.

(31) Dagan G. Flow and transport in porous formations. Berlin ; New York: Springer-Verlag; 1989.

(32) Schulin R, Wierenga PJ, Fluehler H, Leuenberger J. Solute transport through a stony soil. Soil Sci Soc Am J; 1987; 51(1): 36-42.

(33) Ellsworth TR, Jury WA, Ernst FF, Shouse PJ. A three-dimensional field study of solute transport through unsaturated, layered, porous media. 1. Methodology, mass recovery, and mean transport. Water Resour Res; 1991; 27(5): 951-965.

(34) Butters GL, Jury WA, Ernst FF. Field scale transport of bromide in an unsaturated soil 1. Experimental methodology and results. Water Resour Res; 1989; 25(7): 1575-1581.

(35) Severino G, Comegna A, Coppola A, Sommella A, Santini A. Stochastic analysis of a field-scale unsaturated transport experiment. Adv Water Resour; 2010; 33(10): 1188-1198.

(36) Comegna V, Coppola A, Sommella A. Effectiveness of equilibrium and physical non-equilibrium approaches for interpreting solute transport through undisturbed soil columns. J Contam Hydrol; 2001; 50(1-2): 121-138.

(37) Kachanoski RG, Pringle E, Ward A. Field measurement of solute travel times using time domain reflectometry. Soil Sci Soc Am J; 1992; 56(1): 47-52.

(38) Fredericia J. Saturated hydraulic conductivity of clayey tills and the role of fractures. Nordic Hydrol; 1990; 21(2): 119-132.

(39) Nilsson B, Sidle RC, Klint KE, Bøggild CE, Broholm K. Mass transport and scale-dependent hydraulic tests in a heterogeneous glacial till - Sandy aquifer system. J Hydrol; 2001; 243(3-4): 162-179.

(40) Willingham TW, Werth CJ, Valocchi AJ. Evaluation of the effects of porous media structure on mixing-controlled reactions using pore-scale modeling and micromodel experiments. Environ Sci Technol; 2008; 42(9): 3185-3193.

(41) Jose SC, Cirpka OA. Measurement of Mixing-Controlled Reactive Transport in Homogeneous Porous Media and Its Prediction from Conservative Tracer Test Data. Environ Sci Technol; 2004; 38(7): 2089-2096.

(42) Hendry MJ, Wassenaar LI. Inferring heterogeneity in aquitards using high-resolution δD and $\delta^{18}O$ Profiles. Ground Water; 2009; 47(5): 639-645.

(43) Hendry MJ, Wassenaar LI, Kotzer T. Chloride and chlorine isotopes (^{36}Cl and $\delta^{37}Cl$) as tracers of solute migration in a thick, clay-rich aquitard system. Water Resour Res; 2000; 36(1): 285-296.

(44) Desaulniers DE, Cherry JA, Fritz P. Origin, age and movement of pore water in argillaceous Quaternary deposits at four sites in southwestern Ontario. J Hydrol; 1981; 50(C): 231-257.

(45) Remenda VH, Cherry JA, Edwards TWD. Isotopic composition of old ground water from Lake Agassiz: Implications for late Pleistocene climate. Science; 1994; 266(5193): 1975-1978.

(46) McKay LD, Cherry JA, Gillham RW. Field experiments in a fractured clay till 1. Hydraulic conductivity and fracture aperture. Water Resour Res; 1993; 29(4): 1149-1162.

(47) Keller CK, Van Der Kamp G, Cherry JA. A multiscale study of the permeability of thick clayey till. Water Resour Res; 1989; 25(11): 2299-2317.

(48) Gerber RE, Howard K. Recharge through a regional till aquitard: Three-dimensional flow model water balance approach. Ground Water; 2000; 38(3): 410-422.

(49) Reifferscheid L. In situ measurement of the coefficient of molecular diffusion in fine grained till. Saskatchewan, Canada: University of Saskatchewan; 2007.

(50) Hendry MJ, Cherry JA, Wallick EI. Origin and distribution of sulfate in a fractured till in southern Alberta, Canada. Water Resour Res; 1986; 22(1): 45-61.

(51) Timms WA, Hendry MJ. Quantifying the impact of cation exchange on long-term solute transport in a clay-rich aquitard. J Hydrol; 2007; 332(1-2): 110-122.

(52) MacKinnon MD, Sethi A. A comparison of the physical and chemical properties of the tailings ponds at the Syncrude and Suncor oil sands plants; 1993.

(53) MacKinnon MD, Retallack JT. Preliminary characterization and detoxification of tailings pond water at the Syncrude Canada Ltd Oil Sands Plant; 1981: 185–210.

(54) MacKinnon MD. Oil sands water quality issues: properties, treatment, and discharge options. Available at: http://www.conrad.ab.ca/seminars/water_usage/2004/Agenda; 2004.

(55) Nix PG. Detoxification of tailings pond top water. Report prepared for Suncor Energy Inc., Fort McMurray, Alberta; 1983.

(56) Gulley JR. Study of oil sands sludge reclamation under the tailings sludge abandonment research program. Final Report. Canada Centre for Mineral and Energy Technology (CANMET), Energy, Mines and Resources Canada, Edmonton, Alta.; 1992.

(57) Madill REA, Orzechowski MT, Chen G, Brownlee BG, Bunce NJ. Preliminary risk assessment of the wet landscape option for reclamation of oil sands mine tailings: Bioassays with mature fine tailings pore water. Environ Toxicol; 2001; 16(3): 197-208.

(58) Rogers VV, Liber K, MacKinnon MD. Isolation and characterization of naphthenic acids from athabasca oil sands tailings pond water. Chemosphere; 2002; 48(5): 519-527.

(59) Allen EW. Process water treatment in Canada's oil sands industry: I. Target pollutants and treatment objectives. J Environ Eng Sci; 2008; 7(2): 123-138.

(60) Holowenko FM, MacKinnon MD, Fedorak PM. Characterization of naphthenic acids in oil sands wastewaters by gas chromatography-mass spectrometry. Water Res; 2002; 36(11): 2843-2855.

(61) Verbeek A, McKay W, MacKinnon M. Isolation and characterization of the acutely toxic compounds in oil sands process water from Syncrude and Suncor Oil Sands- Our Petroleum Future Conference, Fine Tails Fundamentals Consortium; 1993: F10–1-F10–11.

(62) Fine Tailings Fundamentals Consortium. Advances in oil sands tailings research. Edmonton, Alta.: Alberta Department of Energy, Oil Sands and Research Division; 1995.

(63) Siwik PL, Van Meer T, MacKinnon MD, Paszkowski CA. Growth of fathead minnows in oilsand-processed wastewater in laboratory and field. Environ Toxicol Chem; 2000; 19(7): 1837-1845.

(64) Peng J, Headley JV, Barbour SL. Adsorption of single-ring model naphthenic acids on soils. Can Geotechn J; 2002; 39(6): 1419-1426.

(65) Janfada A, Headley J, Peru K, Barbour S. A laboratory evaluation of the sorption of oil sands naphthenic acids on organic rich soils. J Environ Sci Health Part A Toxic Hazard Subst Environ Eng; 2006; 41(6): 985-997.

(66) Gervais FJM. Fate and Transport of Naphthenic Acids in a Glacial Aquifer. Waterloo, Ontario, Canada: University of Waterloo; 2004.

(67) Oiffer AAL, Barker JF, Gervais FM, Mayer KU, Ptacek CJ, Rudolph DL. A detailed field-based evaluation of naphthenic acid mobility in groundwater. J Contam Hydrol; 2009; 108(3-4): 89-106.

(68) Tompkins TG. Natural Gradient Tracer Tests to Investigate the Fate and Migration of Oil Sands Process-Affected Water in the Wood Creek Sand Channel. Ontario, Canada: University of Waterloo; 2009.

(69) Holden AA, Donahue RB, Ulrich AC. Geochemical interactions between process-affected water from oil sands tailings ponds and North Alberta surficial sediments. J Contam Hydrol; 2011; 119(1-4): 55-68.

(70) Holden AA, Haque SE, Donahue RB, Ulrich AC. Geochemical Impact of Seepage from an Oil Sands Tailings Facility on Groundwater Resources GQ10: Groundwater Quality Management in a Rapidly Changing World. Proc.; 2010 13–18 June 2010.

(71) Gibson JJ, Birks SJ, Moncur M, Yi K, Tattrie K, Jasechko S, et al. Isotopic and Geochemical Tracers for Fingerprinting Process-Affected Waters in the Oil Sands Industry: A Pilot Study. Oil Sands Research and Information Network, University of Alberta, School of Energy and the Environment, Edmonton, Alberta. OSRIN; 2011; TR-12: 109 pp.

Chapter 3: Native Soil Physical Properties

3-1 Introduction

The focus of this thesis is to describe transport of oil sands process affected water into the subsurface and its fate. This chapter will provide an overview of the geology underlying Suncor's South Tailings Pond. The focus will then shift to U of A's specific research field site – the Infiltration Pond, providing construction details, the specific underlying geology, sampling program, as well as field and laboratory tests used to characterize native soil particle size distribution, Atterberg limits, unified classification, water content, specific gravity, and hydraulic conductivity using both falling head and double ring infiltrometer tests.

3-1-1 Overview of Geology Underlying Suncor's South Tailings Pond

As mentioned in the first chapter, the South Tailings Pond (STP) with a 23 km^2 area: 4 km North to South, and 4.5 km East to West and a 336 Mm^3 capacity for tailings and PA water storage was developed by Suncor on the east side of the Athabasca River.

Previous field studies, using boreholes, monitoring wells, surface geophysics and supporting field mapping and air photo interpretation conducted by Suncor's consultants, among them Klohn Crippen Bergere Ltd., Mollard & Associates, and WorleyParsons, provide an overview of the geology underlying the STP and within its vicinity. Thus it provides a wider perspective of the geological units located in this area of the Athabascan oil sands region near the STP.

Three overburden soil layers cover two major bedrock formations in the area. These two bedrock formations consist of the Clear water formation and the McMurray formation [1,2]. As a marine deposit, the Clearwater formation is composed of clay shales on thin carbonate cemented, siltstone beds. The McMurray formation is comprised of clay and fine to medium grained, unconsolidated sand which is predominantly oil-saturated [2,3]. In comparison to "bedrock formations", the "surficial geology" of this area plays the most crucial role in controlling the extent of PA water infiltration from tailings ponds.

According to the 2004 consulting report by Klohn Crippen Consultants Ltd [1]. on data from 336 boreholes, there are three major formations which comprise the surficial geology. In order descending from the surface they are:

1- Muskeg: Dark brown to black colored, thin (~1.5 m), surface soil composed of wood, peat, silt and clay. For the STP construction this thin layer was totally excavated since this layer was not important in this project due to its efficacy in terms of the geotechnical and geo-environmental impacts of the STP.

2- Glacial till: The muskeg lies on an 8 to 35 m-thick- Pleistocene glacial till. Typically, the glacial till is composed of a predominantly clayey till and silty till contribution as well as some gravel and sand content. The STP was built over this layer, due to its low permeability (median value of $2.4*10^{-7}$ m/s from 41 field tests). This thesis focuses mainly on the chemical and physical properties of this glacial till layer, due to its vital role in preventing PA water

migration. In addition, the interesting effect of varying soil types (from clay to silt to sand lenses) in this zone will provide much needed information on PA water migration.

3- Wood Creek Sand Channel: WCSC is a highly permeable Pleistocene glaciofluvial channel with an approximately 20-30 m thickness. Fine to medium sandy soils are the main composite of this channel. In the upper sub-layer, more clay and silt is available. The reason behind high fine content of the upper sub-layer lies in the gradual transition from the upper layer of glacial till to the sandy lower level. However, coarse sand and fine gravel are progressively more predominant at the bottom of WCSC [1,2]. As described in Chapter 1, approximately 50% of the STP overlies the WCSC, providing the Western and Southern dyke walls with more geotechnical stability to avoid flat slopes. On the other hand, this placement could result in adverse environmental impacts. In fact, after seepage through the clay till layer, STP PA water migrates to the McLean Creek and subsequently to the Athabasca River by using the WCSC as a preferential flow pathway. Figure 3-1 shows the WCSC boundary beneath the STP and presents the seepage patterns at the Western dyke.

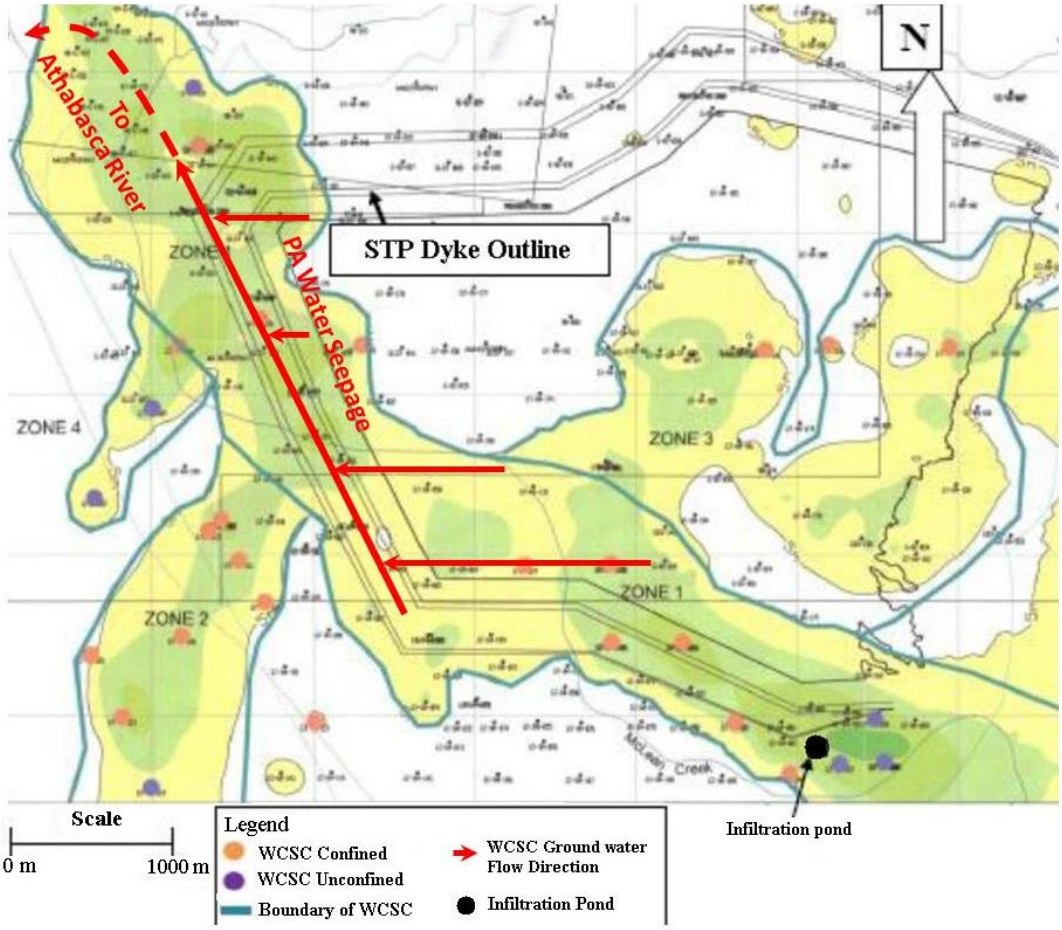

Figure 3-1: Wood Creek Sand Channel boundary beneath clay till layer underlying the STP. Source: [1].

3-1-2 Field Research Infiltration Pond Details

To better characterize the infiltration of PA water into the glacial till, U of A constructed an Infiltration Pond on the South Eastern portion of the WCSC (location shown in Figure 3-1) in August 2008. As a general rule, the 10 m x 10 m infiltration pond was excavated to a 1.3 m depth into the clay till layer to ensure penetration into the clay till. Prior to filling it, a series of double-ring infiltrometer tests were completed on the floor of the pond to provide preliminary hydraulic conductivity data (described in Section 3-2-3-6). In a 5 x 6 grid pattern,

a series of slotted, 15.2 cm (6 in) diameter PVC pipes covered in a geotextile liner were placed into the floor of the pond and 1m of tailings sand was then placed on top of them to hold the slotted pipes in position. These slotted pipes were designed to make future clay till coring easier to avoid coring through the tailings sand. Finally, STP PA water was used to fill the pond during the August 2008 construction visit. A schematic as well as a photo of the Infiltration Pond are shown in Figure 3-2 and Figure 3-3 respectively.

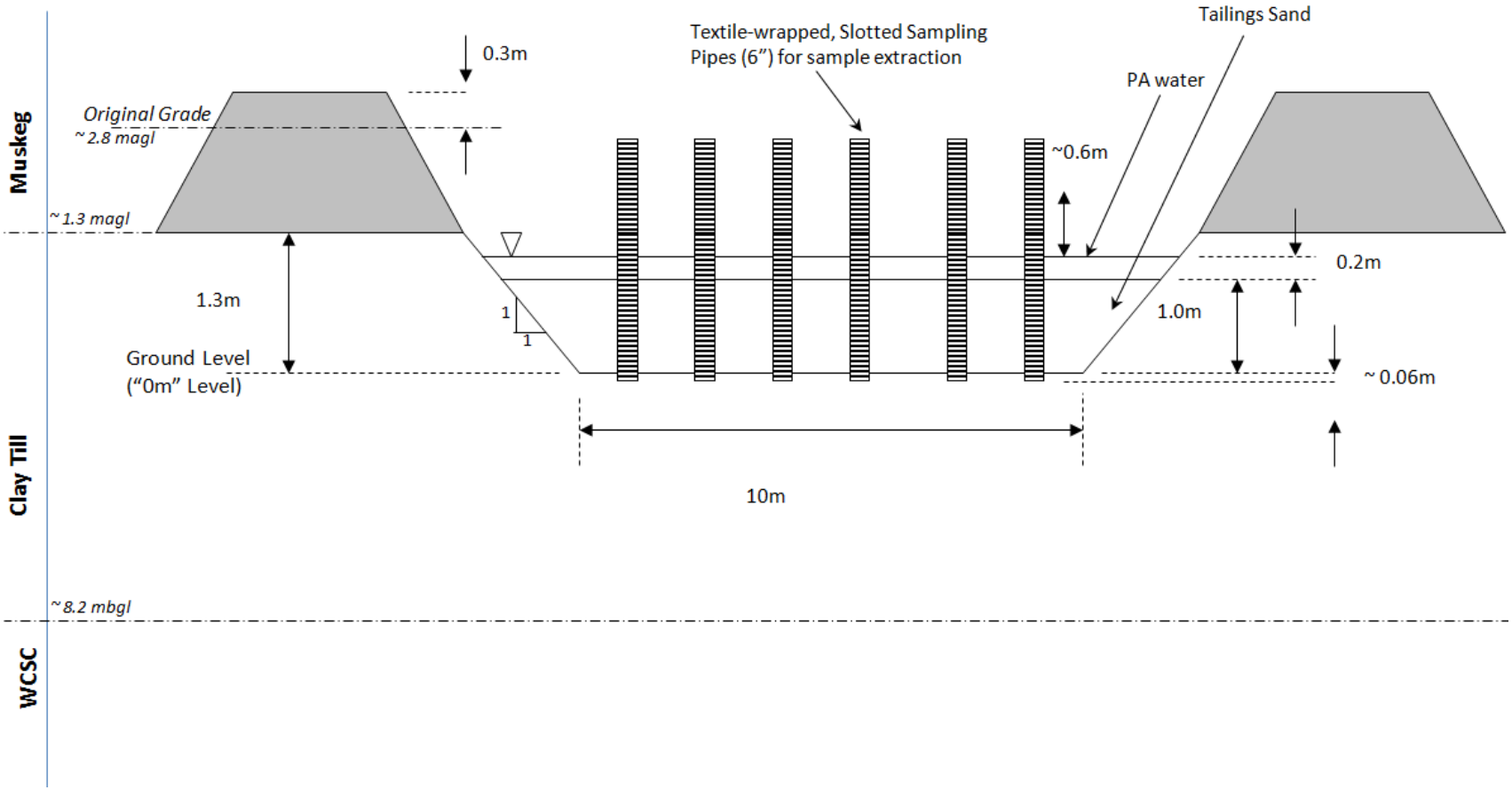

Figure 3-2: Schematic of the infiltration pond (not to scale); magl: metres above ground level; mbgl: metres below ground level; Ground level: Infiltration pond bottom.

Figure 3-3: The North West view of the Infiltration Pond; a: August 2008; b: July 2010.

This Infiltration Pond served as a small scale model of the STP to investigate the PA water migration into the subsurface. A soil core sampling program was used over time to determine the following:

1. Soil properties (discussed in the chapter below):

    Physical properties such as particle size distribution, Atterberg limits, unified classification, water content, specific gravity, and hydraulic conductivity using both the falling head and double ring infiltrometer tests were measured.

2. Pore water properties (discussed in Chapter 4):

    a) pH, alkalinity, electric conductivity, heavy metals, cations and anions.

    b) The isotopic composition of ^{18}O to track the progress of the water molecule from the PA water in the Infiltration pond.

This overall analysis would help to enhance our understanding of the transport of PA water through the clay till, as well as where it ends up.

3-2 Materials and Methods

3-2-1 Soil Coring and Sampling

Soil samples were collected by drilling boreholes inside and outside of the infiltration pond at two time periods – August 2008 (time zero samples) and July 2010 (two year infiltration timeline).

The first series of soil cores were collected in August 2008 at the four corners of the Infiltration Pond after the excavation and before the placement of the tailings (locations shown in Figure 3-4). These soil samples served as a baseline for the soil and pore water chemistry. The drilling started at the surface where muskeg

was encountered, followed by the clay till around 8 m down and stopped as soon as the top of the WCSC was encountered. The total depth of each borehole was around 12 m. 12.7 cm (5 in) diameter, transparent PVC pipes were used to contain the soil cores and were labelled, sealed and transported to the Department of Civil and Environmental Engineering at the University of Alberta. The columns were stored in a -16˚C freezer. Freezing the soil columns helped to preserve the chemical properties of the soil and pore water and kept the soil column undisturbed for the subsequent hydraulic conductivity tests.

The very bottom of each 1 m length of sample was assumed to be a good representative section of the associated 1 m soil cores. Therefore, the last 15 cm section was tested physically and geo-chemically (i.e. 0.85-1 m, 1.85-2 m ...). In some cases, due to partial recovery of soil cores, the aforementioned designated section was not available. Therefore, the closest available 15 cm section has been examined instead. It should be noted that since all soil physical and geo-chemistry analysis were conducted on the soil samples underlying the Infiltration Pond, the bottom of the pond is designated as the "0 mbgl" point. This simplified the comparison of data from samples collected in 2008 and 2010. Each 15 cm soil section was split lengthwise and one half of the sample was used to extract pore water for geochemical analysis at U of A. The other half was sent to Alberta Innovates Technology Futures in Calgary for isotopic analysis.

The remaining soil cores were stored frozen and were used for the soil physical analysis, hydraulic conductivity tests, and also served as a backup for lost or poorly maintained samples.

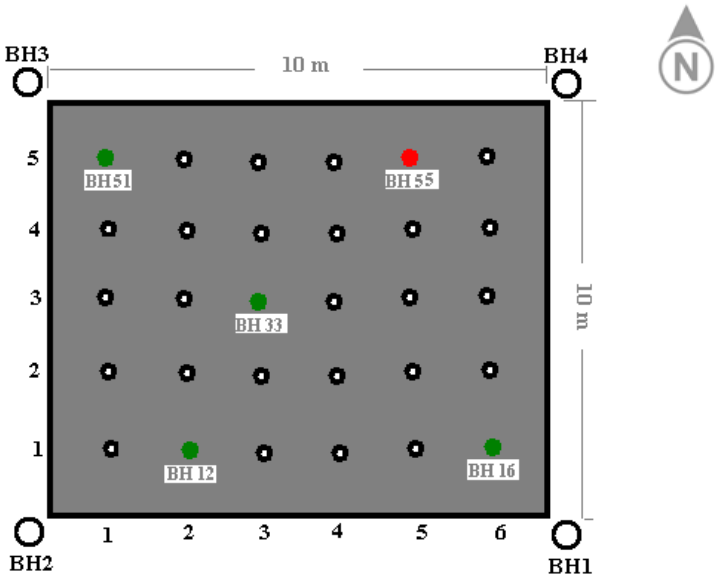

Figure 3-4: Schematic of BHs collected and their location inside and outside the infiltration pond. ○: Slotted sampling pipes; ●: BHs drilled with full recovery August 2010; ●: BH drilled with no recovery August 2010; ○: BHs 1, 2, 3, and 4 drilled August 2008 (used to establish baseline).

Table 3-1: Details of soil samples collected for BH4 in 2008

BH #	Sample ID	Depth Range (m)	Average Depth (m)	Date Taken
BH4	4-1	1.44-1.29 agl	1.365 agl	Aug 23 2008
BH4	4-2	0.95-0.8 agl	0.875 agl	Aug 23 2008
BH4	4-3	0.05-0.20 bgl	0.125 bgl	Aug 23 2008
BH4	4-4	0.86-1.01 bgl	0.935 bgl	Aug 23 2008
BH4	4-7	3.05-3.20 bgl	3.125 bgl	Aug 23 2008
BH4	4-9	4.05-4.20 bgl	4.125 bgl	Aug 23 2008
BH4	4-10	5.43-5.58 bgl	5.505 bgl	Aug 23 2008
BH4	4-14	9.20-9.35 bgl	9.275 bgl	Aug 23 2008

Note: agl, above ground level; bgl, below ground level; Ground level, Infiltration pond bottom

The second soil sampling program was conducted in July 2010 (two years after filling the Infiltration Pond with tailings). The cores were collected by driving a 5.1 cm (2 in) diameter thin-walled aluminium irrigation tubing into the till using a gasoline powered Pionjar 120 portable drill (Figure 3-5). The aluminium core

tubing was driven from the surface to the refusal to a depth of 1 m, following the method of Starr and Ingleton [4].

Figure 3-5: a: Gasoline powered Pionjar 120 portable drill used for coring; b: Driving aluminium tube into the clay till at the bottom of the Infiltration Pond using gas powered drill.

The soil cores were retrieved using a tripod pulling mechanism. In an attempt to get representative samples, five different locations were selected. Figure 3-4 shows the location of these five samples amongst the 5 x 6 grid pattern within the infiltration pond. Four full recovery clay cores were collected (indicated in green in Figure 3-4). The cores' lengths ranged from 0.5 to 1 m. PVC caps and tape were used to seal the soil samples in aluminium pipes to prevent the cores from interacting with the atmosphere. To preserve the soil and pore water chemistry, the samples were placed in a small cooler with ice packs on site immediately after their collection. The core samples were transferred to the same freezer previously mentioned for the 2008 samples at U of A.

The frozen cores were sectioned into 17 to 20 cm lengths. Then, all the sections were split lengthwise to run geochemistry tests on the pore water of one half at U of A and isotopic analysis on the remaining half by Alberta Innovates Technology Futures in Calgary. Table 3-2 summarizes the details of all the soil samples taken in 2010.

Table 3-2: Details of soil samples collected for BHs 12, 33, 51, and 16

BH #	Sample ID	Depth Range (m bgl)	Average Depth (m bgl)	Date Taken
BH12	12-1	0-0.2	0.1	July 7 2010
BH12	12-2	0.2-0.4	0.3	July 7 2010
BH12	12-3	0.4-0.59	0.5	July 7 2010
BH33	33-1	0-0.17	0.08	July 7 2010
BH33	33-2	0.17-0.34	0.25	July 7 2010
BH33	33-3	0.34-0.52	0.42	July 7 2010
BH33	33-4	0.52-0.69	0.59	July 7 2010
BH33	33-5	0.69-0.86	0.76	July 7 2010
BH33	33-6	0.86-1.04	0.93	July 7 2010
BH51	51-1	0-0.18	0.09	July 8 2010
BH51	51-2	0.18-0.36	0.27	July 8 2010
BH51	51-3	0.36-0.55	0.45	July 8 2010
BH16	16-1	0-0.2	0.1	July 8 2010
BH16	16-2	0.2-0.4	0.3	July 8 2010
BH16	16-3	0.4-0.62	0.5	July 8 2010

3-2-2 Visual Inspection of Soil Profiles

To identify the different soil types underlying the infiltration pond, both the 2008 and 2010 soil samples were visually classified. Distinguishing different soil types versus their depth helps to focus on the details of their physical properties. All descriptions were conducted in accordance with ASTM D2488 standards [5]. Beneath the infiltration pond, two distinct soil types including a clay till and a sand layer were found. All physical properties tests were conducted on these two layers.

3-2-3 Soil Physical Properties Tests

To improve our understanding of PA water transport, it was essential to establish the physical properties of the soil layers underlying the infiltration pond. To do so particle size distribution, water content, specific gravity and hydraulic properties of the soil layers were measured. All of these tests have been duplicated to check for consistency.

3-2-3-1 Particle Size Distribution

A particle size distribution (PSD) curve, by showing the particle size and uniformity, plays a big role in understanding soil behavior not only in soil strength and compressibility, from a structural point of view, but also in its interaction with fluids and thermal regimes in hydrogeology and geo-environmental applications [6].

Based on the soil particle size range, two types of tests are performed to establish the particle size distribution: sieve analysis is used on soils larger than 0.075 mm, called coarse-grained, and the hydrometer test is used for particles smaller than 0.075 mm, passed sieve number 200.

3-2-3-1-1 Sieve Analysis

This method uses a known volume of dry soil, which is shaken to pass through a set of sieves sorted from the largest opening size at the top to the smallest at the bottom. A particle size distribution curve is the output of this method and displays the accumulative percentage of soil passing through the different opening size of each sieve. This curve is used to determine particle size ranges and uniformity. C_u and C_c are two coefficients, computed based on Equations 3-1 and 3-2 respectively from the PSD curve for coarse soil classification.

$$C_u = \frac{D_{60}}{D_{10}} \qquad \textbf{Equation 3-1}$$

$$C_c = \frac{}{D_{60} . D_{10}} \qquad \textbf{Equation 3-2}$$

Where: D_x is the grain size diameter corresponding to x% passing (finer) on a PSD curve.

The sieve analysis tests were conducted under the ASTM D421 standard method by Dr. Saied Gitipour, a visiting researcher, at U of A [7]. A 500 g sample of the upper portion of the clay till , a 500 g sample of the lower portion of the clay till and a 500 g sample of sand (type C), were used for the tests and run in duplicate. The sieve numbers were arranged from 4, 10, 20, 40, 60, 100 to 200 respectively from top to bottom. The shaking time was around 10-15 minutes. A bottom pan was placed at the bottom of sieves tray to collect soil particles that passed sieve number 200 for subsequent hydrometer tests.

3-2-3-1-2 Hydrometer Analysis

For fine-grained soils, those with particles smaller than 0.075 mm or that passed through sieve U.S. No 200, hydrometer analysis was completed. The hydrometer analysis was developed based on Stokes' equation for the terminal velocity of a falling sphere [8]. This test was based on the ASTM D421 and D422 standard method procedure and was conducted on clay till soil samples by Dr. Saied Gitipour, a visiting researcher, at U of A [7].

3-2-3-2 Atterberg Limits

The Atterberg Limits include the Liquid Limit (LL), the Plastic Limit (PL), and the Plasticity Index (PI) of soils and are one of the methods used to classify soil. The liquid limit and plastic limit were performed according to ASTM D4318 by Dr. Saied Gitipour, at U of A [7,9]. The plastic index was calculated by subtracting the plastic limit from the liquid limit.

3-2-3-3 Soil Classification

The grain size distribution and the Atterberg Limits were used to classify soil in accordance to the Unified Soil Classification System (USCS) based on ASTM D2487 procedure [7]. The percentage of gravel, sand and fines were obtained based on the USCS in which gravel particles are retained on sieve No.4 (diameter greater than 4.75mm), sand particles pass sieve No. 4 and are retained on sieve

No. 200 (range from 4.75 mm to 0.075 mm in diameter) and finally fine particles pass sieve No. 200 (diameter smaller than 0.075 mm) [7].

3-2-3-4 Water Content

Water content is defined as the ratio between the mass of water and that of oven dry solids in the soil. The procedure for the determination of the water content of soil in the laboratory is given by ASTM D 2216 [7]. The water content of the 2008 soil samples was measured by Alberta Innovates Technology Futures in Calgary. For the 2010 samples, the water content test was performed at U of A. An oven with a temperature of 110º C was used to dry the soil samples over a period of 12 hours.

3-2-3-5 Specific Gravity

Specific gravity is defined as the density of soil divided by the density of 20º C distilled water [10]. The specific gravity tests were conducted using the ASTM D854 procedure by Dr. Saied Gitipour, a visiting researcher, at U of A [7].

3-2-3-6 Hydraulic Conductivity Measurements

Hydraulic conductivity is a fundamental characteristic of soil representing the ease with which water can flow through soil materials. The permeability coefficient of soils (K) is measured using hydraulic conductivity tests. Constant

head and falling head are the two most common permeameters used for coarse sands and fine soils, respectively. As of 2010, the falling head test has not been regulated by ASTM. However, a procedure proposed by Das (1982) is commonly used for the falling head test that is similar to the ASTM D2434-68 standard procedure for constant head permeability coefficient measurements [11,12]. Soil hydraulic conductivity as determined by the falling head test is calculated as shown in Equation 3-3 [12].

$$K = 2.303 \frac{a.L}{A.t} \log\left[\frac{h_1}{h_2}\right] \quad \text{(cm/s)} \qquad \textbf{Equation 3-3}$$

Where h1 and h2 are starting head and ending head respectively; L (cm) is the soil sample length, A (cm^2) and "a" (cm^2) are the area of the sample and the area of the burette tube, respectively [13].

Since soil texture has a large effect on the soil permeability coefficient measured in the laboratory [14] the hydraulic conductivity tests for all soil samples were conducted on undisturbed soil cores. Undisturbed soil columns were trimmed to fit snugly and placed in the permeameter cylinder, which was stainless steel with a 6.3 cm inner diameter and 8 cm length (Figure 3-6). Furthermore, keeping the samples under 4˚C helped to prevent chemical and biological activities in the soil columns.

Utilizing distilled or deionized water in the hydraulic conductivity tests increases the dispersion of clay particles and is not recommended [14,15]. Consequently, the STP PA water was used to simulate the actual reaction of the clay till particles with organic and inorganic substances existing in the PA water.

Figure 3-6: Falling head permeameter testing equipment

Using the grain size distribution results, Hezan's empirical formula was applied to compare laboratory and empirical results. Based on Hezan's suggestion, for sands with C_u<5 and D_{10} of 0.1-3 mm, K can be calculated using Equation 3-4.

$$K = cD_{10}^2 \qquad \textbf{Equation 3-4}$$

Where K (cm/s) is the permeability coefficient and D_{10} (mm) is the grain size diameter corresponding to 10% passing on a PSD curve and c is a constant with the value ranging from 1 to 1.5.

3-2-3-7 Double Ring Infiltrometer

The Double Ring Infiltrometer (DRI) test is a widely used in-situ method to estimate soil characteristics in geotechnical investigations, especially to measure the field-saturated hydraulic conductivity of surface soil layers [2,14-16]. In particular, this method is used for the unsaturated soils above the water table.

As it is clear from the test's name, two open ended, metal cylinders are used to perform the double ring infiltrometer test. One of which is smaller with a diameter of 16.5 cm and one larger with a diameter of 32 cm. These cylinders are driven into the soil layer from 3 to 10 cm using a hydraulic ramp or drop-hammer. The smaller ring is located in the center of the large one. The cylinders' ends will have been sharpened to reduce disturbances in the soil and to move directly through the soil layer.

There are two separate water tanks to supply water for this test. One tank is connected to the inner ring and the other tank is connected to the annular ring. The majority of infiltrometer tests use float valves or siphons to keep a constant water head in the cylinders. Apparently, in constant head infiltrometers, mass balance dictates that "the volume of water conducted from the associated tank to the inner ring" should be equal to "the volume of water infiltrated from the inner ring to the soil".

Due to soil's anisotropic nature, water can infiltrate both horizontally and vertically with a more or less different permeability in these two directions. One of the most important advantages of using double ring infiltrometers is to keep

water from its lateral movement. In fact, as Figure 3-7 presents, the same level of water in both rings forces the inner ring to drain water mainly in the vertical direction. Equation 3-5 was used to calculate the infiltration rate using the volume of water infiltrated through the inner ring over the elapsed time [17].On the other hand, water in the annular ring can move both vertically and horizontally. As a result, the water level fluctuation or volume of water added to the annular ring has no bearing on infiltration rate calculations and can be ignored.

$$I_{IR} = \frac{\Delta V_{IR}}{A_{IR} \cdot \Delta t} \qquad \textbf{Equation 3-5}$$

Where I_{IR} (cm/s) is the infiltration rate of the inner ring, Δt (s) is the time duration, ΔV_{IR} (cm^3) is the volume of water infiltrated during Δt (s) and A_{IR} (cm^2) is the area of the inner ring.

The double ring infiltrometer test was conducted in accordance with ASTM D3385 procedure by Mr. Ojekanmi, a geo-environmental researcher from U of A [17]. In this research, the clay till infiltration rate was measured at two locations on the infiltration pond floor, directly after the excavation of the pond.

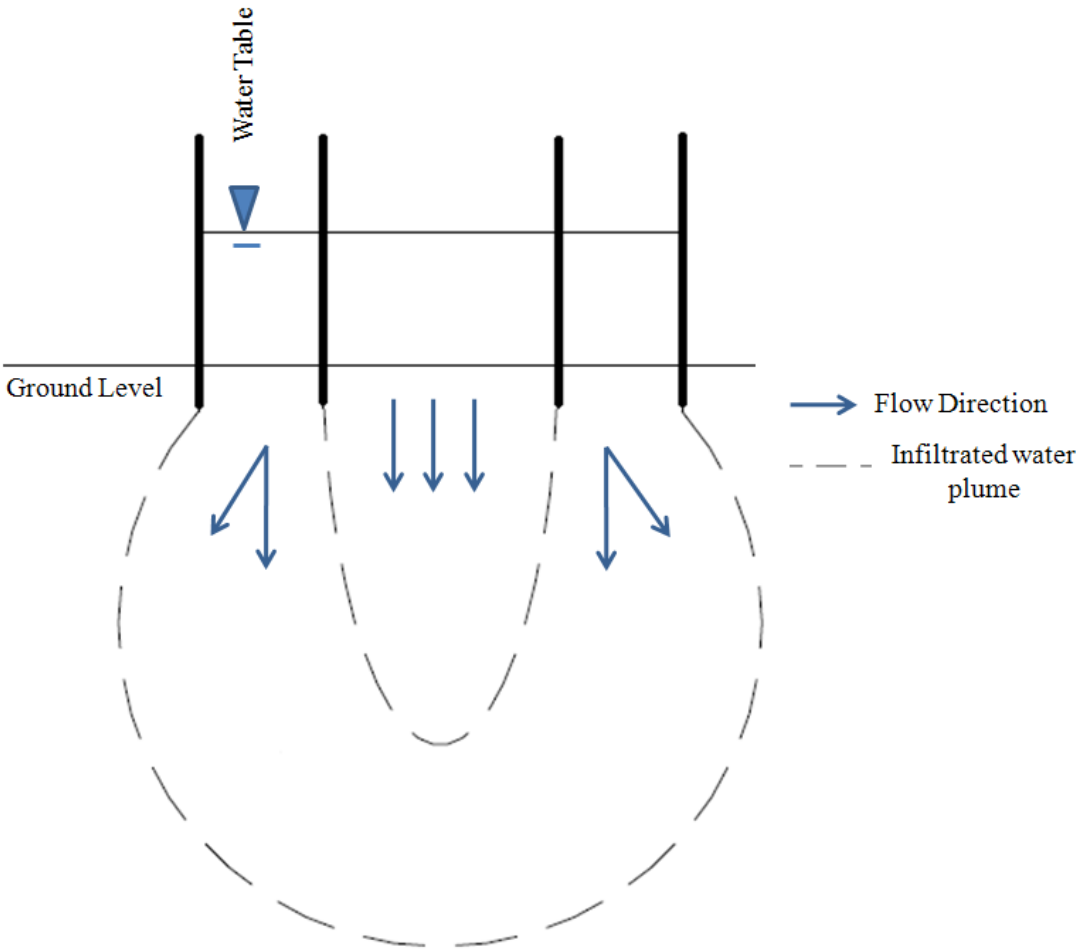

Figure 3-7: Schematic of the Double Ring Infiltrometer [18]

3-3 Results and Discussion

3-3-1 Visual Inspection of Soil Profiles

Based only upon visual inspection, there are three distinguishable soil types in the 2008 soil cores. The first layer at the top of boreholes 1 to 4 was muskeg with a composition of silt, clay, peat, organic soil and wood. This roughly 1.5-metre thick, black layer overlies a clay till layer with medium plasticity which contains large clasts and red staining. The clay layer was seen at a 1.5 to around a 10.5 metre depth. Upper portions are brown clay with a progressively higher dark grey-silt content found with depth.. Finally, light brown glaciofluvial sand and gravel was detected in all samples deeper than 10.5 metre. Interlaminated soil layers between different soil types were observed.

Since the STP and the infiltration pond were excavated on the clay till layer and the focal point of this study is to characterize the PA water seepage through clay till, the physical and chemical properties of the muskeg layer have been ignored.. The visual inspection results are illustrated graphically in Figure 3-8.

Likewise, 2010 soil samples were visually inspected after they were split. Predominantly, the soil of these samples was brown clay with stones, large clasts and red and dark gray staining with medium to high plasticity (clay till). BH16-1 was the only sample with a sand lens which covered around 60% of that sample (Figure 3-9).

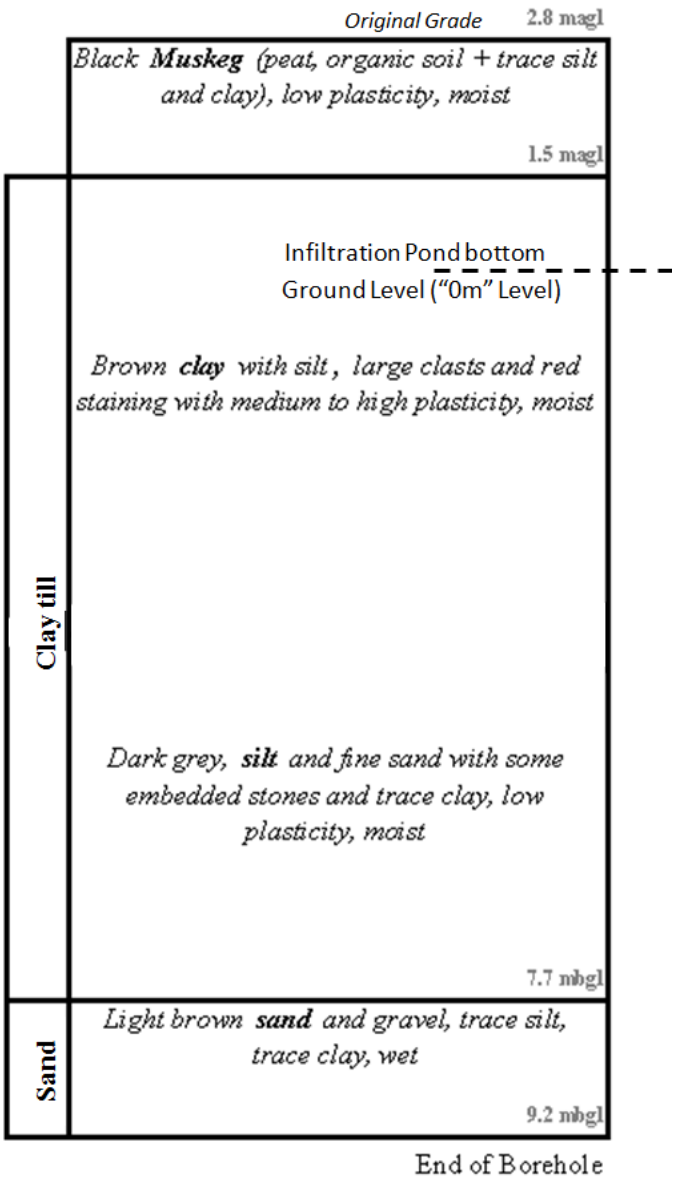

Figure 3-8: Borehole log of BH2 based on visual classification; agl: above ground level; bgl: below ground level; Ground level: Infiltration pond bottom.

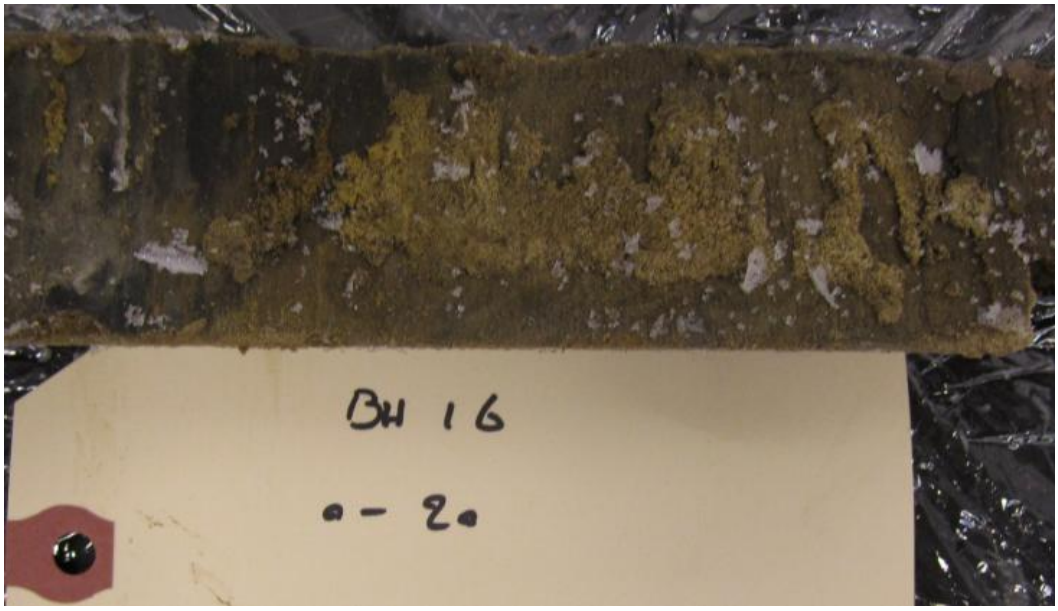

Figure 3-9: Photo of BH16-1(0-0.2 mbgl), brown clay with stones and sandy lens.

3-3-2 Grain Size Distribution Test

Figures 3-10 to 3-12 show the grain size distribution of the two soil types. To show the total grain size distribution of the clay till soil, the hydrometer results were combined with the sieve results and plotted on a semi-log graph paper (Figures 3-10 and 3-11). The results of the sieve analysis for sandy soil are available in Figure 3-12. Detail results of the sieve and hydrometer test can be found in appendix A.

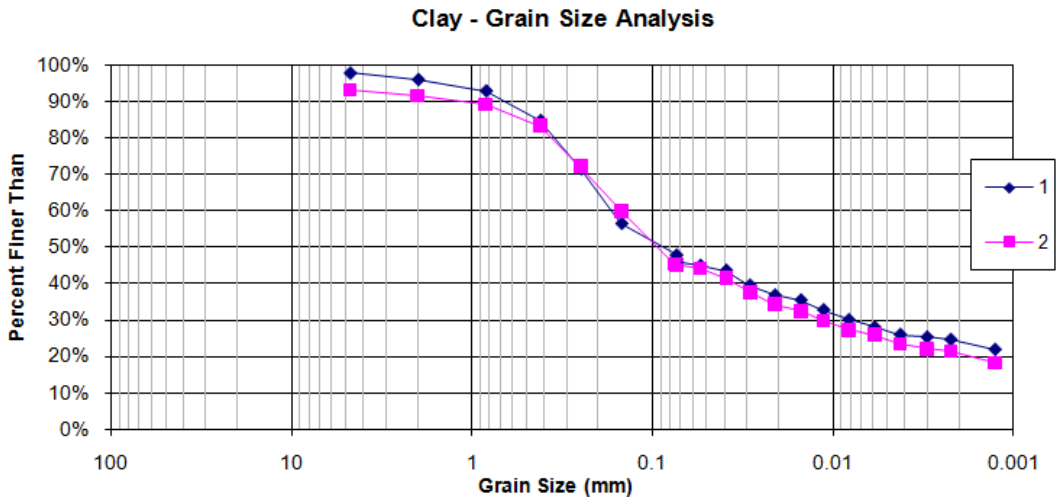

Figure 3-10: Grain Size Distribution Curve for BH1 clay till; 1: 0-0.1 mbgl; 2: 0.1-0.2 mbgl.

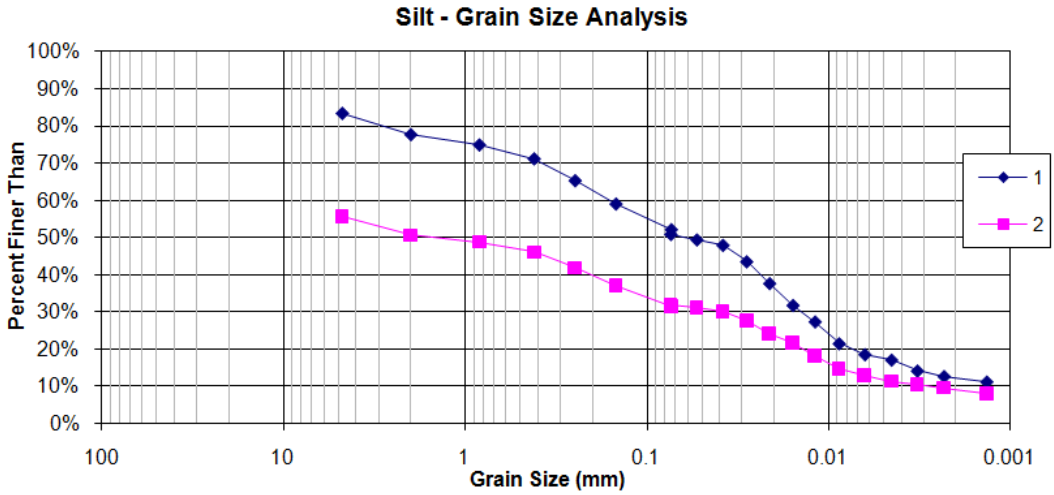

Figure 3-11: Grain Size Distribution Curve for BH1 clay till; 1: 4.1-4.2 mbgl; 2: 4.3-4.4 mbgl.

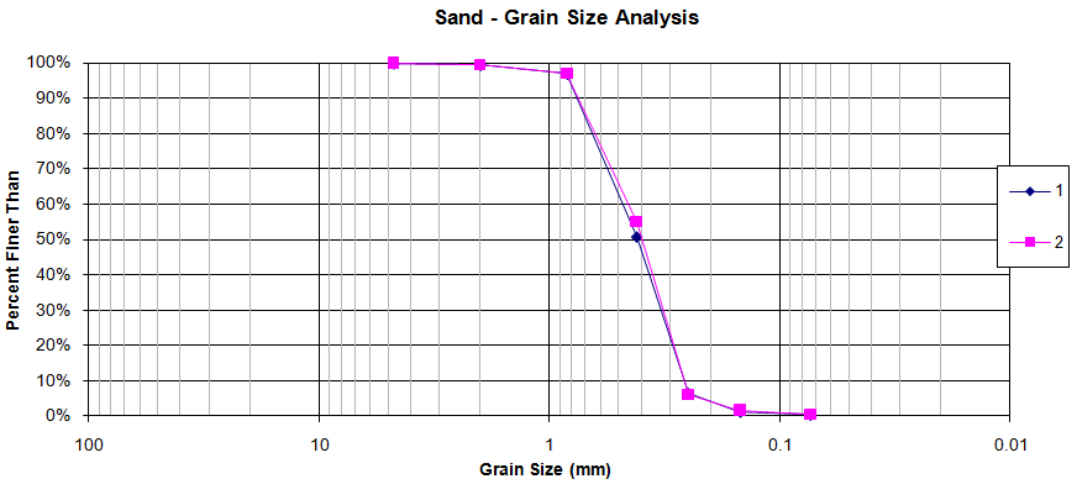

Figure 3-12: Grain Size Distribution Curve for BH1 sand; 1: 8.7 -8.8 mbgl; 2: 9.2-9.3 mbgl.

3-3-3 Atterberg Limits

The Atterberg Limit test results including the Liquid Limit, Plastic Limit, and Plasticity Index of clay and silt soils are summarized in Table 3-3. The results of these tests were used for fine grained soils classifications based on USCS.

Table 3-3: Average Atterberg Limits for clay till soil samples

Soil Type	Sample ID (BH: Depth (mbgl))	Liquid Limit	Plastic Limit	plasticity index
Clay till	BH1: 0-0.2	23.5	16.7	6.8
Clay till	BH1: 4.1-4.3	20.3	19.4	0.8

3-3-4 Soil Classification

The particle size distribution of BH1: 0 to 0.1 mbgl is continuous and shows that the upper portion of the clay till soil is relatively uniformly graded and smoothly distributed. The PSD curve, Figure 3-10, also indicates a 4.5% gravel, 48.9% sand and 46.5% fines (including silt and clay) content. Based on the Atterberg Limit test results (LL<50 and 4<PI>7), this soil is classified as SM-SC which indicates sand that contains a high percentage of low plasticity clay and silt.

The PSD curve of BH1: 4.1-4.3 mbgl shows a gap graded distribution especially in the fine sands size range. However, this soil contains a higher percentage of gravel in comparison to the upper portion of the clay till sample. The PSD indicates a 16.6 % gravel, 31.1% sand and 52.2% fine content for the first run. Combining the first sample PSD result with the Atterberg Limit test results (LL<50 and PI<4), this soil is classified as ML, predominantly silt plus sand and gravel. Surprisingly, the PSD of the second soil sample of lower clay till soil sample indicates a 44.3 % gravel, 24.1% sand and 31.6% fine content which classifies this soil as GM, which is poorly graded silty gravel with sand. This difference, between two samples, reveals a high heterogeneity in this layer of soil.

Based on the PSD curve for the of the sand soil (Figure 3-12), the composition of soil is less than 0.1% gravel, 99.5% sand and 0.4% fines. Therefore, it has a textural class of sand. Where D_{10}=0.23 mm, D_{30}=0.31 mm and D_{60}=0.47 mm, the C_u and C_c were calculated 2 and 0.89 respectively. With C_u<6 and a Cc that is not in the range of 1 to 3, this soil is classified as SP, a poorly graded sand.

3-3-5 Water Content

A water content test was conducted on BH1,2 as well as the 2010 samples at different depths. For the 2008 samples, the average water content for upper clay till soil samples is 13.4%, for deeper clay till soil samples is 18.2% and for the sand layer samples is 7.5%. The graph in Figure 3-13 illustrates the average water content of the 2008 samples for the depth range of 0 m to 1 m bgl and 2010 samples water content versus depth. As it is clear from the figure of water content versus depth, Figure 3-13, all three 2010 soil samples show similar patterns. The water content is highest near the top, close to the Infiltration Pond bottom, and decrease with depth to the average water content of the 2008 samples (indicated in black dotted line in Figure 3-13) which serves as a background water content.

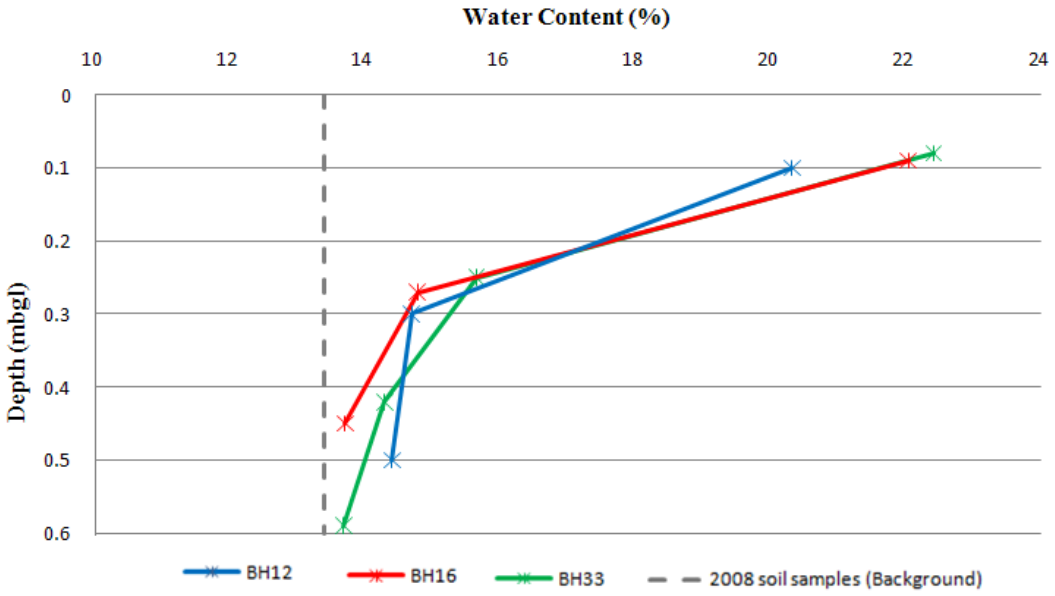

Figure 3-13: Water content of 2010 soil samples (BHs 12, 16, and 33) versus depth as they compare to 2008 soil samples (background) water content. Average value of Background, is shown in vertical dotted lines to make the comparison easier.

3-3-6 Specific Gravity

A specific gravity test was conducted on clay till and sand soil samples of BH1. The results of these specific gravity tests are available in Table 3-4.

Table 3-4: Specific gravity for the native soils

Soil Type	Depth (mbgl)	specific gravity (Average)
Clay till	0.1	2.59
Clay till	4.2	2.61
Sand	9.0	2.65

3-3-7 Hydraulic Conductivity

The coefficients of Permeability (K) for soil samples were measured by a falling head hydraulic conductivity test performed on undisturbed soil samples. The permeability coefficient increases from the upper clay till soil samples to the sand soil samples. Table 3-5 lists the average results of permeability.

Table 3-5: Average hydraulic conductivity of the native soils

Soil type	Depth (mbgl)	K (cm/s)
Clay till	0.1	$3.1*10^{-6}$
Clay till	4.5	$7.2*10^{-5}$
Sand	1.4	$1.9*10^{-4}$

The lowest hydraulic conductivity belongs to the upper clay till soil and it is comparable to the K of lower clay till soil. Although both of these two soil samples have approximately the same percentage of fine amendments, lower soil

sample has a higher K due to a higher percentage of gravel in comparison to upper clay till. Moreover, based on the Atterberg Limits findings, the fine particles of the upper clay till soil, passed sieve 200, are more clay, which absorbs water, expands and results in a lower permeability. On the other hand, for the lower clay till soil the majority of its fine particles are silt. The higher permeability of the sand soil sample is due to its sandy texture and the higher percentage of particles retained on sieves number 40 and 60, 46.1% and 44.3% respectively. Using D_{10}=0.23 mm, measured in the grain size distribution test, and by the knowledge of C_u=2, which satisfies Hazen's empirical equation limits, the sand soil K is calculated at $5.3*10^{-4}$ cm/s which is in agreement with the laboratory falling head results. More details from the hydraulic conductivity tests may be found in Appendix A.

The low percentage of gravel particles, the high percentage of fine sand and the location at the silt/sand interface zone of glacial till and wood creek sand channel, are the reasons behind the low permeability of the sand soil sample compared with the typical K of WCSC measured by Klohn Crippen Berger Ltd., $6.5*10^{-2}$ cm/s [1].

3-3-8 Double Ring Infiltrometer

Two infiltrometer tests were performed on the infiltration pond floor immediately after the excavation and before the tailings placement in the pond. Because of the low permeability of clay till, the gauge readings were taken every 24 hours. The

infiltration rate was measured at $4.3*10^{-7}$ cm/s for the first location and $2.6*10^{-7}$ cm/s for the duplicate run.

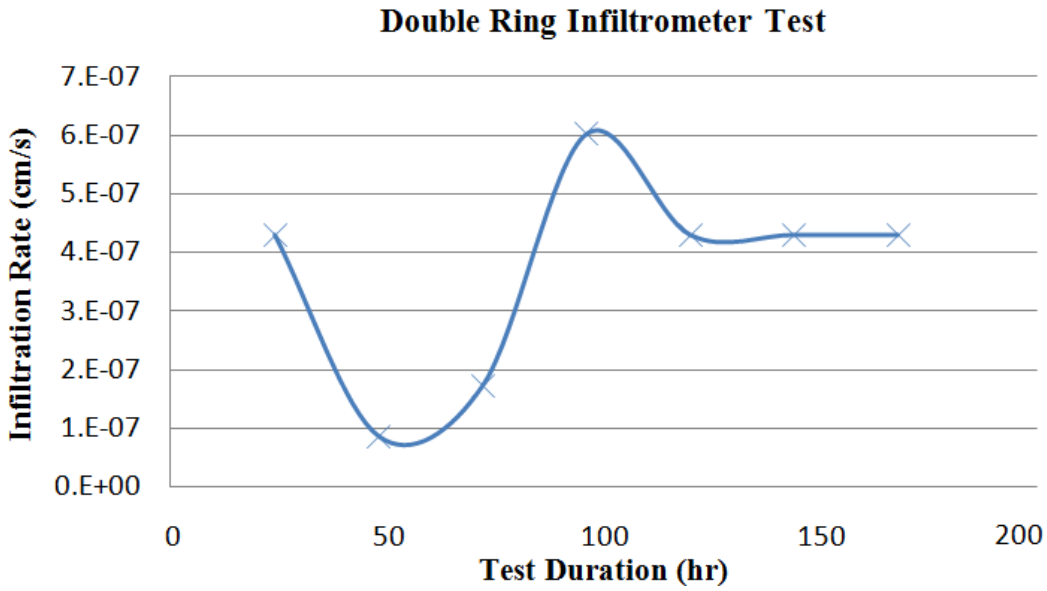

Figure 3-14: Graphical representation of clay till layer double ring infiltrometer test result

Figure 3-14 demonstrates the graphic results of the infiltrometer test. It is clear that the infiltration rate stabled out at $4.3*10^{-7}$ cm/s after around 5 days. The infiltration rate is reported as field-saturated vertical hydraulic conductivity as well.

The comparison of the falling head hydraulic conductivity test results, presented in the previous section, with the saturated permeability indicated by the infiltrometer test shows that, the laboratory value is around 80% larger than the field measurement. Also, Klohn Crippen Berger (KCB) Ltd's site investigation in "Millennium Mine Design of the South Tailings Pond" project indicates that the hydraulic conductivity of the clay till layer ranges from $1.5*10^{-6}$ cm/s to $9*10^{-4}$

cm/s with the median value of $2.4*10^{-5}$ cm/s [1]. These permeability values suggest that the falling head result ($3.1*10^{-6}$ cm/s) is in the range of the KBC value, whereas the infiltrometer results are not.

In essence, the permeability values obtained from the infiltrometer test are likely lower than the laboratory findings. It should be noted that there are several reasons for the introduction of error during the infiltrometer test besides the difficulties of field tests that would adversely affect the results.

Major potential sources of error include:

- Short circuiting of water as a consequence of side wall leakage.
- Water evaporation which could influence the water table in the gauges.
- Soil disturbance during cylinder installation.

There is also an uncertainty as to the proper evaporation and rain isolation of the cylinders and gauges for the experiment's duration (more than five days). This could have been the major contributor to the relatively erroneous test results.

3-4 Conclusions

As it is described in the introduction chapter, the objectives of this thesis have been accomplished in a number of steps. In this step the Infiltration Pond construction details, the specific underlying geology, the sampling program, as well as the field and laboratory tests were described.

The surficial geology of the study area is comprised of three major formations including muskeg, glacial till, and WCSC. Due to its low permeability, the STP was built over the glacial till. To be in harmony with it, the Infiltration Pond which serves as a small scale model of the STP was excavated approximately 2.8 m below the original ground level, 1.3 m below the glacial till layer's surface.

Prior to filling the Infiltration Pond with PA water, the first series of soil cores were collected in August 2008 at the four corners of the Infiltration Pond with the median depth of 12m. The second soil sampling program was conducted in 2010 from the Infiltration Pond bottom with an average depth of 0.7m.

The native soil characterizations underlying the constructed Infiltration Pond were determined by soil physical analysis. The following conclusions can be made from the physical tests results:

- Based upon the results of visual soil inspection and soil classification for the 2008 soil samples, two layers of very distinguishable soils were found under the Infiltration Pond bottom; Including: clay till (from 0 to 7.7 mbgl) and sand (from 9.2 mbgl).

- The Atterburg Limit results on the first soil layer, SM-SC, with 46.5% fines content revealed a higher percentage of clay content compared to the other layers. Therefore, there should be a strong possibility for PA water interaction with this layer during seepage.
- The water content of the soil cores recovered in 2010 decreases with depth and reaches the average water content of 2008 sample at approximately 0.7 mbgl.
- The 2010 samples' water content trend looks like a diffusion-dominated seepage from the Infiltration Pond bottom to approximately 0.7m below.
- The saturated permeability coefficient for the first layer of soil obtained from the falling head test is $3.1*10^{-6}$ cm/s. Based on previous laboratory and in-situ tests conducted within the vicinity of the Infiltration Pond, the falling head result is likely more reliable than the DRI.

3-5 References

(1) Klohn Crippen Consultants Ltd. Millenium Mine Design of the South Tailings Pond – Final Report. Report submitted to Suncor Energy, Inc.; November 2004.

(2) Tompkins TG. Natural Gradient Tracer Tests to Investigate the Fate and Migration of Oil Sands Process-Affected Water in the Wood Creek Sand Channel. Ontario, Canada: University of Waterloo; 2009.

(3) Schramm LL, Stasiuk EN, MacKinnon M. Surfactants in Athabasca Oil Sands Slurry Conditioning, Flotation Recovery, and tailings Processes. In: Schramm LL, editor. Surfactants, Fundamentals, and Applications in the Petroleum Industry Cambridge, UK: Cambridge University Press; 2000. p. 365-430.

(4) Starr RC, Ingleton RA. A new method for collecting core samples without a drilling rig. Ground Water Monit. Rev.; 1992; 12(1): 91-95.

(5) ASTM. American Society for Testing Materials. "Standard Practice for Description and Identification of Soils (Visual-Manual Procedure)" ASTM D2488 - 09a. Testing Standard. West Conshohocken, PA: ASTM International; 2009a.

(6) Hillel D. Fundamentals of soil physics. New York: Academic Press; 1980.

(7) Bowles JE. Engineering properties of soils and their measurement. 4th ed. New York: McGraw-Hill; 1992.

(8) Wray WK. Measuring engineering properties of soil. Englewood Cliffs, NJ: Prentice-Hall; 1986.

(9) Das BM. Principles of geotechnical engineering. 2nd ed. Boston: PWS-KENT Pub. Co.; 1990.

(10) Flint AL, Flint LE. Particle Density in Soil Science Society of America Book Series: 5 – Method of Soil Analysis: Part 4 – Physical Methods. Madison, Wisconsin: Soil Science Society of America, Inc.; 2002.

(11) Das BM. Soil mechanics laboratory manual. San Jose, Calif.: Engineering Press; 1982.

(12) Bowles JE. Engineering properties of soils and their measurement. 4th ed. New York: McGraw-Hill; 1992.

(13) Das BM. Advanced soil mechanics. 3rd ed. London ; New York: Taylor & Francis; 2008.

(14) Reynolds WD, Elrick DE, Youngs EG. Single-Ring and Double- or Concentric-Ring Infiltrometers in Soil Science Society of America Book Series: 5 – 118 Method of Soil Analysis: Part 4 – Physical Methods. Madison, Wisconsin: Soil Science Society of America, Inc.; 2002.

(15) Naujock LJ. Development of Hydraulic and Soil Properties for Soil Amendments and Native Soils for Retention Ponds in Marion County, Florida. Florida, USA: University of Central Florida; 2008.

(16) Charbeneau RJ. Groundwater Hydraulics and Pollutant Transport. Long Grove, IL: Waveland Press, Inc; 2000.

(17) ASTM. Standard Test Method for Infiltration Rate of Soils in Field Using Double-Ring Infiltrometer. Testing Standard ASTM D 3385-03. West Conshohocken, PA: ASTM International; 2003a.

(18) Hayden AH. Correlation between falling head and double ring testing for a full-scale infiltration study. Florida, USA: The Florida State University; 2010.

Chapter 4: Pore Water Geo-chemistry

4-1 Introduction

This research takes a multidisciplinary approach to comprehensively characterize the fate and transport of oil sands process affected water into the subsurface of Suncor's South Tailings Pond (STP). U of A's specific research field site, the Infiltration Pond, served as a small scale of STP to investigate the process-affected (PA) water migration into the subsurface. The first goal (discussed in Chapter 3) focused on characterizing the physical properties of soil layers underlying the Infiltration pond.

The second goal, and the focus of this chapter, is to geo-chemically evaluate the PA water seepage.

The impact of PA water migration on the underlying pore water was investigated through isotopic and inorganic geo-chemistry analysis on the pore water of soil samples underlying the Infiltration Pond at two time points: (i) prior to filling with PA water (Aug. 2008) and (ii) two years after filling (Jul. 2010). Pore water was analyzed for the composition of isotopes (δ^2H and $\delta^{18}O$), pH, alkalinity, electric conductivity, heavy metals, cations and anions. Initial soil pore water chemistry was defined by the 2008 analysis. Any changes in the pore water isotopic composition and chemistry at different depths underlying the pond and over time would indicate PA water seepage.

The results of soil physical properties measured in Chapter 3 enhance our understanding of PA water transport and allow us to interpret the behavior of dissolved heavy metals and major ions. Soil is a "chemically active" component that should be considered in contaminant fate investigations [1-3]. Soils,

particularly clay particles, do not react the same as purified porous media [1-3]. There are several complicated processes, physical, chemical and biological, which may govern the fate and transport of PA water in a clay till.

Movement of dissolved inorganic compounds (heavy metals and major ions) in soil is mainly regulated by adsorption, precipitation and ion exchange reactions. In the case of ion exchange reactions, the ions adsorbed on the surface of clay can be replaced by other dissolved ions in the solution. Therefore, due to the high ion exchange capacity of clay soils, it is hypothesised that adsorption and desorption of ions from the clay particles will be foremost factors controlling and leading changes in pore water chemistry [4]. Furthermore, by the adsorption reactions, the adsorbed solute on the soil is retained from moving and as a result, its transportation is slower than the velocity of seepage flow. Pore water chemistry properties including pH, redox potential and ionic strength have a critical role in the partitioning of ions and heavy metals between pore water and soil surface and accordingly the metals and ions availability and toxicity [4].

For simplicity the investigation of PA water mobility through the clay till was conducted by creating profiles of pore water major ions and heavy metals as a function of depth for 2008 (time zero/ background) and 2010 soil cores underlying the Infiltration Pond. This comparison provided a better understanding of changes in pore water chemistry and the processes governing the fate and progress of inorganic compounds of PA water into the clay till.

4-2 Materials and Methods

4-2-1 Pore water extraction

Pore water was extracted from the soil cores at the U of A geo-chemistry lab using a centrifuge technique. This technique proved to be the most suitable, as compared to other methods such as mechanical squeezing with a hydraulic press [5-7] or vacuum filtration [8], due to the simplicity and capacity to seal the samples from an aerobic atmosphere. The centrifuge technique is a commonly used method in environmental geotechnics research (e.g., [9-11])

All phases of sample preparation such as defrosting soil cores, filling and balancing the centrifuge tubes were conducted in an anaerobic chamber (Figure 4-1) to prevent oxidation of ions and heavy metals. The chamber was filled by gas mix with the composition of N_2: CO_2: H_2 (80: 10: 10). Maintenance of the anaerobic environment is crucial to simulating the field conditions.

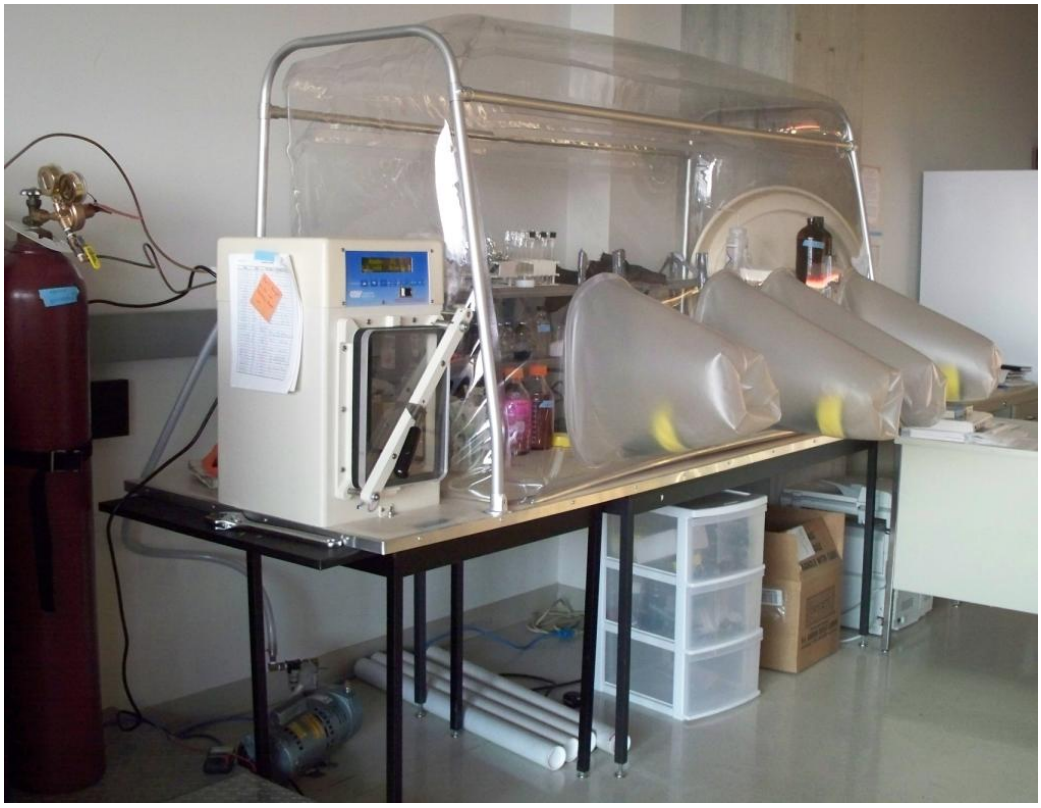

Figure 4-1: Anaerobic chamber to isolate the soil samples from an aerobic atmosphere.

All centrifugations were performed in a Sorvall PC-5B refrigerated superspeed centrifuge. Due to the limited core samples acquired from the clay till and the need to extract enough pore water for subsequent geo-chemistry analysis, the centrifuge speed and duration for each sample were designed based on a trial and error approach. Indeed, speed and duration of centrifuge were dictated by the water contents of soil samples. As discussed in section 3-3-5 higher water contents were observed in the soil samples from the top of the cores and lower water content belonged to deeper soil samples. An extraction time of 10 minutes with 10,000 rotations per minute (rpm) was used for the wetter top samples (with

the maximum water content of 22.4%) and in the case of dryer samples (with the minimum water content of 13.6%) 20 minutes duration with 15,000 rpm.

As a note, all frozen cores were sectioned into 15 to 20 cm lengths (described in Section 3-2-1). To make data plots easier to read, the extracted pore water results were reported for the average depth of each section.

4-2-2 Isotopic Analysis

^{18}O and ^{2}H composition in different water bodies are reported relative to a global standard, the Vienna Standard Mean Ocean Water (VSMOW). Equation 4-1 is used to compute a particular water body relative ^{18}O isotope ratio to VSMOW [12].

$$\delta^{18}O = \left(\frac{(\frac{^{18}O}{^{16}O})_{Sample}}{(\frac{^{18}O}{^{16}O})_{VSMOW}} - 1 \right) \times 1000 \qquad (‰) \qquad \textbf{Equation 4-1}$$

It has been discovered that, on a global scale there is a linear correlation between $\delta^{2}H$ and $\delta^{18}O$ in fresh waters which is termed the "Global Meteoric Water Line" (GMWL) [13-15]. On the other hand, Local Meteoric Water Line (LMWL) is developed for a more local description of the GMWL in different areas.

The water bodies analysed for this project include: 1) PA water sampled in 2008 and 2010, 2) soil pore water samples taken in 2008 and 2010, 3) regional ground water of WCSC, under the infiltration pond, and 4) Athabasca River water and were differentiated based on their unique isotopic signatures.

To characterize the PA water migration through the clay till layer underlying the Infiltration pond, a comparison of the unique isotopic signatures can identify the infiltration depth. In this study, isotopic composition of ^{18}O was used as an indicator to track the progress of the water molecule from the PA water in the Infiltration pond to the underlying soil layers.

Falcone [14] isotopic values for Athabasca River water were used as the Athabasca River water isotopic signature. Local meteoric water line (LMWL) was obtained from Wolfe et al. [16]. Isotope compositions of the PA water and pore water samples collected from the Infiltration Pond and groundwater samples taken from monitoring wells in the WCSC within the vicinity of the Infiltration Pond, were measured by "Alberta Innovates Technology Futures" in Calgary, AB. CO_2 equilibration and chromium reduction techniques were used to analyze oxygen and hydrogen isotopes, respectively. Vienna Standard Mean Ocean Water (VSMOW) was used as the reference standard for $\delta^{18}O$ and $\delta^{2}H$ in the water. Furthermore, to ensure the consistency of both samples and standard ratios, a dual inlet mass spectrometer was used.

4-2-3 pH

To better track the ions fate, an accumet® AB15 Fisher Scientific pH meter which calibrated with pH 4, 7, and 10 standard solutions was used to measure PA water and soil samples pore water.

4-2-4 Electrical conductivity

Electric current can be carried by dissolved ions in a solution. Indeed, the total amount of dissolved ions/salts (TDS) dictates the ability of a solution to conduct electricity and is termed the Electrical Conductivity (EC). A higher TDS correlates to a higher EC. In other words, EC could be used as an indicator to estimate the amount of TDS in different samples. The EC values of all samples were measured using a Thermo Orion model 130A calibrated with standard solution at 5000 and 1000 µS/cm at 25ºC.

4-2-5 Alkalinity

The waste water of some industrial activities, salts, soils, rocks are the sources of the alkalinity in water bodies, which is the neutralizing acids in the solutions. Bromcresol green/ methyl red indicator with a 0.16 N sulphuric acid Hatch digital titrator was used to measure the alkalinity of the PA water and pore water samples extracted from soil cores.

4-2-6 Heavy Metals

Heavy metals concentrations in the pore water samples were measured using a highly sensitive Inductively Coupled Plasma-Mass Spectrometry (ICP-MS) instrument named PerkinElmer SCIEX, ELAN 9000. Calibration solutions were prepared using two standard solutions including: 1) PerkinElmer Pure Plu, USA (multi-element standard) and 2) SPEXcertiPrep, USA (Mo solution). PA water and pore water extracted from soil samples were filtered using Fisherbrand PTFE

0.22µm syringe filters and the internal standard (45Sc, 89Y, 159Tb at 100 µg l-1, VHG LABS, Manchester) was added to all samples. A rinse, a standard solution, a multi-element spiked sample as well as a duplicated sample were designed to run after each 20 sample run for quality assurance and control.

4-2-7 Major Ions and Cations

Fisherbrand PTFE 0.45µm filters were used to syringe filter extracted pore water from the soil samples. The filtered pore water samples were analyzed for cations and anions using Ion Chromatography (IC). In the case of anions, Dionex 2500 equipped with IonPac® AS14A (4X250mm) column with highly pure (>99%) methanosulfonic acid effluent was adopted. Major cations were measured using a Dionex ICS-2000 with an IonPac® CS12A (4X250mm) column and 8 mM sodium carbonate and 1 mM sodium bicarbonate as the eluent. For both anions and cations analysis the designed flow rate was 1 mL/min.

Profiles of the six most abundant major ions in PA water and pore water for 2008 and 2010 soil samples is evaluated in the results section.

4-3 Results and Discussion

Soil samples averaging 10 cm in length roughly yielded 10 mL of pore water through the centrifugation technique. These samples were then analyzed for isotopic composition and inorganic geochemistry.

4-3-1 Isotopic Analysis

^{2}H, and ^{18}O and ^{17}O are stable isotopes of hydrogen and oxygen that naturally occur in water molecules in addition to ^{1}H and ^{16}O. Over the past 50 years, mass-dependent partitioning of stable isotopes (unique isotopic signatures) of water was used by several researchers in hydrogeology studies as tracers [14,17-22]. Conservative properties of these isotopes when they interact with soils below $50^{o}C$ help to track the depletion or enrichment of a specific body of water during its seepage [23,24].

The results of isotopic analysis on $\delta^{18}O$ and $\delta^{2}H$ indicate that Athabasca River water, 2008 and 2010 PA water, pore water of 2008 and 2010 soil samples, as well as groundwater in the study area are isotopically distinct. $\delta^{18}O$ versus $\delta^{2}H$ plots for different water samples, lakes in that area and LMWL are provided in Figure 4-2.

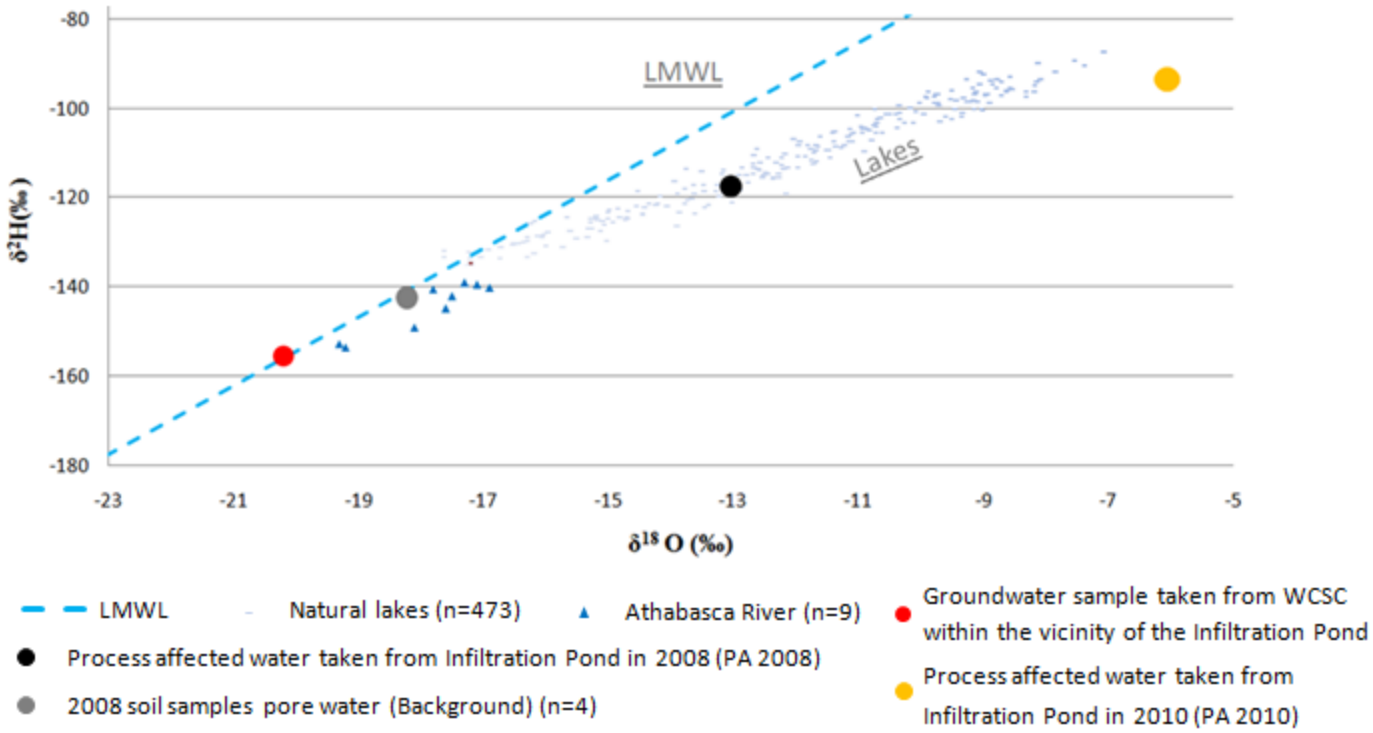

Figure 4-2: Stable water isotope compositions of various water bodies relative to the local meteoric water line (LMWL) [16]; n indicates the number of samples.

As Figure 4-2 shows, groundwater and background (2008 soil samples pore water) data lie along the LMWL of the study area. As it is expected, data from Athabasca River water samples, lakes, and PA from 2008 and 2010 do not plot on the LMWL. Due to evaporation in the Athabasca River water samples, data show enriched values of $\delta^{18}O$ and $\delta^{2}H$. It is to be noted that, Suncor uses Athabasca River water and recycled PA water for oil sands extraction processes.

For the PA 2008 and PA 2010 water samples, the deviations from the LMWL indicate isotopic enrichment due to evaporation. PA water originally starts as Athabasca River water, which undergoes evaporative enrichment during steam generation for oil sands extraction processes and atmospheric exposure after its placement in tailings ponds. Furthermore, PA water evaporation from the Infiltration Pond over a two year time period (August 2008 to July 2010) underwent more enrichment through evaporation. Isotope analysis of PA water samples indicates that they are distinct from other bodies of water in the area. This property of PA water could be used to identify and trace its migration.

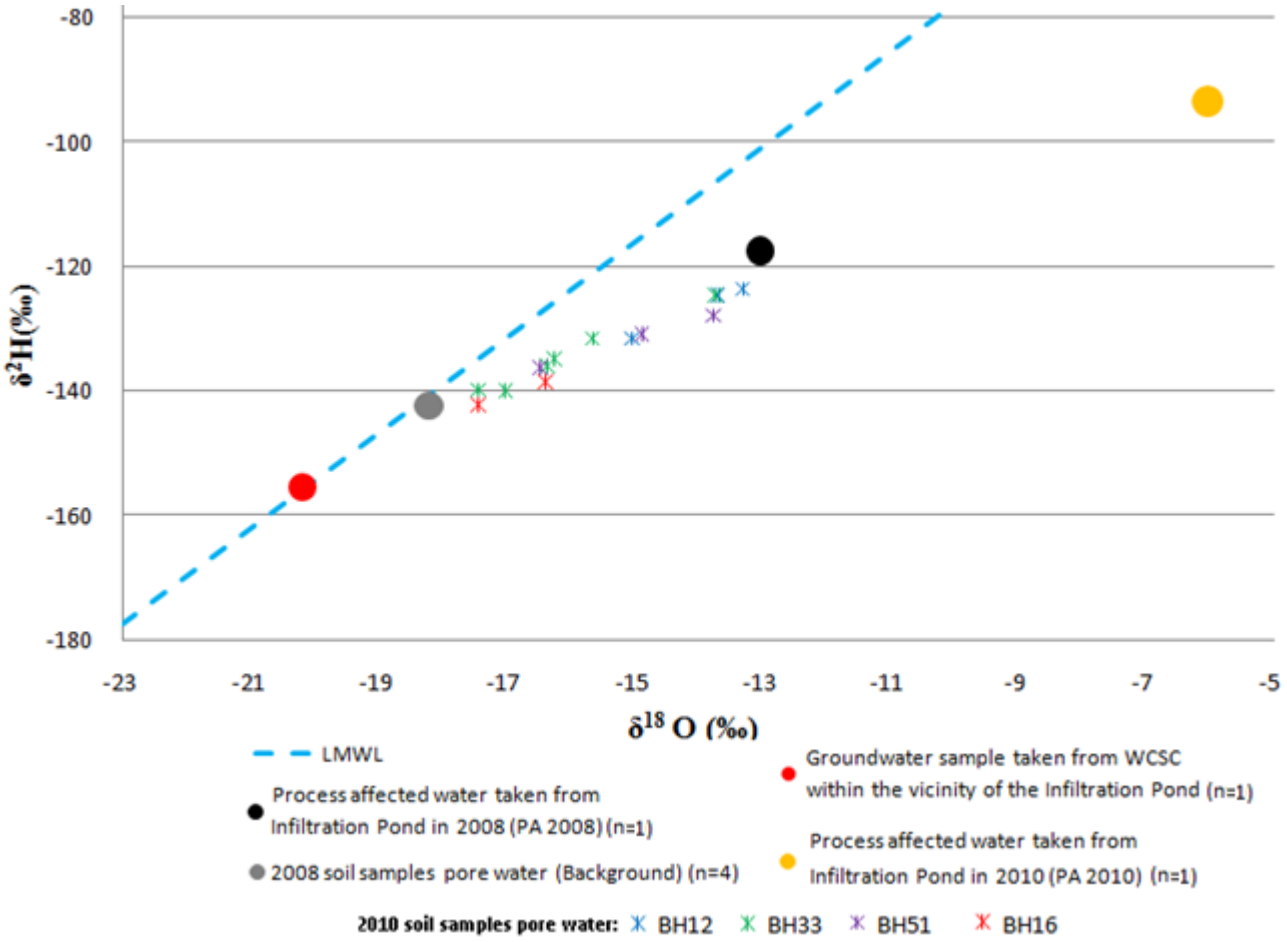

Figure 4-3: Stable water isotope compositions of various water bodies relative to the local meteoric water line (LMWL) [16]; n indicates the number of samples.

As provided in Figure 4-3, $\delta^{18}O$ vs. $\delta^{2}H$ isotopic analysis results for 2010 soil samples fall within the range of PA 2008 and the background data. The enriched values of $\delta^{18}O$ and $\delta^{2}H$ in pore water of 2010 soil samples in comparison to the background samples could be interpreted as the mixture of the background pore water with PA 2008 during its infiltration through the clay till. In other words, PA water infiltration through clay till would cause enrichment of heavier isotopes in pore water, which subsequently can be used as a conservative tracer for PA water migration. Profiles of $\delta^{18}O$ versus depth for 2010 soil samples were plotted in Figure 4-4. Recall from Chapter 3, to simplify the process of comparing the physical and geo-chemical analysis results, the bottom of the Infiltration Pond is acting as the ground level (0 mbgl).

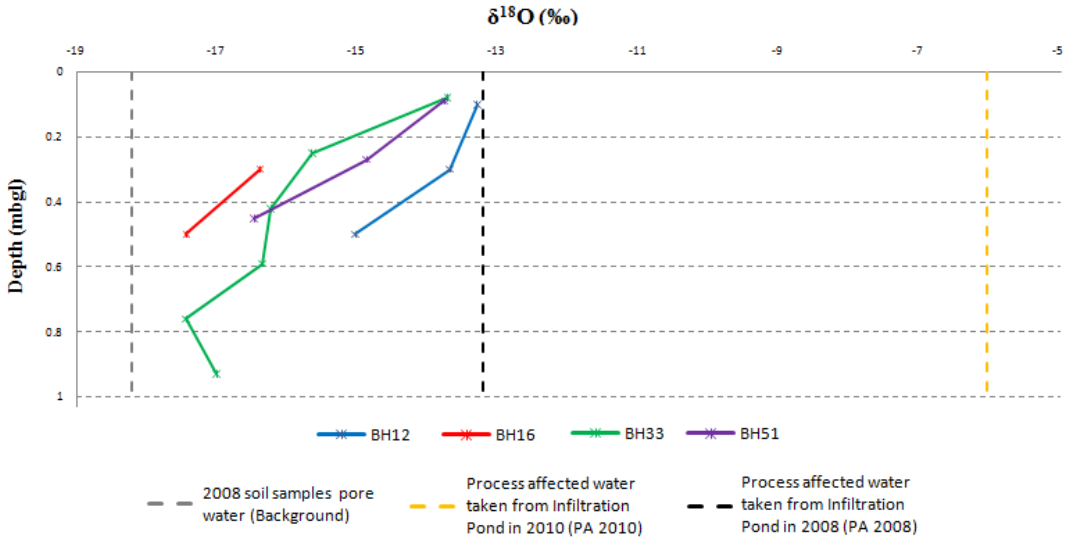

Figure 4-4: $\delta^{18}O$ profiles versus depth for 2010 pore water soil samples (BHs 12, 16, 33, and 51). Average values of Background, PA 2010 and PA 2008 samples are shown in vertical dotted lines to make the comparison easier.

The average values of $\delta^{18}O$ for the background pore water soil samples (0-1 mbgl), PA 2008 and PA 2010 are plotted on Figure 4-4. As it is clear from the figure above, the levels of $\delta^{18}O$ in PA 2008 and to a higher extent in PA 2010 are greater than background levels. $\delta^{18}O$ values of all 2010 soil samples are greater than background levels. Higher $\delta^{18}O$ values than background, indicate that soil pore water has mixed with another water source enriched in heavier isotopes (PA water) during the two years. The isotopes show a similar pattern versus depth, which resembles a typical diffusion profile. The $\delta^{18}O$ values are higher near the top, close to the Infiltration Pond bottom, and gradually show more negative isotope values with depth approaching the average background value of $\delta^{18}O$ (-18.2 ‰). Gradual decrease of $\delta^{18}O$ values versus depth, with no evidence of an advective front, implies that diffusion was the dominant PA water migration process between August 2008 and July 2010. Furthermore, 2010 soil trends in Figure 4-4 reveal that PA water diffused to approximately 1m below the Infiltration Pond bottom. It is to be noted that both infiltration depth and $\delta^{18}O$ trends of 2010 soil samples are in agreement with the findings of water content versus depth discussed in section 3-3-5.

4-3-2 pH

PA 2008 water samples had a pH of 8.48, which is in the range of typical pH of PA water [25]. On the other hand, PA 2010 water samples had a pH of 7.32. The lower pH of the PA water from 2010 is due to the dilution of Infiltration Pond water by rain fall and melt-water discharged into the Infiltration pond from September 2008 to July 2010.

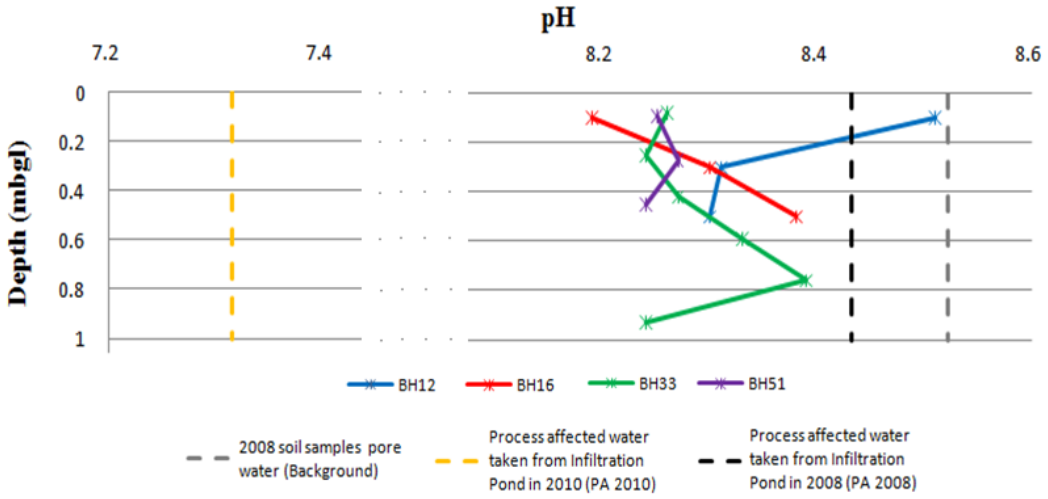

Figure 4-5: pH values of 2010 pore water soil samples (BHs 12, 16, 33, and 51) versus depth as they compare to PA 2008 and 2010 values and background. Average values of Background, PA 2010 and PA 2008 samples are shown in vertical dotted lines to make the comparison easier.

Figure 4-5 illustrates the pH of 2010 pore water soil samples versus depth and the average pH values of background, PA 2008 and 2010 samples. The average pH of 2008 and 2010 pore water soil samples was measured at 8.52 (depth of 0-1 mbgl) and 8.30 (depth of 0-1 mbgl), respectively. From Figure 4-5, pH of 2010 pore water soil samples remains relatively unchanged with depth, with the exception of BH12 at the depth range of 0-0.2 mbgl. A visual inspection of this sample shows

that it was the only soil core with a sand lens which covered around 60% of the core length providing a preferential flow path for PA water.

All 2010 soil samples show lower pH in comparison to background and PA 2008 samples with no discernable trend. More details on pH of PA water and soil samples at different depths may be found in Appendix B.

Typically, the pH of soil pore water ranges from 4 to 7 and 7 to 9 in humid and arid regions, respectively [26,27]. Based upon this, the clay till soil samples both in 2008 and 2010 are in the category of arid soils (pH range of 7-9). The pore water pH is also subject to change due to infiltration of anthropogenic sources such as industrial waste water. Numerous studies were conducted on the effect of the soil solution pH and heavy metals and ions sorption on soils such as McBride et al., Gray et al., and Sauve et al. [26,28-30]. These studies state that pH is the most important factor affecting ions sorption. Higher pH of the soil solution results in an increase in the amount of hydroxyl complexes of cations and higher adsorption of metals on soil surfaces accordingly [31,32]. In case of the ion exchange property of clay soils, higher electrostatic surface charges of minerals due to higher pH of the soil solution can lead to higher adsorption of ions. Based on this knowledge and the pore water samples pH (> 8), high ion exchange and adsorption interactions between PA water and clay till layer are expected.

4-3-3 Electrical Conductivity

The values of electric conductivity of PA water and pore water of soil samples versus depth are graphically shown in Figure 4-6. PA water sampled in 2008 with an EC of 2.67 mS/cm at 25ºC has the highest value, which shows the high value of TDS in the process affected water. The average background EC for the 2008 pore water soil samples in the range of 0 to 1 mbgl, obtained 0.50 mS/cm. As it is interpreted from Figure 4-6, all four 2010 soil samples show a similar pattern, which resembles the $\delta^{18}O$ pattern shown in Figure 4-4. The EC is highest near the top, close to the Infiltration Pond bottom, and decreases with depth to the average EC of 2008 samples (indicated in gray dotted line in Figure 4-6). BH33, the longest core, shows EC values for 2010 samples reached the background average EC at approximately 0.8 mbgl (Figure 4-6). Dilution of PA water with rain and melt-water during the two year study corresponds to the lowest EC reading for the 2010 Infiltration pond water sample (PA 2010).

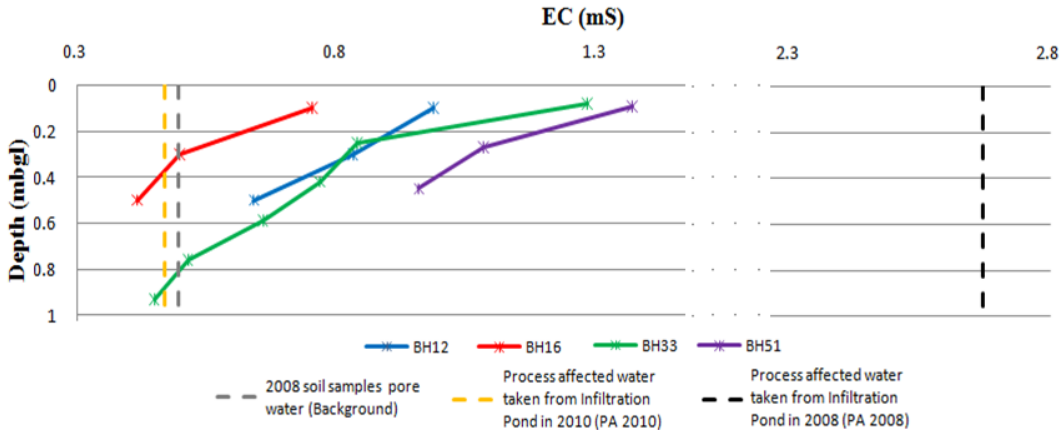

Figure 4-6: EC values of 2010 pore water soil samples (BHs 12, 16, 33, and 51) versus depth as they compare to PA water samples collected in 2008 and 2010 and 2008 background pore water soil samples. Average values of Background, PA 2010 and PA 2008 samples are shown in vertical dotted lines to make the comparison easier.

4-3-4 Alkalinity

The alkalinity of PA 2008 was measured around 530 mg/L $CaCO_3$. While the average alkalinity of 2010 soil samples was 172 mg/l $CaCO_3$. Alkalinity trends for the 2010 soil samples versus depth show the highest alkalinity at the top and gradually decrease with depth and reach the background soil alkalinity at approximately 0.4 mbgl (Figure 4-7). A comparison between the alkalinity and $\delta^{18}O$ trends of 2010 soil samples reveals that the alkalinity of pore water is highly affected by chemical reactions, especially ion exchange reactions, during PA water infiltration through clay till layer. As a result the alkalinity of pore water cannot be used as an indicator for PA water seepage.

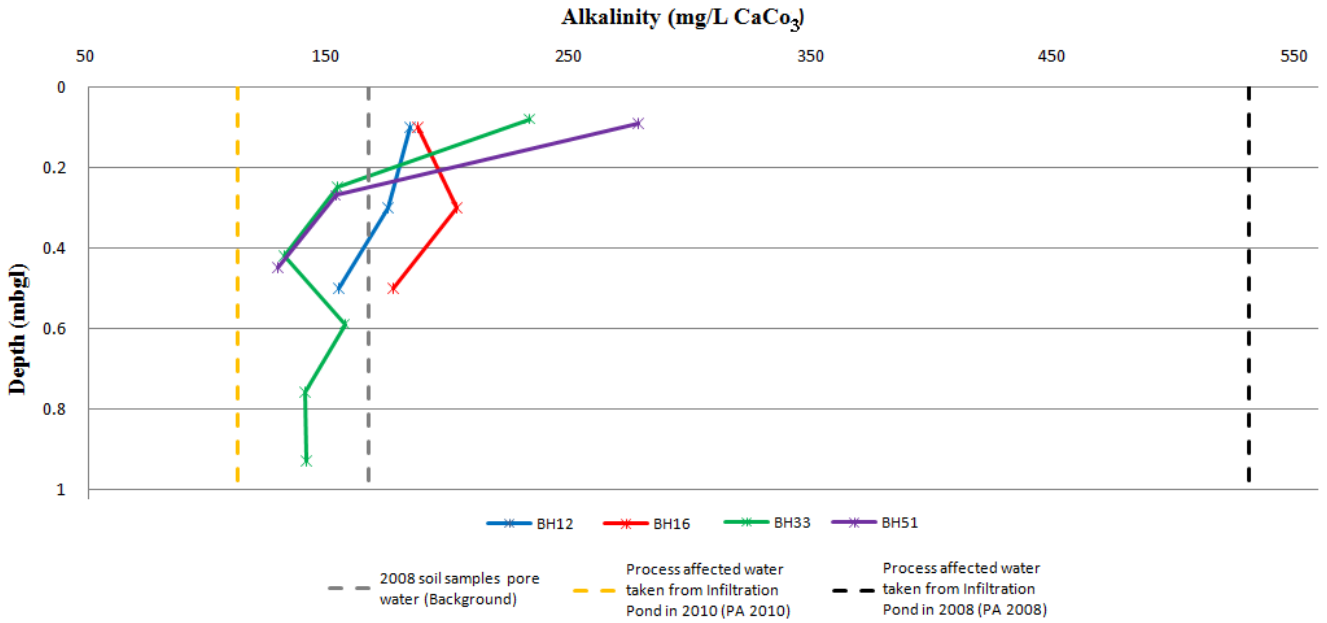

Figure 4-7: Alkalinity values of 2010 pore water soil samples (BHs 12, 16, 33, and 51) versus depth as they compare to PA 2008 and 2010 values and background. Average values of Background, PA 2010 and PA 2008 samples are shown in vertical dotted lines to make the comparison easier.

4-3-5 Heavy Metals

Based on ICP-MS results for 2008 and 2010 PA and pore water soil samples, concentration levels are low and results of analyses are provided in units of µg/L. Mo, Sr, Ba, Pb, Mn and Ni, ordered from most to least abundant dissolved heavy metals, were detected in PA 2008. U and Zn are two trace elements that were not detected in PA 2008, but were observed in pore water of background and 2010 soil samples.

A previous study by Smedley et al. [33] states that, due to high adsorption properties of clay till, small quantities of heavy metals (µg/L) observed in typical PA waters could not pose a risk to the environment.

The measured concentration of Mo in PA 2008 was around 17 times higher than the background level of Mo. While ICP-MS results show the concentration of Mo in the pore water of 2010 soil samples is close to background levels (Figure 4-8 a) and soil cores produce significant scatter with no discernable pattern. Due to the large difference in Mo levels observed in PA 2008 and 2010 soil samples, Mo may have been dramatically influenced by attenuation processes such as adsorption and precipitation activities during PA water diffusion. Holden et al.'s [34] studies on the clay till in the South Tailings Pond area, using radial diffusion cells, confirm Mo mitigation (uptake) by clay till particles during PA water diffusion.

Likewise, the measured Pb concentration in PA 2008 is much higher than the background level. Three of four 2010 soil cores show higher concentrations at the top, while two of these cores (BHs 12 and 51) rapidly decrease with depth to the

background level at approximately 0.5 mbgl (Figure 4-8 b). Attenuation processes such as precipitation, reduction and to a greater extent adsorption could play a big role in the fate of dissolved Pb during PA water diffusion. In contrast, radial diffusion cell tests conducted by Holden et al. [34] on the same clay till reveals Pb release from clay till particles during PA water diffusion.

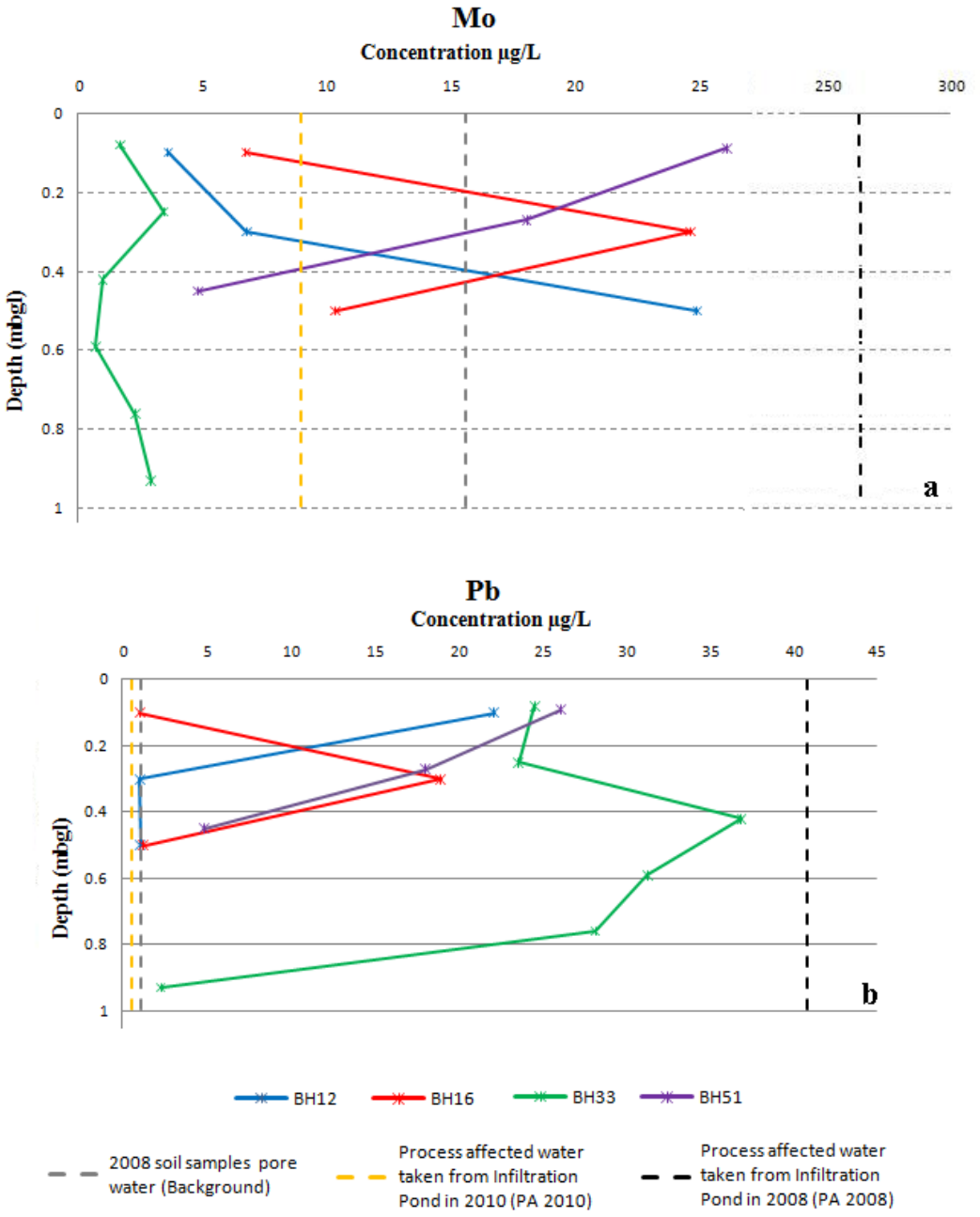

Figure 4-8: Dissolved heavy metals concentrations of 2010 pore water soil samples (BHs 12, 16, 33, and 51) versus depth as they compare to PA 2008 and 2010 values and background. Average values of Background, PA 2010 and PA 2008 samples are shown in vertical dotted lines to make the comparison easier. a) Mo; b) Pb.

PA 2008 and background soil pore water show relatively the same levels of dissolved Mn (39 and 25 µg/L respectively). With the exemption of BH12 and samples BH51-1 (0-0.18 mbgl) and BH33-6 (0.86-1.04 mbgl), all other 2010 soil samples show the same Mn level as background and PA 2008. Furthermore, 2010 soil samples produce significant scatter with no specific trend (Figure 4-9 a).

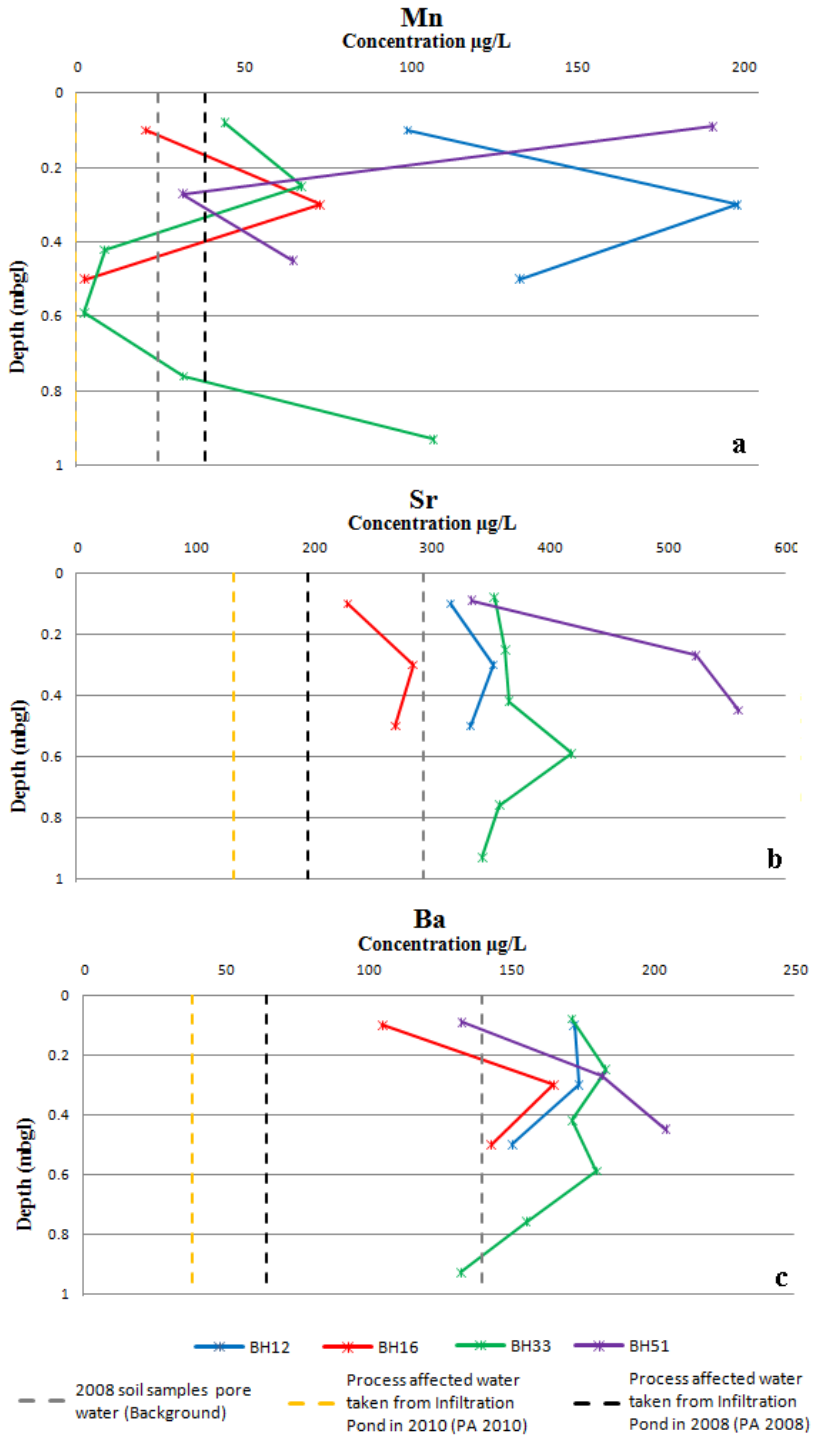

Figure 4-9: Dissolved heavy metals concentrations of 2010 pore water soil samples (BHs 12, 16, 33, and 51) versus depth as they compare to PA 2008 and 2010 values and background. Average values of Background, PA 2010 and PA 2008 samples are shown in vertical dotted lines to make the comparison easier. a) Mn; b) Sr; c) Ba.

Measured concentrations of Ba and Sr in PA 2008 are lower than their background levels. The background concentrations of Ba and Sr are respectively around 1.5 and 2 times higher than PA 2008. However, higher concentrations of Ba and Sr are observed in the majority of 2010 soil samples as shown in Figures 4-9 b and 4-9 c. Using radial diffusion cell tests, Holden et al. 2010 stated Ba and Sr release from clay till particles during PA water diffusion [34]. Accordingly, increase in the concentration of these two trace metals in the pore water of 2010 soil samples can be attributed to the release of them from the clay content after PA 2008 seepage through clay till.

Although Zn is not detected in PA 2008, notable concentrations (227 µg/l) of Zn were measured in the pore water of background soil samples. Zn concentration in 2010 soil samples ranged from around 0 to 170 µg/l. The average concentration of Zn in 2010 soil samples is lower than background level. Dilution of pore water by PA 2008 seepage through the soil layer could be the reason behind the lower Zn detected in 2010 soil samples. Zn trends in BHs 16 and 51 indicate a gradual increase with depth and in the case of BH 33 up to BH33-3 (0.34-0.52 mbgl) it also follows the same pattern. These patterns indicate dilution of pore water by PA 2008. It is to be noted that the highest level of Zn in 2010 soil samples is detected at approximately 0.6 mbgl (Figure 4-10).

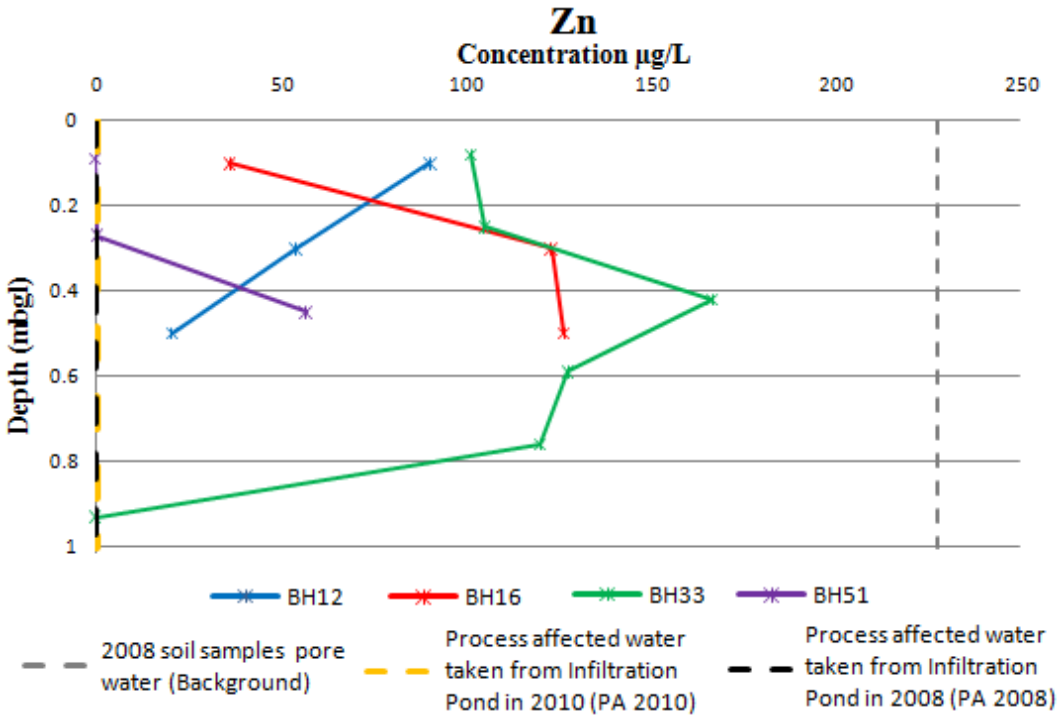

Figure 4-10: Dissolved Zn concentrations of 2010 pore water soil samples (BHs 12, 16, 33, and 51) versus depth as they compare to PA 2008 and 2010 values and background. Average values of Background, PA 2010 and PA 2008 samples are shown in vertical dotted lines to make the comparison easier.

4-3-6 Major Ions and Cations

Based on IC test results for PA 2008, the six most abundant species of ions detected are sodium, chloride, sulphate, potassium, magnesium and calcium (ordered from most to least abundant as well). On the other hand, the concentrations of ammonium, nitrate, nitrite and fluoride are low (<1 mg/L) both in PA water and soil samples. The profiles of these ions were created for 2008 and 2010 soil and PA water samples and are presented in groups as cations and anions:

4-3-6-1 Cations

The measured concentration of calcium in PA 2008 and background soil pore water are 7.639 mg/L and 54.013 mg/L respectively, while in 2010 the pore water for the very top soil cores is roughly 95 mg/L. As shown in Figure 4-11 a, the concentration of calcium slightly decreases with depth. Comparably, magnesium profiles (Figure 4-11 b) show roughly the same trend as calcium. Likewise calcium, dissolved magnesium quantities in 2010 soil samples pore water is much higher than PA 2008.

Higher concentrations of dissolved calcium and magnesium in 2010 soil samples in comparison to PA 2008 and background levels reveal that these components may be released from clay particles to the pore water during the PA water infiltration. It does not give a clear indication of the change in the status of each ion on the exchange complex. However, it matches laboratory batch adsorption test findings by Holden, et al. [35].

In contrast, the concentration of dissolved sodium in PA 2008 is around 16 times higher than its concentration in background samples. Moreover, sodium concentration for the top cores of 2010 soil samples is around one fourth of PA 2008. This high difference reveals sodium uptake by the clay particles in this soil layer during PA water infiltration. As Figure 4-11 c presents, the sodium concentration decreased rapidly with depth and reached the assumed background concentration at approximately 0.4 mbgl.

These observations indicate that sodium in the PA water replaces exchangeable magnesium and calcium on clay particle surfaces. Therefore, exchangeable calcium and magnesium greatly increased in the pore water up to 80% and 40% of initial concentration, respectively. Consequently, sodium diffusion was impacted by cation competition. Apparently, high amounts of sodium adsorbed reflects the high cation exchange capacity of the clay fraction of soil. These results are in agreement with previous batch sorption study conducted by Holden et al. [35] on the clay till samples within the vicinity of Infiltration Pond.

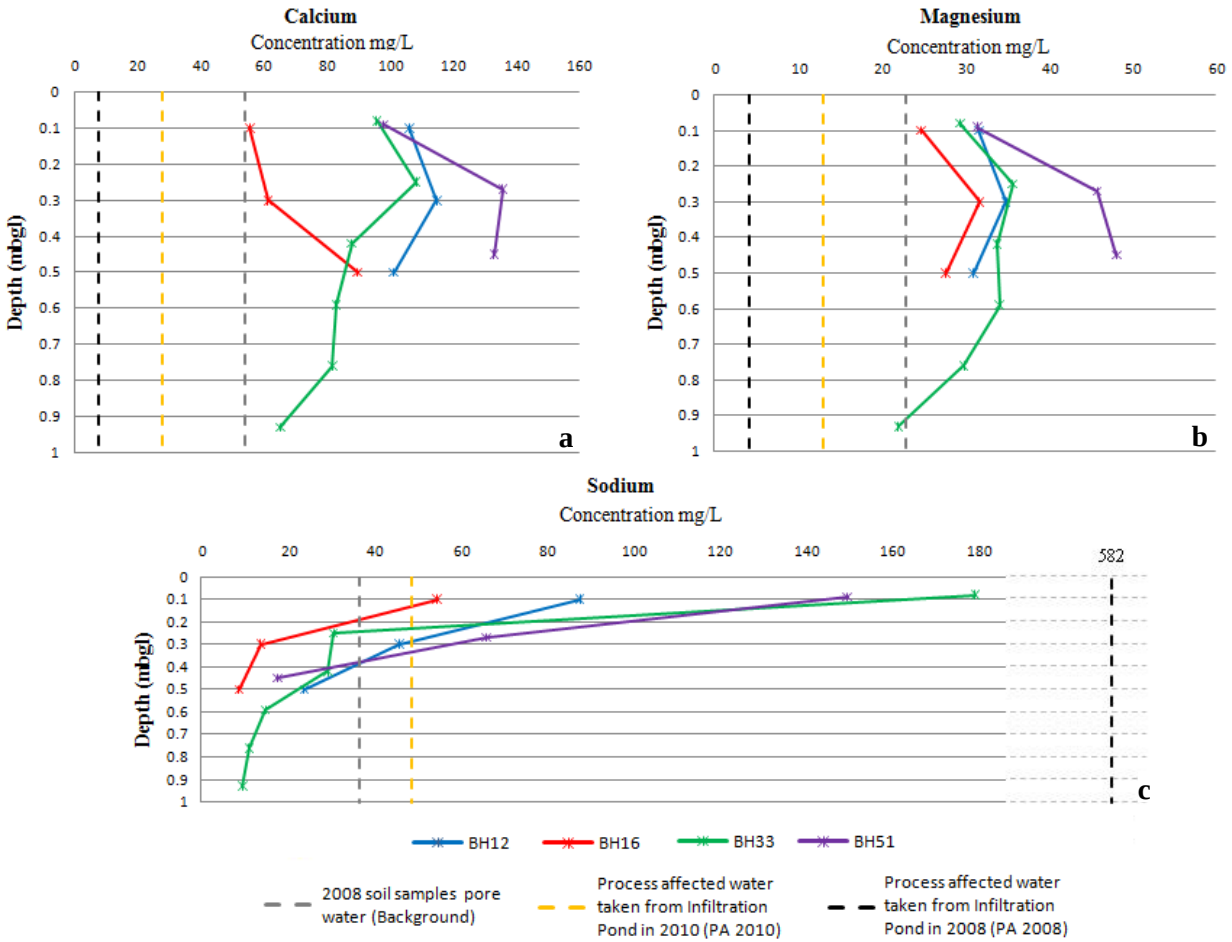

Figure 4-11: Dissolved cations concentrations of 2010 pore water soil samples (BHs 12, 16, 33, and 51) versus depth as they compare to PA 2008 and 2010 values and background. Average values of Background, PA 2010 and PA 2008 samples are shown in vertical dotted lines to make the comparison easier. a) Calcium; b) Magnesium; c) Sodium.

Measured potassium concentrations for all 2010 pore water soil samples were lower than background soil pore water and PA 2008. Figure 4-12 shows that potassium concentrations of 2010 soil samples remain relatively unchanged with depth indicating that it is likely not involved in any exchange reactions.

It is to be noted that odd cation patterns obtained from BH16 which is not consistent with the other three boreholes could be due to the sand lens observed in BH16-1 (0-0.2 mbgl) which occupied around 60% of its volume (see Section 3-3-1).

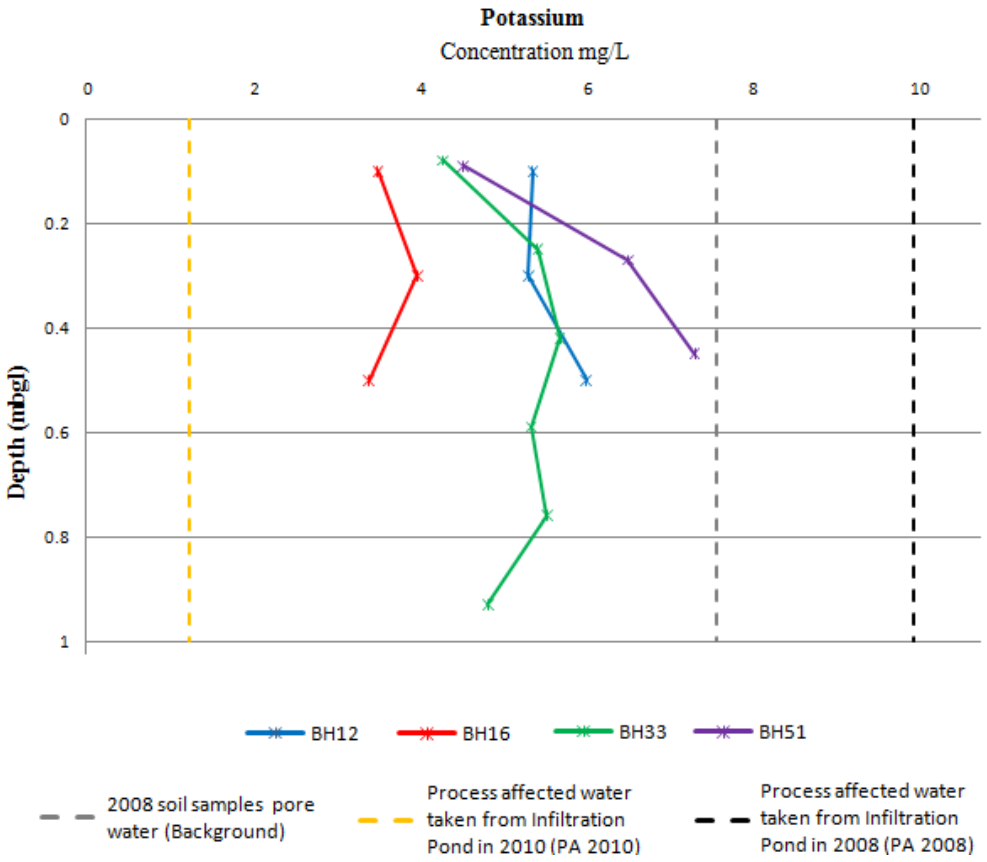

Figure 4-12: Dissolved Potassium concentrations of 2010 pore water soil samples (BHs 12, 16, 33, and 51) versus depth as they compare to PA 2008 and 2010 values and background. Average values of Background, PA 2010 and PA 2008 samples are shown in vertical dotted lines to make the comparison easier.

4-3-6-2 Anions

Of the anions analysed, chloride is the dominant species in PA water. The dissolved chloride concentration in PA 2008 measured around 386 mg/L, which makes it the second most abundant ion after sodium in PA water. The chloride concentration of 2010 pore water soil samples ranged from 20 to 190 mg/L. As illustrated in Figure 4-13, 2010 soil samples show higher concentrations at the top of the cores (an order of magnitude higher than background concentration) and gradually decrease with depth. The chloride concentration of BH33, the longest retrieved soil core, shows that at approximately 0.9 mbgl it reaches the assumed background level of chloride. Chloride follows the same pattern as the stable isotopes shown in Figure 4-4, which resembles a typical diffusion profile. This consistency was expected and also proves the conservative behaviour of chloride diffusing through the clay till.

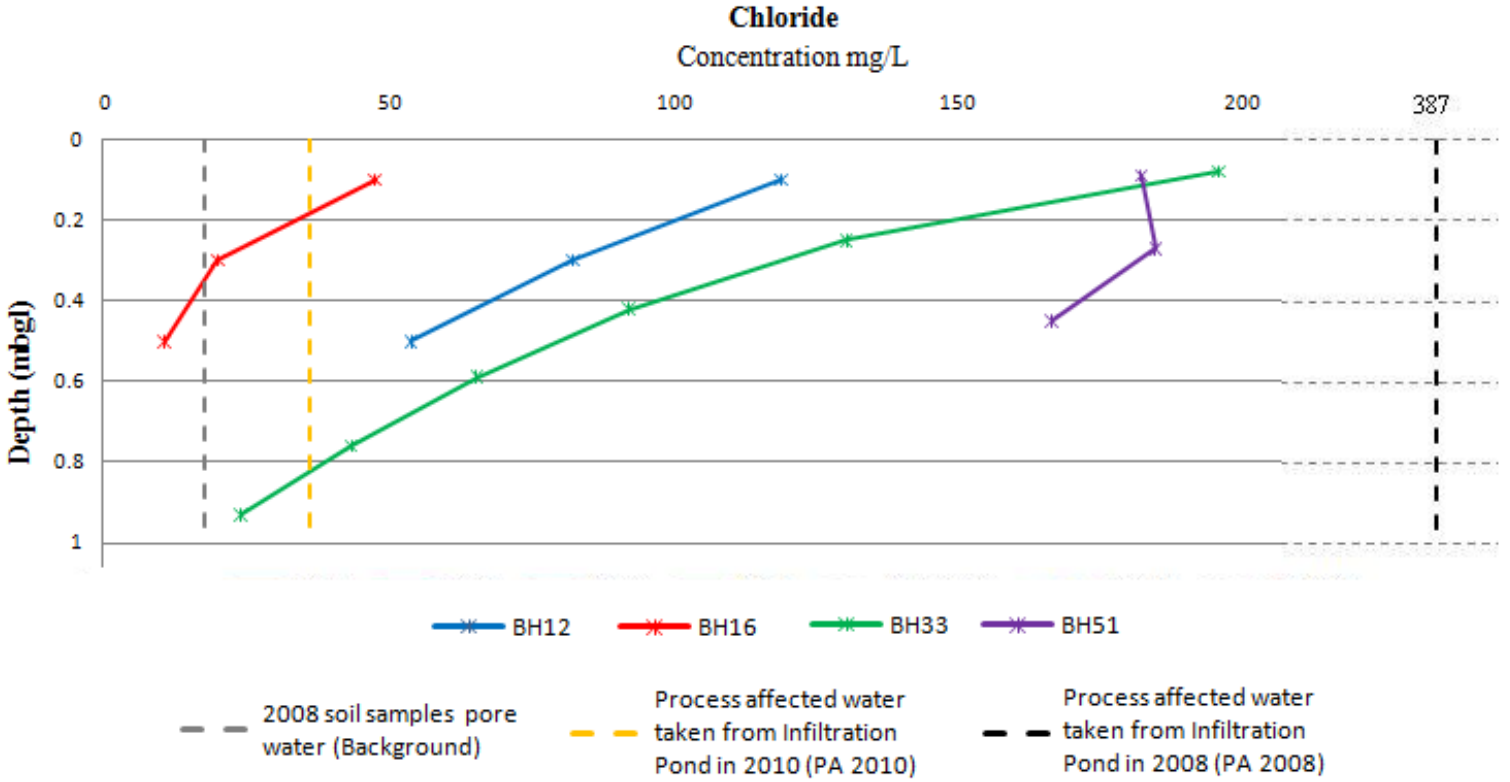

Figure 4-13: Dissolved Chloride concentrations of 2010 pore water soil samples (BHs 12, 16, 33, and 51) versus depth as they compare to PA 2008 and 2010 values and background. Average values of Background, PA 2010 and PA 2008 samples are shown in vertical dotted lines to make the comparison easier.

Sulphate concentration in the PA 2008 sample was measured around 150 mg/L and the sulphate concentration of 2010 pore water soil samples ranged from around 22 (very bottom of soil core) to 140 mg/L (very top of soil core). In comparison to the background level of sulphate, 2010 soil cores had triple the sulphate content at the top and rapidly decreased with depth and subsequently reached background levels at approximately 0.5 mbgl.

These observations show an indiscernible pattern for sulphate diffusion, which suggests that sulphate is not behaving conservatively. A large difference between the level of dissolved sulphate in PA 2008 and background pore water samples and the rapid decrease of 2010 soil sample sulphate concentrations with depth (Figure 4-14) reveal that PA water sulphate may have been influenced by attenuation processes such as precipitation, reduction or microbial activities during PA water seepage [35,36].

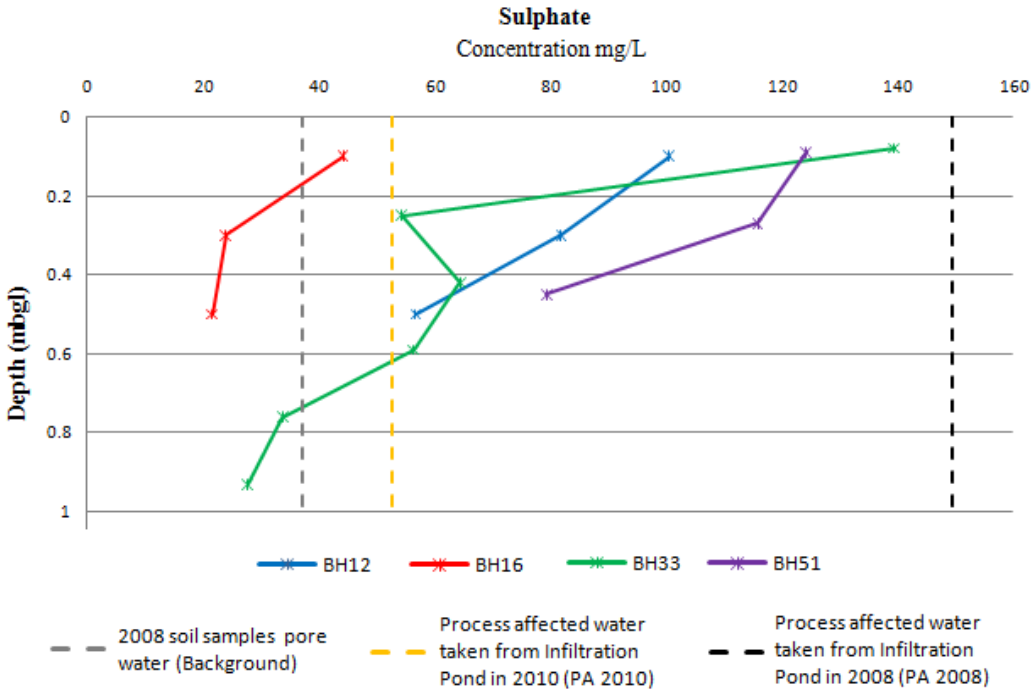

Figure 4-14: Dissolved Sulphate concentrations of 2010 pore water soil samples (BHs 12, 16, 33, and 51) versus depth as they compare to PA 2008 and 2010 values and background. Average values of Background, PA 2010 and PA 2008 samples are shown in vertical dotted lines to make the comparison easier.

4-4 Conclusion

As the focal point of this study, the pore water chemistry of 2010 soil samples was compared to the background results (2008 soil samples). Observed changes in pore water chemistry were explained through ion exchange, precipitation, and microbial processes involved in the fate and transport of inorganic compounds of PA water in the clay till. The research described herein identified the following:

- Isotope analysis of PA water indicates it is distinct from other natural bodies of water in the area such as river water, and groundwater. PA water is enriched compared to all other sources in $\delta^{18}O$ and $\delta^{2}H$, providing an opportunity to use isotopes as a signature to trace PA water infiltration. $\delta^{18}O$ profiles versus depth for 2010 soil samples showed that the PA water infiltrated to a depth of approximately 0.9 mbgl over a two year time period.
- Metal mobility lagged as compared to chloride and isotopic trends. It could be the result of attenuation processes, which affected the heavy metals such as Mo and Pb infiltration. Trends in metal mobility showed uptake of Mo and Pb from PA water and release of Ba and Sr from clay particles. Generally, no specific infiltration indicator was observed with respect to heavy metals behaviour. Small quantities of trace metals observed in pore water samples (in the order of ug/L) do not exceed the water quality guidelines.
- Ions (except for chloride) lag the water penetration line from 0.3 to 0.6 m. Trends in major ions for the 2010 soil samples indicated release of calcium and magnesium into the pore water and sodium and sulphate uptake by clay particles

after PA water infiltrated the clay till layer. The major ions concentrations observed in soil samples pore water do not exceed the water quality guidelines.

- The concentration of exchangeable calcium and magnesium greatly increased in the pore water up to 80% and 40% of background levels respectively; indicating that high levels of calcium and magnesium were held off exchange sites by competing cations, mainly sodium. In contrast, potassium data shows that it is not involved in any exchange reactions.
- Analyzing the changes in cation concentration revealed that ion exchange is the dominant factor affecting transport of cations.
- Large chloride concentrations in PA water and its similar behaviour as the stable isotopes indicates that chloride can be used as a conservative ion and a reliable tracer to track PA water infiltration through these clay soils.
- $\delta^{18}O$ and chloride profiles versus depth for 2010 soil samples resemble typical diffusion profiles, which are in agreement with the findings of EC and water content trends versus depth as shown in Chapter 3.
- Advective transport of PA water is likely minimal and there is good agreement between the depth of diffusion indicated by these profiles (approximately 0.9 mbgl). Field studies of ion and isotope profiles could be used to examine the diffusion process (will be discussed in Chapter 5).

4-5 References

(1) Gustafsson JP, Pechova P, Berggren D. Modeling metal binding to soils: The role of natural organic matter. Environ Sci Technol; 2003; 37(12): 2767-2774.

(2) Lofts S, Woof C, Tipping E, Clarke N, Mulder J. Modelling pH buffering and aluminium solubility in European forest soils. Eur J Soil Sci; 2001; 52(2): 189-204.

(3) McDonald JD. The partitioning of CD, Cu, Pb and Zn between the solid and solution phase of forest floor horizons in polzolic soils near metal smelters. Quebec, Canada: McGill University, Canada; 2005.

(4) Essington ME. Soil and water chemistry: an integrative approach. Boca Raton: CRC Press; 2004.

(5) Smyth DJA. Hydrology and geochemical studies above the water table in an active uranium impoundment near Elliot Lake, Ontario. Ontario, Canada: Waterloo university; 1981.

(6) Blowes DW, Reardon EJ, Jambor JL, Cherry JA. The formation and potential importance of cemented layers in inactive sulfide mine tailings. Geochim Cosmochim Acta; 1991; 55(4): 965-978.

(7) Moncur MC, Ptacek CJ, Blowes DW, Jambor JL. Release, transport and attenuation of metals from an old tailings impoundment. Appl Geochem; 2005; 20(3): 639-659.

(8) Bufflap SE, Allen HE. Sediment pore water collection methods for trace metal analysis: A review. Water Res; 1995; 29(1): 165-177.

(9) Toifl M, Nash D, Roddick F, Porter N. Effect of centrifuge conditions on water and total dissolved phosphorus extraction from soil. Aust J Soil Res; 2003; 41(8): 1533-1542.

(10) Giesler R, Lundström US, Grip H. Comparison of soil solution chemistry assessment using zero-tension lysimeters or centrifugation. Eur J Soil Sci; 1996; 47(3): 395-405.

(11) Geibe CE, Danielsson R, van Hees PAW, Lundström US. Comparison of soil solution chemistry sampled by centrifugation, two types of suction lysimeters and zero-tension lysimeters. Appl Geochem; 2006; 21(12): 2096-2111.

(12) Clark ID, Fritz P. Environmental isotopes in hydrogeology. Boca Raton, FL: CRC Press/Lewis Publishers; 1997.

(13) Craig H. Isotopic variations in meteoric waters. Science; 1961; 133(3465): 1702-1703.

(14) Falcone MD. Assessing hydrological processes controlling the water balance of lakes in the Peace- Athabasca Delta, Alberta, Canada using water isotope tracers. Ontario, Canada: University of Waterloo; 2007.

(15) Swart PK. Climate change in continental isotopic records. Washington, DC: American Geophysical Union; 1993.

(16) Wolfe BB, Karst-Riddoch TL, Hall RI, Edwards TWD, English MC, Palmini R, et al. Classification of hydrological regimes of northern floodplain basins (Peace-Athabasca Delta, Canada) from analysis of stable isotopes ($\delta^{18}O$, $\delta^{2}H$) and water chemistry. Hydrol Processes 2007;21(2):151-168.

(17) Gibson JJ. Short-term evaporation and water budget comparisons in shallow Arctic lakes using non-steady isotope mass balance. J Hydrol; 2002; 264(1-4): 242-261.

(18) Gibson JJ, Edwards TWD, Prowse TD. Development and validation of an isotopic method for estimating lake evaporation. Hydrol Processes; 1996; 10(10): 1369-1382.

(19) Gibson JJ, Edwards TWD, Prowse TD. Runoff generation in a high boreal wetland in northern Canada. Nordic Hydrol; 1993; 24(2-3): 213-224.

(20) Gibson JJ, Reid R, Spence C. A six-year isotopic record of lake evaporation at a mine site in the Canadian subarctic: results and validation. Hydrol Processes; 1998; 12(10-11): 1779-1792.

(21) Kendall C, McDonnell JJ. Isotope tracers in catchment hydrology. Amsterdam; New York: Elsevier; 1998.

(22) Gat JR. Lakes: Stable Isotope Hydrology- Deuterium and Oxygen-18 in the Water Cycle; 1981; 210: 203-221.

(23) Lawrence JR, Taylor Jr. HP. Hydrogen and oxygen isotope systematics in weathering profiles. Geochim Cosmochim Acta, 1972; 36(12): 1377-1393.

(24) Zeng H. Web-Based High Performance Simulation System for Transport and Retention of Dissolved Contaminants in Soils. Mississippi, USA: Mississippi State University; 2002.

(25) Tompkins TG. Natural Gradient Tracer Tests to Investigate the Fate and Migration of Oil Sands Process-Affected Water in the Wood Creek Sand Channel. Ontario Canada: University of Waterloo; 2009.

(26) Chinu Wa T. Nonequivalent transport of heavy metals in soils and its influence of soil remediation. Hong Kong: Hong Kong university of Scence and Technology; 2006.

(27) Alloway BJ. Heavy metals in soils. 2nd ed. London: Blackie; 1995.

(28) Gray CW, McLaren RG, Roberts AHC, Condron LM. Solubility, sorption and desorption of native and added cadmium in relation to properties of soils in New Zealand. Eur J Soil Sci; 1999; 50(1): 127-137.

(29) McBride M, Martínez CE, Sauvé S. Copper(II) activity in aged suspensions of goethite and organic matter. Soil Sci Soc Am J; 1998; 62(6): 1542-1548.

(30) Sauvé S, Norvell WA, McBride M, Hendershot W. Speciation and complexation of cadmium in extracted soil solutions. Environ Sci Technol; 2000; 34(2): 291-296.

(31) Tiller KG, Nayyar VK, Clayton PM. Specific and non-specific sorption of cadmium by soil clays as influenced by zinc and calcium. Aust J Soil Res; 1979; 17(1): 17-28.

(32) Bruemmer GW, Gerth J, Tiller KG. Reaction kinetics of the adsorption and desorption of nickel, zinc and cadmium by goethite. I. Adsorption and diffusion of metals. J Soil Sci; 1988; 39(1): 37-52.

(33) Smedley PL, Kinniburgh DG. A review of the source, behaviour and distribution of arsenic in natural waters. Appl Geochem; 2002; 17(5): 517-568.

(34) Holden AA, Haque SE, Donahue RB, Ulrich AC. Geochemical Impact of Seepage from an Oil Sands Tailings Facility on Groundwater Resources GQ10: Groundwater Quality Management in a Rapidly Changing World. Proc 2010; 13–18 June 2010.

(35) Holden AA, Donahue RB, Ulrich AC. Geochemical interactions between process-affected water from oil sands tailings ponds and North Alberta surficial sediments. J Contam Hydrol; 2011; 119(1-4): 55-68.

(36) Reifferscheid L. In situ measurement of the coefficient of molecular diffusion in fine grained till. Saskatchewan, Canada: University of Saskatchewan; 2007.

Chapter 5: One-Dimensional Analytical Models

5-1 Introduction

As the final step of this research, the main focus of this chapter is to determine the dominant process governing the PA water seepage from the Infiltration Pond into the underlying clay till layer. To do so, simple analytical models were used to define the fundamental mechanisms of PA water seepage from the Infiltration. Advection, dispersion and molecular diffusion are three physical processes that may govern the transport of solutes. During advection, the solute moves through the porous media with the same velocity as the flow in the system. Convection processes through porous media, such as mechanical dispersion, cause hydraulic mixing due to pore-to-pore variation in the velocity of the flow, which changes the distribution of the flow. In extremely low flow velocity systems, a concentration gradient causes solutes to spread through diffusion, which is the slowest form of contaminant transport. In other words, solute movement from a higher concentration to a lower concentration is the driving force behind the diffusion process. During contaminant migration through soil, each of these three processes may dominate separately, or can govern the migration simultaneously [1]. One of the foremost factors controlling the type and extent of these processes is flow velocity. Figure 5-1 suggests dominant migration processes based on Darcy's velocity of solute in the soil system [2].

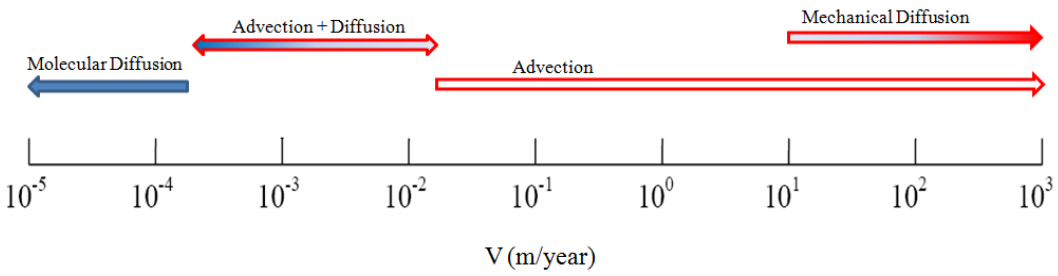

Figure 5-1: Dominant contaminant migration processes through soil based on Darcy velocity [2]**.**

To describe and predict the dissolved chemical contaminant transport through porous media, numerical and analytical methods are extensively studied by researchers particularly in the geo-environmental engineering field. In this capacity, analytical methods were developed based on mathematical principals to estimate the contaminant plume and evaluate the governing processes in ideal systems of contaminant transport. In spite of the simplicity of usage and analytical models' estimation accuracy, due to some restrictions associated to analytically developed equations, they cannot be used to simulate complexities in heterogeneous systems with complicated boundary conditions and geometries [3].

To simplify the complexity of the experimental results obtained in geochemistry analysis (discussed in Chapter 4), one-dimensional analytical models were developed for the soil system underlying the infiltration pond. The output from the analytical models was compared to the field results obtained for conservative chemicals in Chapter 4. These comparisons: 1) identify the dominant process governing PA water seepage through the clay till layer and 2) provide a simple

model to estimate the progress and extent of PA water seepage into the underlying soil.

5-2 Materials and Methods

By assuming that the vertical seepage under the infiltration pond occurs under unit hydraulic conductivity (free drainage) [4] and using the permeability coefficient measured in Chapter 3, $3.1*10^{-6}$ and $4.3*10^{-7}$ cm/s by falling head and double ring infiltrometer test respectively, the average Darcy velocity of seepage calculated in the range of $1.4*10^{-1}$ to 1.1 m/y based on Equation 5-1.

$$\bar{q} = -K\left(\frac{dH}{dX}\right) \qquad \textbf{Equation 5-1}$$

Where:

$\bar{q}$: Darcy velocity or fluid flux (L/T)

K: Hydraulic conductivity of soil (L/T)

$\left(\frac{dH}{dX}\right)$: Hydraulic gradient (i) (L/L)

Based on Figure 5-1, this seepage velocity falls close in the range of Darcy velocities over which advection and diffusion are suggested to be dominant and dispersion could be neglected. Thus, two scenarios were one-dimensionally modeled: (1) pure advection; and (2) pure diffusion of a solute through the clay till layer. Due to the conservative transport characteristics of chloride and $\delta^{18}O$ [5-8], both models were developed for these two tracers.

5-2-1 Advection

The direction of seepage flow under the Infiltration Pond is downward through the clay till. Therefore, the infiltrated PA water "advective front" position under the pond can be calculated using Equation 5-2 [12].

$$Z(t) = \bar{V} \times t \qquad \textbf{Equation 5-2}$$

Where:

Z(t): Depth of advective front (the same concentration as the source) at time t (L)

t: time (T)

$\bar{V}$: Average solute velocity (L/T)

The average solute velocity is computed based on Equation 5-3.

$$\bar{V} = \frac{q}{\eta} \qquad \textbf{Equation 5-3}$$

Where:

η: Effective porosity of the soil

Effective porosity is defined as the portion of the soil total porosity that is available for flow. The value of effective porosity is commonly estimated based on available literature or engineering experience [9,10]. In this project η=0.22 was used in the advection calculations. This value of effective porosity for Cl^- is reported by Hendry et al. [11] based on diffusion cell testing on clay till samples.

5-2-2 Diffusion

Adolf Fick explained diffusion behaviour by Equation 5-4 which is known as Fick's first law [12].

$$J = -D^* \frac{\partial C}{\partial Z} \qquad \textbf{Equation 5-4}$$

Where:

J: Diffusion mass flux ($M/L^2/T$)

D*: Effective diffusion coefficient (L^2/T)

C: Solute concentration (M/L^3)

D* which is known as the effective diffusion coefficient is dependent both on porous media and solute characteristics which can be defined based on Equation 5-5.

$$D^* = \tau \times D_0 \qquad \textbf{Equation 5-5}$$

Where: D_0 (L^2/T) is free-solution diffusion coefficient which depends on the viscosity, size and charge of ion and temperature of the solute of interest [10,13]. τ (tortuosity coefficient) is a dimensionless empirical coefficient to account for the longer distance that a solute must diffuse in a porous media in comparison to free solution diffusion. Based on soil physical characteristics, τ ordinarily ranges from 0.1 to 0.85 [3]. In the absence of advective flow, one-dimensional diffusion of a continuous solute input in a homogeneous, saturated and infinite column of porous media with zero initial concentration of the solute is represented by Fick's second law (Equation 5-6). Fick's second law is developed from Fick's first law.

$$\frac{\partial C}{\partial t} = D^* \frac{\partial^2 C}{\partial^2 Z}$$ **Equation 5-6**

Where:

∂C/∂t: change in the solute concentration with time.

The analytical solution for Equation 5-5 (for Z≥ 0) is given in Equation 5-7 [12].

$$C_{(z,t)} = C_0 \times \mathrm{ERFC}\left[\frac{z}{2\sqrt{D^* t}}\right]$$ **Equation 5-7**

Where:

$C_{(z,\,t)}$: Solute concentration at depth z and time t.

C_0: Source concentration of the solute.

ERFC: Statistical complementary error function

To simplify the complexity of the experimental results, one-dimensional simulation for chloride and $\delta^{18}O$ were conducted.

Free solution coefficient (D_0) of chloride is about $2.03*10^{-9}$ m^2/s at 25ºC [10,14] and with τ= 0.3, D* is calculated as $6*10^{-10}$ m^2/s. A D* value of $3.5*10^{-10}$ m^2/s was obtained for ^{18}O in a previous field study by Reifferscheid [10] in clay till consisting of 39% sand and 51% fine particle. This effective diffusion coefficient value was used for our study for ^{18}O, due to the similarity in clay till composition to our study.

Commonly, as an empirical coefficient, the effective diffusion coefficient is either measured in the actual field or in the laboratory (using radial diffusion cell tests). In this study, however, both for Cl^- and $\delta^{18}O$, one dimensional diffusion models for the base case, D* which is the literature suggested value have been created. In

addition, the similar outputs for 2D* and 3D* have been generated. In this capacity, each model outputs were compared to the field geo-chemistry findings in order to find the best fit diffusion coefficient. To do so, the correlation coefficients and minimum relative error (MRE) for the aforementioned models and field results were calculated base on Equations 5-8 and 5-9.

$$Corr(Cm,Cp)=\frac{\sum(Cm-\overline{Cm})(Cp-\overline{Cp})}{\sqrt{\sum(Cm-\overline{Cm})^2\sum(Cp-\overline{Cp})^2}} \qquad \textbf{Equation 5-8}$$

$$MRE=\frac{1}{n}\sum_{i=1}^{n}\left|\left((Cpi-Cmi)\middle/Cmi\right)\right|\times 100 \qquad \textbf{Equation 5-9}$$

Where:

C_m and $C_{p:}$ The measured concentration and predicted concentration value by model

$\overline{C_m}$ and $\overline{C_p}$: The average values of measured and model predicted concentration respectively

N: The number of samples, respectively.

All calculations were conducted using Microsoft Excel 2007.

5-3 Results and discussion

To properly compare model outputs to the field geo-chemistry results the following modifications were conducted on the 2010 soil pore water geo-chemistry results:

1- To provide a "good guess" for the source concentration of the tracers for each borehole, a trend for concentration versus depth was plotted and then extrapolated to the horizontal axis (concentration). It is to be noted that different contamination sources associated to different boreholes could be caused by their locations in Infiltration Pond (near or far from the edge), clay till layer heterogeneity or uneven excavated bottom of the pond.

2- To better track pore water chemistry changes after PA water seepage, the average background levels of tracers were deducted from the 2010 soil pore water concentrations.

It is to be noted that, as mentioned in Chapter 4, all pore water samples were extracted from core sections, around 20 cm in length. These samples then underwent chemistry analysis and are reported by the average depth of each section, which reflects the average chemistry of the whole section. As a result, the maximum and minimum depths of each soil section are shown in dotted curves as shown in Figure 5-2.

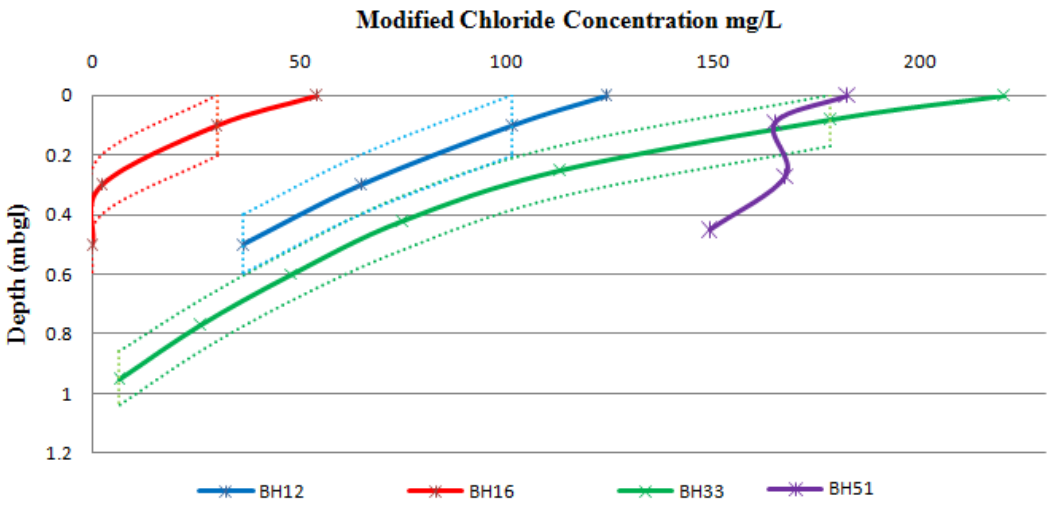

Figure 5-2: Modified chloride levels versus depth for 2010 soil samples (BHs 12, 16, 33, and 51); curves were brought to the concentration axis (x-axis) and the maximum and minimum depths of each soil section are indicated as dotted curves.

Figure 5-2 shows the odd behaviour of BH51 trend for chloride concentration versus depth in comparison to the other field results for boreholes 12, 16, and 33. To explain the different behaviour of BH51, one could claim the routine errors, introduced in field experiments, as a possible reason. Consequently, BH51 results have been eliminated and comparison to the outputs of chloride advection and diffusion models have been conducted on boreholes 12, 16, and 33.

5-3-1 Advection

The advection analytical calculation yielded the advective front progress for PA water to approximately 1 mbgl after 2 years. This claims that the levels of dissolved tracers, chloride and $\delta^{18}O$, in the pore water of the 2010 clay till samples should be the same as the source concentration at any depth less than 1

mbgl. However, the trends for measured chloride (Figure 5-2) and $\delta^{18}O$ (Figure 4-3 in Chapter 4) versus depth for the 2010 soil samples show that no advective front is observable. For example, the concentration of dissolved chloride (after deducting the background average level) in the soil pore water of BH33 at 0.95 mbgl is about 6.5 mg/L while the source concentration of chloride is 220 mg/L. To further support this observation, the advection model results are in contrast with the water content trends of 2010 soil samples which showed a gradual decrease with depth (see Section 3-3-5).

These observations strongly indicate that advection has not happened to this depth. The effect of advective transport is felt to be minimal and based on experimental observation it is hypothesized that it could happen to 0.1-0.2 mbgl. It is to be noted that the permeability coefficient used in the advection calculations was measured on saturated soil samples, while unsaturated permeability of soil can be up to an order of magnitude lower than the saturated ones. The significant difference in saturated and unsaturated permeability coefficients could be the reason behind the poor estimation of the advection model.

5-3-2 Diffusion

The simulation model and experimental results for chloride are compared in Figure 5-3.

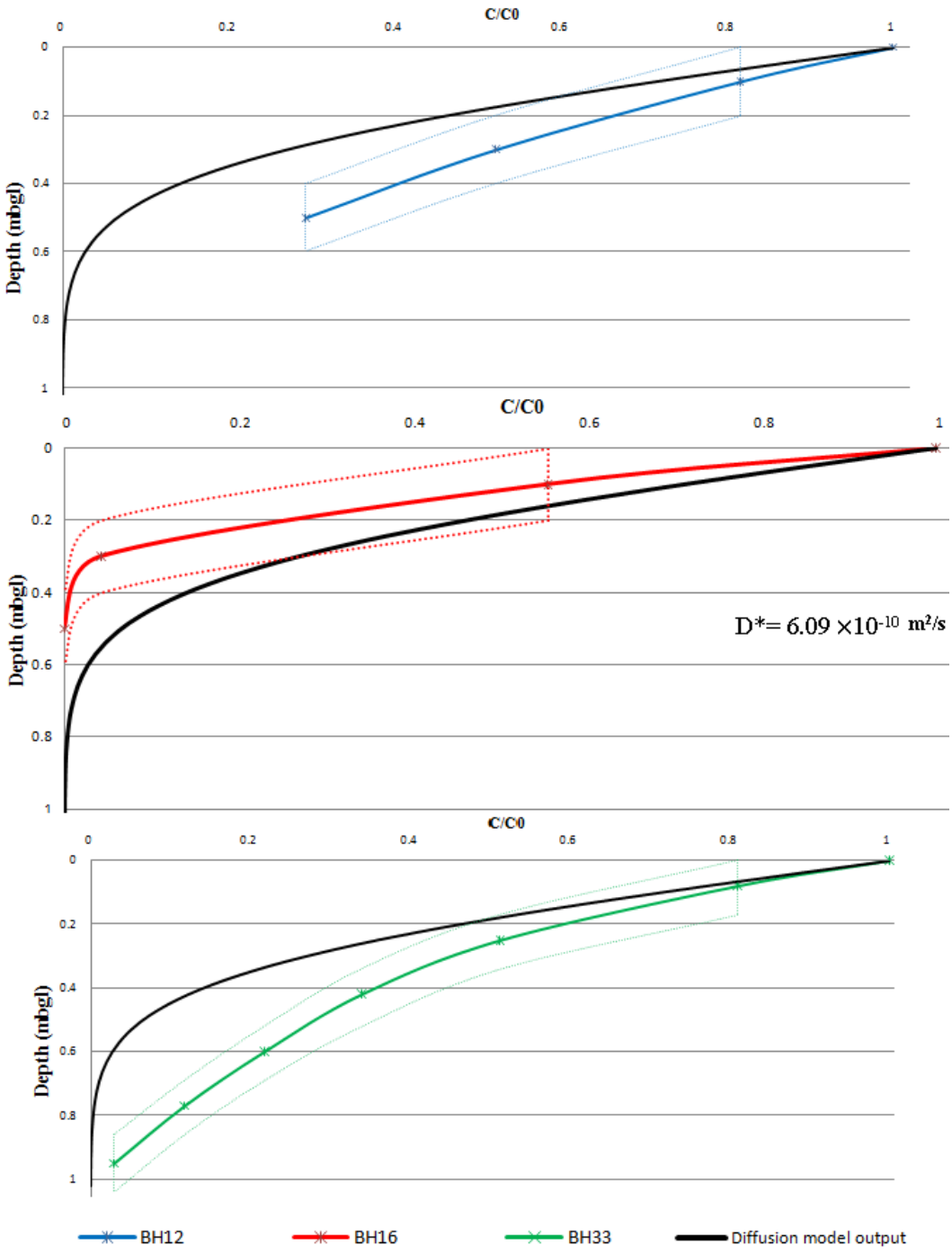

Figure 5-3: Dissolved Chloride concentrations of 2010 pore water soil samples (BHs 12, 16, and 33) versus depth as they compare to one dimensional diffusion model output (t=2 Years and D* = 6.09*10^{-10} m^2/s); the maximum and minimum depths of each soil section are indicated as dotted curves.

As shown in Figure 5-3, the one-dimensional diffusion model for chloride over a two year time period, from August 2008 to July 2010, fits the field results. The correlation coefficients between the model prediction and field measurements were: 0.99, 0.96, and 0.96 for boreholes 12, 16, and 33 respectively. These results indicate that PA water seepage under the Infiltration Pond is a diffusion dominant process. However, the mean relative errors (MRE) between the model and target points (experiments findings) are: 46.3%, 370.7%, and 63.6% for boreholes 12, 16, and 33, respectively. The MRE values reveal that the model and field results are not a perfect match. The diffusion depth suggested by the model is around 0.7 to 0.8 mbgl, while field data shows the leading edge of the Cl^- plume between 0.9 and 1 mbgl. This deviation from the field results could have been associated with several factors including inappropriate D* used in modelling.

Trial and error attempts to find a D* better representing the clay till system resulted in a new value of $D^* = 1.83*10^{-9}$ m^2/s, equivalent to three-folds of the first attempt. Using the new D* value, correlation coefficients between the diffusion curve and experimental findings have improved to 0.99, 0.92, 0.99 for boreholes 12, 16, and 33, respectively. Furthermore, the model yielded significantly lower MRE values in comparison to the first try (1.32% and 16.69% for boreholes 12 and 33).

Figure 5-4 illustrates the adjusted model and its fit to the field results. As shown in Figure 5-4, the model output yielded a good visual fit to the measured data and there is a very good approximation of experimental data with some minor

deviations. Moreover, the diffusion depth is estimated around 1 mbgl, which is in agreement with the field results.

In this case, BH16 trend showed very poor fitting with diffusion curve. Clay till layer heterogeneity, an uneven excavated bottom of the pond and the location of BH16 in the infiltration pond, which is near a corner and could receive more discharge from rain snow melt water, or routine errors introduced in field experiments, may be reasons behind the odd behaviour of BH16 compared to other boreholes.

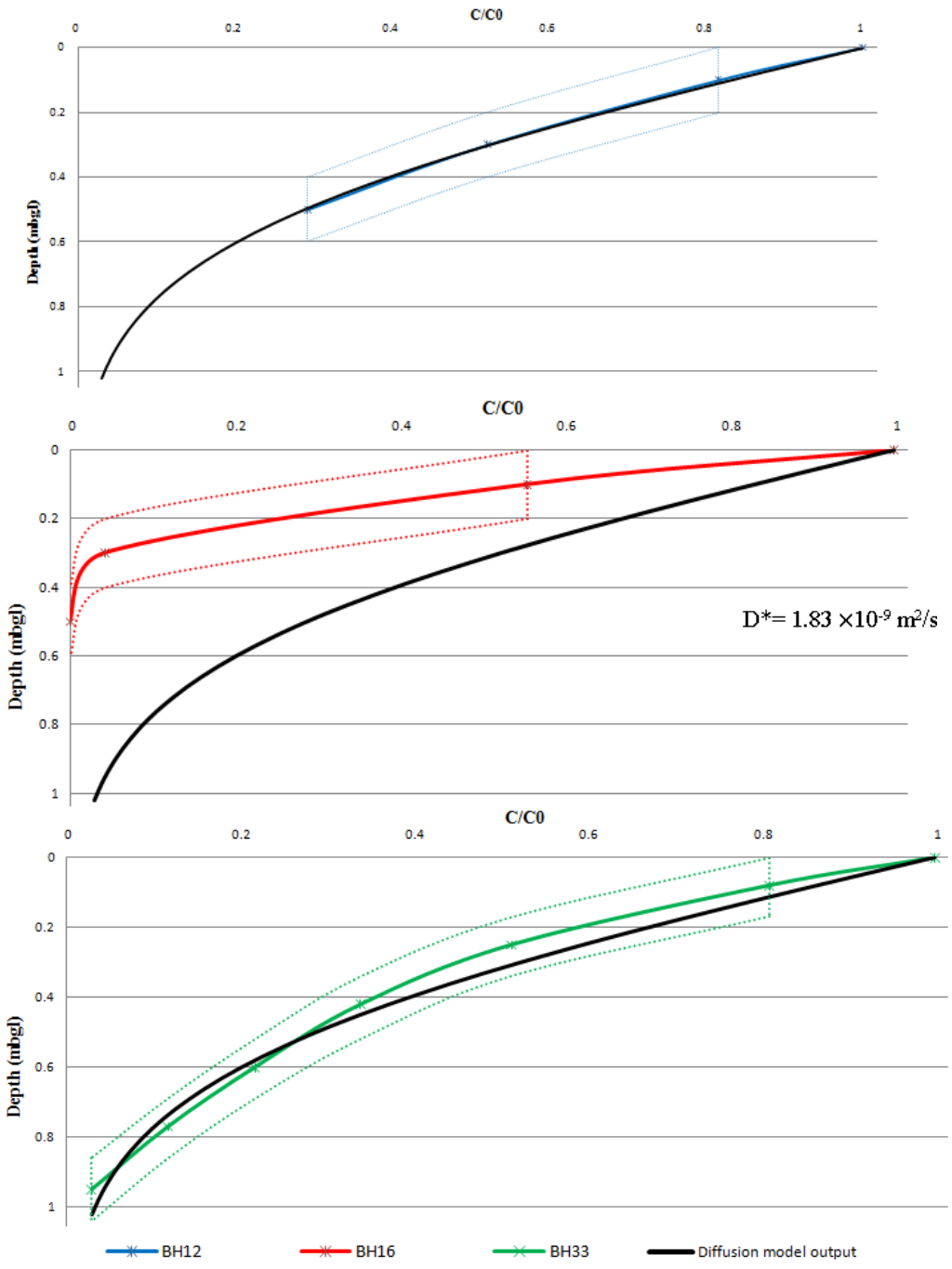

Figure 5-4: Dissolved Chloride concentrations of 2010 pore water soil samples (BHs 12, 16, and 33) versus depth as they compare to one dimensional diffusion model output (t=2 Years and D* = $1.83*10^{-9}$ m^2/s); the maximum and minimum depths of each soil section are indicated as dotted curves.

Similarly, the diffusion models developed for $\delta^{18}O$ fit well with the field results as shown in Figure 5-5. As a starting point a diffusion model was developed with $D^* = 3.5*10^{-10}$ m^2/s. The model produced a similar pattern as the $\delta^{18}O$ 2010 soil samples versus depth, but deviated significantly from the field results (shown in Figure 5-5). It is to be noted that due to the shortage of pore water extracted from BH16, the isotopic analysis was not conducted on the first section of soil, BH16-1 (0-0.2 mbgl). Consequently, this borehole was ignored in models outputs comparison figures.

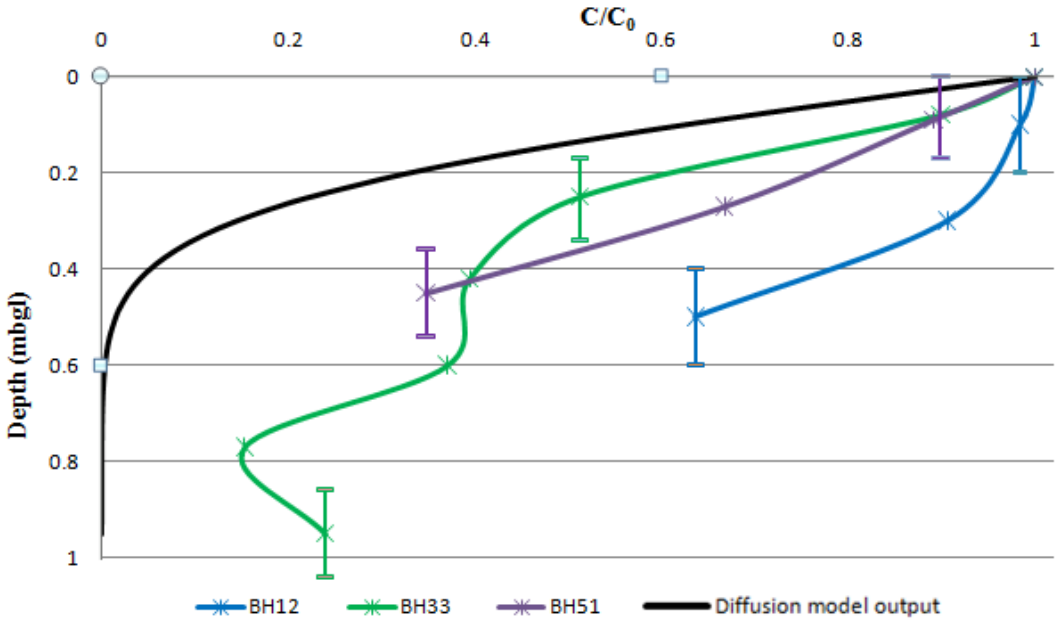

Figure 5-5: Relative $\delta^{18}O$ values of 2010 pore water soil samples (BHs 12, 16, and 33) versus depth as they compare to one dimensional diffusion model output (t=2 Years and $D^* = 3.5 *10^{-10}$ m^2/s); the maximum and minimum depths of soil section are indicated as vertical bars.

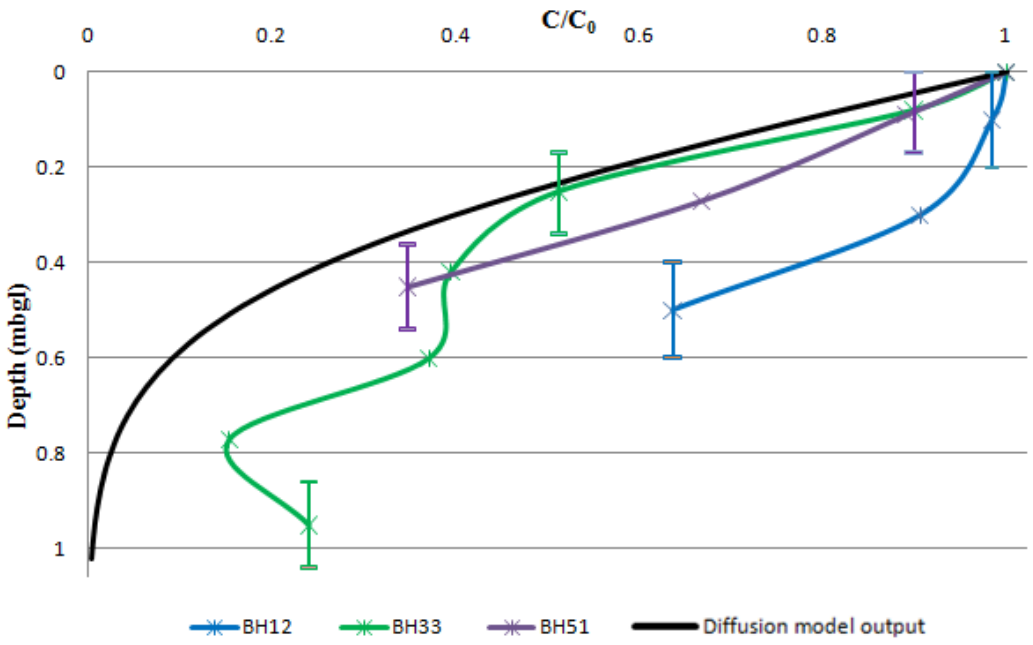

Figure 5-6: Relative $\delta^{18}O$ values of 2010 pore water soil samples (BHs 12, 16, and 33) versus depth as they compare to one dimensional diffusion model output (t=2 Years and D* = 1 *10^{-9} m^2/s); the maximum and minimum depths of soil section are indicated as vertical bars.

By using D*=1*10^{-9} m^2/s which is three fold of the first diffusion coefficient used, the resultant model shows quantitatively closer results to the experimental findings (Figure 5-6). In this case, the correlation coefficients between the diffusion curve and field results were: 0.90, 0.97, and 0.98 of boreholes 12, 33 and 51 respectively. Plus, the associated MRE values have been explored as 50.5%, 51.01%, and 27.91%. Additionally, the predicted diffusion depth is in a reasonable range of 1 to 1.1 mbgl.

$\delta^{18}O$ trend of BH12 is inconsistent with the results of BHs 33 and 51. Since BH12 fits perfectly with the Cl^- diffusion curve (Figure 5-4), it can interpreted that routine errors introduced in isotopic analysis in field experiments or poor maintenance of pore water samples could be the reason behind this error.

The detailed outputs of the one-dimensional simulations for Cl^- and $\delta^{18}O$ are provided in Appendix C (Tables C-1 to C-6).

5-4 Conclusions

Generally, modelling of contaminant transport through soil systems needs great attention to the details of solute and soil characteristics. But, at the final step of this research, a simple analytical one-dimensional model was adopted to discover the dominant processes governing PA water seepage into the clay till. The following conclusions can be made from the analytical models evaluation:

- There was no agreement between the advection analytical model and field test results, which concludes that the effect of advective transport is minimal.
- The diffusion models for chloride and $\delta^{18}O$ fit well with the field results providing evidence of a diffusion-dominated system. For instance, the correlation coefficient of the diffusion curves and BH33 field measurements for both of Cl^- and $\delta^{18}O$, were higher than 0.96.
- For chloride one-dimensional diffusion modelling, a better fit between the model and field results was obtained by applying $D^* = 1.83*10^{-9}$ m^2/s (e.g. correlation factor of 0.99 and MRE value of 16.7% between BH33 field results and diffusion model outputs) indicating that it is a good estimation for the effective diffusion coefficient of chloride in the clay till layer.

- $D^*=1*10^{-9}$ m^2/s for $\delta^{18}O$ one dimensional diffusion modelling yielded an excellent fit to the field results with the correlation coefficient of 0.98 and MRE value of 27.9% for BH33.
- For both chloride and $\delta^{18}O$, using modified D* values resulted to models which estimated the diffusion edge at approximately 1 mbgl, which is in agreement with the geo-chemistry and water content findings.

5-5 References

(1) Gorelick SM. Groundwater contamination : optimal capture and containment. Boca Raton: Lewis Publishers; 1993.

(2) Pollutant Transport Through Barriers. Geotechnical Special Publication; 1987.

(3) Mendoza CA. Contaminant Hydrogeology (EAS 425) Course Notes. University of Alberta; 1998.

(4) McCray JE, Nieber J, Poeter EP. Groundwater mounding in the vadose zone from on-site wastewater systems: Analytical and numerical tools. J Hydrol Eng; 2008; 13(8): 710-719.

(5) Oiffer LAA. Integrated Solid Phase, Aqueous Phase and Numerical Investigation of Plume Geochemistry at an Oil Sand Mining Facility. Ontario, Canada: University of Waterloo; 2006.

(6) Gervais FJM. Fate and Transport of Naphthenic Acids in a Glacial Aquifer. Ontario, Canada: University of Waterloo; 2004.

(7) Baker KM. Identification of Process Water in a Surficial Aquifer at Syncrude's Mildred Lake Site. Ontario, Canada: University of Waterloo; 1999.

(8) Thomson NR, editor. Indicators for assessing transport of oil sands process-affected waters. Bringing Groundwater Quality Research to the Watershed Scale, Proceedings of GQ2004 ,The 4th International Groundwater Quality Conference; 2004.

(9) Stephens DB, Hsu K-, Prieksat MA, Ankeny MD, Blandford N, Roth TL, et al. A comparison of estimated and calculated effective porosity. Hydrogeol J; 1998; 6(1): 156-165.

(10) Reifferscheid L. In situ measurement of the coefficient of molecular diffusion in fine grained till. Saskatchewan, Canada: University of Saskatchewan; 2007.

(11) Hendry MJ, Wassenaar LI, Kotzer T. Chloride and chlorine isotopes (36Cl and δ37Cl) as tracers of solute migration in a thick, clay-rich aquitard system. Water Resour Res; 2000; 36(1): 285-296.

(12) Fetter CW. Contaminant hydrogeology. New York: Macmillan Pub. Co.; Toronto; New York: Maxwell Macmillan Canada; Maxwell Macmillan International; 1993.

(13) Shackelford CD, Daniel DE. Diffusion in saturated soil. 1. Background. J Geotech Eng; 1991; 117(3): 467-484.

(14) Yuan-Hui L, Gregory S. Diffusion of ions in sea water and in deep-sea sediments. Geochim Cosmochim Acta; 1974; 38(5): 703-714.

Chapter 6: Conclusions and Future Recommendations

6-1 Conclusions

The experimental project summarized in this thesis, has extensively characterized the PA water migration into the clay till layer by tracking oxygen stable isotopes, heavy metals and major ions under a small scale Infiltration Pond over a 2 year time period. Separate conclusions are available at the final section of every chapter. In this chapter, overall findings and integrated conclusions are presented. Recommendations to improve the thesis through additional studies follow the summarized conclusions.

With respect to the thesis objectives and based on the results of the study, the following conclusions were developed:

- Two distinguishable soil layers were found in the surficial geology of the study area, underlying the Infiltration Pond, including: clay till layer (from 0 to 7.7 mbgl) and sand layer (from 9.2 mbgl). The saturated permeability coefficient based on a falling head test was $3.1*10^{-6}$ cm/s for the upper portion of clay till layer. This top soil layer has the lowest permeability as compared to the other soil type (sand layer). The low permeability of the clay till layer was one of the design criteria for STP construction, which was confirmed in the physical properties tests completed in this thesis.
- The unsaturated condition of the soil underlying the Infiltration Pond can be interpreted by soil water content trends versus depth. In which, water content of the soil cores recovered in 2010 decreases (from ~22% water content at top sections) with depth and reaches the average water content of 2008 sample (~14%) at approximately 0.7 mbgl.

- Enriched in $\delta^{18}O$ and $\delta^{2}H$, PA water has a distinct signature from other natural water bodies in the study area, therefore providing an opportunity to use isotopic signatures to track PA water infiltration. Chloride can also be used as a tracer of PA water seepage due to the large available Cl concentrations in PA water (~ 390 mg/L), conservative behaviour and similar behaviour as compared to isotopic trends in concentration versus depth graphs for 2010 soil samples.
- $\delta^{18}O$ and chloride profiles versus depth for 2010 soil samples showed that PA water infiltrated to a depth of approximately 0.9 mbgl over a two year time period.
- Metal mobility lagged as compared to chloride and isotopic trends. It could be the result of attenuation processes such as precipitation, reduction and to a greater extent adsorption which could highly affect the heavy metals infiltration. Trends in metal mobility showed uptake of Mo and Pb from PA water and release of Ba and Sr (increase up to 20% of background levels) from clay particles. Small quantities of trace metals observed in pore water samples (in the order of ug/L) do not exceed the water quality guidelines.
- Analyzing the changes in cations and anions concentrations revealed that ion exchange is one of the foremost processes affecting the fate and transport of major ions. Ions (except for chloride) lag the water penetration line 0.3 to 0.6 m. Trends in major ions for the 2010 soil samples indicated release of calcium and magnesium into the pore water (concentrations increased up to 80% and 40% of background levels respectively) and sodium and sulphate uptake by clay particles after PA water infiltrated the clay till layer. For instance, high levels of calcium

and magnesium exchange sites were substituted by competing cations, mainly sodium. As a result, the concentration of exchangeable calcium and magnesium greatly increased in the pore water up to 80% and 40% of background levels respectively. The major ions concentrations observed in soil samples pore water do not exceed the water quality guidelines.

- The one-dimensional analytical models developed for PA water infiltration confirmed that the effect of advective transport is minimal as shown through chloride, $\delta^{18}O$ and water contents trends. Over estimation of the unsaturated permeability coefficient of the clay till layer could also explain the poor results of the advection model.
- The diffusion models for chloride and $\delta^{18}O$ fit well with the field results providing evidence of a diffusion-dominated system. The effective diffusion coefficients of $1.83*10^{-9}$ m^2/s and $1*10^{-9}$ m^2/s for chloride and $\delta^{18}O$ respectively for an one-dimensional diffusion model yielded a very good fit to the field results. For example, correlation coefficient of 0.99 and MRE value of 16.7% obtained between the Cl^- diffusion curve and field results of borehole 33. Based on the diffusion models the estimated diffusion exists at approximately 1 mbgl. This is in agreement with the geo-chemistry and water content findings.

6-2 Recommendations for future research

Recommendations to improve the thesis and expand the research are outlined below:

- In this project the geo-chemistry analysis was conducted on the pore water of the samples taken at two time points: (i) prior to filling with process-affected water and (ii) two years after filling. By continuing once every two years soil coring under the Infiltration Pond, it would be possible to track and monitor the infiltration of PA water over a longer period of time which may result in more detailed characterization of PA water seepage.
- Although conceptual understandings of the types of chemical reactions occurring in the soil system were used in this study, details of chemical and biological attenuation processes were not studied. More multidisciplinary work on chemical and biological activities (such as redox reactions and potential bioaccumulation of metals by indigenous microorganisms in clay layer) using batch tests and column studies of native clay till soils underlying the Infiltration pond may provide more precise results with a better experimental control on the processes.
- To apply the findings of this research to other soils and environments, it would be advisable to analyze the native soil clay mineralogy, adsorption coefficients and cation exchange capacity.
- Geochemical transport numerical models are better suited to model transport involving attenuation processes. As a result, two or three dimensional numerical models developed for seepage through unsaturated soil and capable of considering

attenuation processes should be adopted to verify the findings of the field experiments.

Appendix A

Table A-1: Clay till sieve analysis BH1; 1: 0-0.1 mbgl

Borehole Number: 1
Sample Depth Range (mbgl): 0-0.1
Mass of oven dry sample, W (g): 402.15

Sieve Number	Sieve Opening (mm)	Mass retained on each sieve, W_n (g)	Percent of mass retained of each sieve, R_n	Percent of mass finer of each sieve, F_n
4	**4.76**	8.93	2.2%	97.8%
10	**2**	7.11	1.8%	96.0%
20	**0.84**	12.41	3.1%	92.9%
40	**0.42**	32.58	8.1%	84.8%
60	**0.25**	53.22	13.2%	71.6%
100	**0.149**	60.04	14.9%	56.7%
200	**0.074**	34.75	8.6%	48.0%
passing 200		188.69	46.9%	

Table A-2: Clay till sieve analysis BH1; 1: 0.1-0.2 mbgl

Borehole Number: 1
Sample Depth Range (mbgl): 0.1-0.2
Mass of oven dry sample, W (g): 406.99

Sieve Number	Sieve Opening (mm)	Mass retained on each sieve, W_n (g)	Percent of mass retained of each sieve, R_n	Percent of mass finer of each sieve, F_n
4	**4.76**	27.86	6.8%	93.2%
10	**2**	6.71	1.6%	91.5%
20	**0.84**	9.74	2.4%	89.1%
40	**0.42**	23.4	5.7%	83.4%
60	**0.25**	45.39	11.2%	72.2%
100	**0.149**	50.04	12.3%	59.9%
200	**0.074**	60.39	14.8%	45.1%
passing 200		183.46	45.1%	

Table A-3: Clay till hydrometer analysis BH1; 1: 0-0.1 mbgl

Borehole Number: 1
Sample Depth Range (mbgl): 0-0.1
Mass of oven dry sample, W (g): 50

D (mm)	% Finer	Adjusted % Finer
0.0756	77.2	46.2
0.0543	74.3	44.9
0.0390	71.4	43.5
0.0289	62.8	39.5
0.0210	57.1	36.8
0.0151	54.2	35.4
0.0113	48.5	32.7
0.0082	42.7	30.0
0.0059	38.4	28.0
0.0042	34.1	26.0
0.0030	32.7	25.3
0.0022	31.2	24.7
0.0013	25.5	22.0

Table A-4: Clay till hydrometer analysis BH1; 1: 0.1-0.2 mbgl

Borehole Number: 1
Sample Depth Range (mbgl): 0.1-0.2
Mass of oven dry sample, W (g): 50

D (mm)	% Finer	Adjusted % Finer
0.0756	82.9	45.4
0.0543	80.0	44.1
0.0390	74.3	41.5
0.0289	65.7	37.6
0.0210	58.5	34.4
0.0151	54.2	32.4
0.0113	48.5	29.8
0.0082	42.7	27.3
0.0059	39.8	26.0
0.0042	34.1	23.4
0.0030	31.2	22.1
0.0022	29.8	21.4
0.0013	22.6	18.2

Table A-5: Clay till sieve analysis BH1; 4.1-4.2 mbgl

Borehole Number: 1
Sample Depth Range (mbgl): 4.1-4.2
Mass of oven dry sample, W (g): 402.15

Sieve Number	Sieve Opening (mm)	Mass retained on each sieve, W_n (g)	Percent of mass retained of each sieve, R_n	Percent of mass finer of each sieve, F_n
4	4.76	70.85	16.6%	83.4%
10	2	24.16	5.7%	77.7%
20	0.84	11.81	2.8%	74.9%
40	0.42	15.83	3.7%	71.2%
60	0.25	24.96	5.9%	65.3%
100	0.149	26.48	6.2%	59.1%
200	0.074	29.25	6.9%	52.2%
passing 200		217.74	51.1%	

Table A-6: Clay till sieve analysis BH1; 4.3-4.4 mbgl

Borehole Number: 1
Sample Depth Range (mbgl): 4.3-4.4
Mass of oven dry sample, W (g): 421.93

Sieve Number	Sieve Opening (mm)	Mass retained on each sieve, W_n (g)	Percent of mass retained of each sieve, R_n	Percent of mass finer of each sieve, F_n
4	4.76	186.84	44.3%	55.7%
10	2	21.41	5.1%	50.6%
20	0.84	7.82	1.9%	48.8%
40	0.42	11.35	2.7%	46.1%
60	0.25	17.94	4.3%	41.8%
100	0.149	20.11	4.8%	37.1%
200	0.074	23.25	5.5%	31.6%
passing 200		126.04		

Table A-7: Clay till hydrometer analysis BH1; 4.1-4.2 mbgl

Borehole Number: 1
Sample Depth Range (mbgl): 4.1-4.2
Mass of oven dry sample, W (g): 50

D (mm)	% Finer	Adjusted % Finer
0.0743	80.0	50.9
0.0534	77.2	49.5
0.0384	74.3	48.0
0.0285	65.7	43.6
0.0213	54.2	37.7
0.0158	42.7	31.8
0.0120	34.1	27.4
0.0088	22.6	21.6
0.0064	16.9	18.6
0.0046	14.0	17.2
0.0033	8.3	14.2
0.0023	5.4	12.8
0.0014	2.5	11.3

Table A-8: Clay till sieve analysis BH1; 4.3-4.4 mbgl

Borehole Number: 1
Sample Depth Range (mbgl): 4.3-4.4
Mass of oven dry sample, W (g): 50

D (mm)	% Finer	Adjusted % Finer
0.0743	80.0	31.9
0.0534	77.2	31.1
0.0384	74.3	30.2
0.0285	65.7	27.6
0.0213	54.2	24.2
0.0158	45.6	21.6
0.0120	34.1	18.2
0.0088	22.6	14.8
0.0064	16.9	13.0
0.0046	11.1	11.3
0.0033	8.3	10.5
0.0023	5.4	9.6
0.0014	0.0	8.0

Table A- 9: Sand soil sieve analysis BH1; 8.7 -8.8 mbgl

Borehole Number: 1
Sample Depth Range (mbgl): 8.7 -8.8
Mass of oven dry sample, W (g): 434.18

Sieve Number	Sieve Opening (mm)	Mass retained on each sieve, W_n (g)	Percent of mass retained of each sieve, R_n	Percent of mass finer of each sieve, F_n
4	4.76	0.51	0.1%	99.9%
10	2	1.8	0.4%	99.5%
20	0.84	10.82	2.5%	97.0%
40	0.42	200.375	46.1%	50.8%
60	0.25	192.5	44.3%	6.5%
100	0.149	22.8	5.3%	1.2%
200	0.074	3.72	0.9%	0.4%
passing 200		1.66		

Table A-10: Sand soil sieve analysis BH1; 1: 9.2-9.3 mbgl

Borehole Number: 1
Sample Depth Range (mbgl): 9.2-9.3
Mass of oven dry sample, W (g): 516.9

Sieve Number	Sieve Opening (mm)	Mass retained on each sieve, W_n (g)	Percent of mass retained of each sieve, R_n	Percent of mass finer of each sieve, F_n
4	4.76	0	0.0%	100.0%
10	2	2.405	0.5%	99.5%
20	0.84	12.795	2.5%	97.1%
40	0.42	217.15	42.0%	55.0%
60	0.25	252.92	48.9%	6.1%
100	0.149	22.75	4.4%	1.7%
200	0.074	6.33	1.2%	0.5%
passing 200		2.55		

Table A-11: Clay till hydraulic conductivity test BH1; 2.5 mbgl

Test number	Beginning head difference, h1 (cm)	Ending head difference, h2 (cm)	Test duration, t (s)	Length of specimen, L (cm)	Area of specimen, A (cm^2)	Volume of water flow through the specimen, Vw (cm3)	Hydraulic conductivity, k(cm/s)
1	104.7	88.1	10390	5.04	31.16	31.80	5.1E-06
2	88.0	79.9	7626	5.04	31.16	15.40	3.8E-06
3	79.9	66.5	18991	5.04	31.16	25.80	3.0E-06
4	66.3	60.9	8112	5.04	31.16	10.40	3.2E-06
5	60.9	55.3	9748	5.04	31.16	10.80	3.1E-06
6	55.3	50.0	9967	5.04	31.16	10.00	3.1E-06

Average K (test numbers 3-6) = 3.1E-06 (cm/s)

Table A-12: Clay till hydraulic conductivity test BH1; 9 mbgl

Test number	Beginning head difference, h1 (cm)	Ending head difference, h2 (cm)	Test duration, t (s)	Length of specimen, L (cm)	Area of specimen, A (cm^2)	Volume of water flow through the specimen, Vw (cm3)	Hydraulic conductivity, k(cm/s)
1	102.0	96.8	189.08	5.0	31.16	10.00	8.6E-05
2	96.3	91.6	187.62	5.0	31.16	9.00	8.3E-05
3	91.6	86.3	257.97	5.0	31.16	10.00	7.1E-05
4	86.3	81.1	283.41	5.0	31.16	10.00	6.8E-05
5	81.1	75.9	285.26	5.0	31.16	10.00	7.2E-05
6	75.9	70.7	285.5	5.0	31.16	10.00	7.7E-05

Average K (test numbers 3-6) = 7.2E-05 (cm/s)

Table A-13: Sand soil hydraulic conductivity test BH1; 11 mbgl

Test number	Beginning head difference, h1 (cm)	Ending head difference, h2 (cm)	Test duration, t (s)	Length of specimen, L (cm)	Area of specimen, A (cm^2)	Volume of water flow through the specimen, Vw (cm3)	Hydraulic conductivity, k(cm/s)
1	76.8	72.5	37.91	4.7	31.16	4.00	2.1E-04
2	70.4	67.2	28.16	4.7	31.16	3.00	2.3E-04
3	65.1	58.7	105.15	4.7	31.16	6.00	1.4E-04
4	57.6	45.9	244.5	4.7	31.16	11.00	1.3E-04
5	45.9	35.2	347.24	4.7	31.16	10.00	1.1E-04
6	88.5	76.8	124.52	4.7	31.16	11.00	1.6E-04
7	74.7	50.1	254.72	4.7	31.16	23.00	2.2E-04
8	49.1	45.9	103.31	4.7	31.16	3.00	9.1E-05
9	44.8	42.7	43.76	4.7	31.16	2.00	1.6E-04
10	41.6	36.3	216.79	4.7	31.16	5.00	8.9E-05

Average K (test numbers 5-10) = 1.4E-04 (cm/s)

Appendix B

Table B-1: Values of pH, Alkalinity and EC of soil samples pore water and Infiltration Pond PA water

Samples		Depth range (mbgl)	Ave. Depth (mbgl)	pH	Alkalinity (mg/L $CaCO_3$)	EC (mS)
BH2&4 Aug. 2008	2-3, 2-5, 4-3 & 4-4	0-1	0.5	8.52	166.14	0.50
BH12	12-1	0-0.2	0.1	8.51	183.10	0.99
July 2010	12-2	0.2-0.4	0.3	8.31	173.82	0.83
	12-3	0.4-0.59	0.5	8.30	153.49	0.64
BH16	16-1	0-0.2	0.1	8.19	186.39	0.75
July 2010	16-2	0.2-0.4	0.3	8.30	202.46	0.50
	16-3	0.4-0.62	0.5	8.38	176.01	0.42
BH33	33-1	0-0.17	0.08	8.26	232.40	1.28
	33-2	0.17-0.34	0.25	8.24	153.04	0.84
	33-3	0.34-0.52	0.42	8.27	130.86	0.77
July 2010	33-4	0.52-0.69	0.59	8.33	156.01	0.66
	33-5	0.69-0.86	0.76	8.39	139.78	0.51
	33-6	0.86-1.04	0.93	8.24	140.05	0.45
BH51	51-1	0-0.18	0.09	8.25	277.42	1.37
July 2010	51-2	0.18-0.36	0.27	8.27	152.28	1.08
	51-3	0.36-0.55	0.45	8.24	128.43	0.96
PA	PA 2008	-	-	8.43	529.97	2.67
	PA 2010	-	-	7.32	111.90	0.47

Table B-2: Dissolved metals concentrations of soil samples pore water and Infiltration Pond PA water

Samples		Depth range (mbgl)	Ave. Depth (mbgl)	Heavy Metals (µg/L)							
				Mn	Ni	Zn	Sr	Mo	Ba	Pb	U
BH2&4 Aug. 2008	2-3, 2-5, 4-3 & 4-4	0-1	0.5	24.85	6.77	227.48	294.09	15.64	140.31	1.14	10.50
BH12 July 2010	12-1	0-0.2	0.1	99.61	4.80	90.48	316.98	3.65	172.74	22.19	2.93
	12-2	0.2-0.4	0.3	198.52	5.59	54.32	353.19	6.81	174.37	1.02	2.70
	12-3	0.4-0.59	0.5	133.20	5.64	20.78	333.65	24.97	151.03	1.07	2.01
BH16 July 2010	16-1	0-0.2	0.1	21.22	4.88	36.34	229.76	6.79	105.35	1.03	2.51
	16-2	0.2-0.4	0.3	73.33	5.91	123.29	284.96	24.71	165.57	19.00	2.74
	16-3	0.4-0.62	0.5	2.77	2.75	126.71	270.04	10.40	143.58	1.26	2.18
BH33 July 2010	33-1	0-0.17	0.08	44.82	5.46	101.59	354.05	1.72	171.96	24.61	4.26
	33-2	0.17-0.34	0.25	67.80	4.96	105.18	363.22	3.48	183.71	23.63	3.07
	33-3	0.34-0.52	0.42	8.78	5.39	166.77	366.33	1.02	172.06	36.95	2.43
	33-4	0.52-0.69	0.59	2.58	19.78	127.77	418.89	0.73	180.61	31.34	1.87
	33-5	0.69-0.86	0.76	32.42	3.52	120.22	358.44	2.33	155.87	28.23	0.95
	33-6	0.86-1.04	0.93	107.40	3.34	0.00	343.93	2.96	132.89	2.28	0.56
BH51 July 2010	51-1	0-0.18	0.09	191.20	5.89	0.00	334.75	26.17	133.28	1.04	2.28
	51-2	0.18-0.36	0.27	32.20	6.07	0.54	524.42	18.10	182.54	1.07	3.97
	51-3	0.36-0.55	0.45	65.39	9.20	56.91	560.41	4.87	205.06	1.06	3.30
PA	PA 2008	–	–	39.05	14.75	0.00	196.05	262.90	64.60	40.90	0.00
	PA 2010	–	–	0.13	2.47	0.00	133.55	9.01	38.39	0.51	0.91

Table B-3: Dissolved ions concentrations of soil samples pore water and Infiltration Pond PA water

Samples		Depth range (mbgl)	Ave. Depth (mbgl)	Cations(mg/L)					Anions(mg/L)				
				Calcium	Magnesium	Potassium	Sodium	Ammonium	Nitrate	Chloride	Fluoride	Sulphate	Nitrite
BH2&4 Aug. 2008	2-3, 2-5, 4-3 & 4-4	0-1	0.50	54.013	22.970	7.577	36.710	0.077	0.603	17.891	0.579	37.380	0.452
BH12	12-1	0-0.2	0.10	106.114	31.689	5.372	87.844	0.299	0.030	119.241	0.224	100.683	n.a.
July 2010	12-2	0.2-0.4	0.30	114.722	34.918	5.319	45.880	0.359	0.068	82.661	0.192	82.071	n.a.
	12-3	0.4-0.59	0.50	101.193	31.033	6.016	23.903	0.322	0.129	54.243	0.145	56.895	n.a.
BH16	16-1	0-0.2	0.10	55.570	24.826	3.512	54.717	0.220	0.298	47.920	0.364	44.377	0.208
July 2010	16-2	0.2-0.4	0.30	61.362	31.767	3.983	13.822	0.268	0.052	20.198	0.141	24.148	0.056
	16-3	0.4-0.62	0.50	89.717	27.743	3.409	8.827	0.176	0.051	10.975	0.211	21.763	n.a.
BH33	33-1	0-0.17	0.08	95.741	29.408	4.299	179.565	0.704	n.a.	196.123	0.387	139.577	n.a.
	33-2	0.17-0.34	0.25	108.220	35.739	5.433	30.692	0.465	n.a.	130.749	0.159	54.532	n.a.
	33-3	0.34-0.52	0.42	87.908	33.864	5.700	29.447	0.443	n.a.	92.550	0.135	64.604	n.a.
July 2010	33-4	0.52-0.69	0.59	82.930	34.136	5.357	14.931	0.339	0.107	65.745	0.122	56.575	n.a.
	33-5	0.69-0.86	0.76	81.691	29.908	5.543	11.181	0.331	n.a.	43.720	0.160	33.961	n.a.
	33-6	0.86-1.04	0.93	65.227	22.070	4.832	9.620	0.314	n.a.	24.364	0.190	27.926	0.468
BH51	51-1	0-0.18	0.09	97.974	31.507	4.539	149.869	0.689	0.015	182.567	0.266	124.379	n.a.
July 2010	51-2	0.18-0.36	0.27	135.658	45.836	6.514	66.203	0.608	0.214	185.080	0.094	115.985	n.a.
	51-3	0.36-0.55	0.45	132.921	48.140	7.315	17.699	0.511	0.071	166.810	0.230	79.532	n.a.
PA	PA 2008	–	–	7.639	4.179	9.946	581.974	0.561	0.773	386.351	1.961	149.641	0.000
	PA 2010	–	–	27.793	13.089	1.248	48.963	n.a.	n.a.	36.290	0.286	52.833	0.508

Appendix C

Table C-1: Outputs of Cl^- one-dimensional diffusion model $D^* = 6.09 \times 10^{-10}$

$D^*(m^2/s)$ =	6.09E-10	
T (years)=	1.917	(23 months)
Dpeth (mbgl)	β	erfc (β)= C/C_0
0	0	1
0.003	0.007818186	0.991178301
0.006	0.015636373	0.982357681
0.009	0.023454559	0.973539217
0.01	0.026060621	0.970600394
0.03	0.078181863	0.911960629
0.06	0.156363726	0.824989887
0.09	0.234545589	0.740117649
0.1	0.26060621	0.712461056
0.12	0.312727451	0.65829861
0.15	0.390909314	0.580380337
0.18	0.469091177	0.507077541
0.21	0.54727304	0.438953887
0.24	0.625454903	0.3764119
0.27	0.703636766	0.319691202
0.3	0.781818629	0.268874542
0.33	0.860000491	0.223899613
0.36	0.938182354	0.184578163
0.39	1.016364217	0.150616917
0.42	1.09454608	0.12164113
0.45	1.172727943	0.097219084
0.5	1.303031048	0.065363464
0.51	1.329091669	0.060159969
0.57	1.485455394	0.035662821
0.6	1.563637257	0.027013894
0.63	1.64181912	0.020239246
0.66	1.720000983	0.014997116
0.69	1.798182846	0.010990066
0.72	1.876364709	0.007964279
0.78	2.032728434	0.00404396
0.81	2.110910297	0.002833207
0.84	2.18909216	0.001962537
0.87	2.267274023	0.001344025
0.9	2.345455886	0.000909976
0.93	2.423637749	0.000609073
0.96	2.501819612	0.000403006
0.99	2.580001474	0.000263598
1.02	2.658183337	0.000170431

$$\beta = \frac{z}{2\sqrt{D^* \times t}}$$

Where:

z: Depth (m) t: time (s)

D*: Effective diffusion coefficient (m^2/s)

$$\frac{C_{(z,t)}}{C_0} = \text{ERFC}(\beta)[1]$$

Where:

C(z, t): Solute concentration at depth z and time t.

C_0: Source concentration of the solute.

Table C-2: Outputs of Cl^- one-dimensional diffusion model D*= $1.22*10^{-9}$

$D^*(m^2/s)$ =	1.22E-09	
T (years)=	1.917	(23 months)
Dpeth (mbgl)	β	erfc (β)= C/C_0
0	0	1
0.003	0.005528293	0.993762053
0.006	0.011056585	0.987524488
0.009	0.016584878	0.981287685
0.01	0.018427642	0.979208986
0.03	0.055282925	0.937683389
0.06	0.110565851	0.875746328
0.09	0.165848776	0.814561445
0.1	0.184276418	0.794396201
0.12	0.221131702	0.754487738
0.15	0.276414627	0.695864269
0.18	0.331697552	0.639004466
0.21	0.386980478	0.584191165
0.24	0.442263403	0.531672538
0.27	0.497546329	0.481659011
0.3	0.552829254	0.434321172
0.33	0.608112179	0.389788773
0.36	0.663395105	0.34815071
0.39	0.71867803	0.309456215
0.42	0.773960956	0.273715768
0.45	0.829243881	0.240905056
0.5	0.92138209	0.192564261
0.51	0.939809732	0.183817799
0.57	1.050375583	0.13742327
0.6	1.105658508	0.117902825
0.63	1.160941433	0.100627529
0.66	1.216224359	0.08543229
0.69	1.271507284	0.072148049
0.72	1.32679021	0.060605228
0.78	1.43735606	0.042079972
0.81	1.492638986	0.034780028
0.84	1.547921911	0.028590145
0.87	1.603204836	0.023373495
0.9	1.658487762	0.019003829
0.93	1.713770687	0.015365925
0.96	1.769053613	0.012355687
0.99	1.824336538	0.00987999
1.02	1.879619463	0.007856314

$$\beta = \frac{z}{2\sqrt{D^* \times t}}$$

Where:

z: Depth (m) t: time (s)

D*: Effective diffusion coefficient (m^2/s)

$$\frac{C_{(z,t)}}{C_0} = \text{ERFC}(\beta)\ [1]$$

Where:

C(z, t): Solute concentration at depth z and time t.

C_0: Source concentration of the solute.

Table C-3: Outputs of Cl^- one-dimensional diffusion model D*= $1.83*10^{-9}$

$D^*(m^2/s)$ = 1.83E-09		
T (years)= 1.917 (23 months)		
Dpeth (mbgl)	β	erfc (β)= C/C_0
0	0	1
0.003	0.004513832	0.994906721
0.006	0.009027664	0.989813649
0.009	0.013541496	0.984720992
0.01	0.015046107	0.983023568
0.03	0.04513832	0.949101431
0.06	0.090276639	0.898409778
0.09	0.135414959	0.848129438
0.1	0.150461065	0.831495382
0.12	0.180553278	0.798459817
0.15	0.225691598	0.749592966
0.18	0.270829917	0.701711354
0.21	0.315968237	0.654985847
0.24	0.361106557	0.609573895
0.27	0.406244876	0.565617991
0.3	0.451383196	0.523244415
0.33	0.496521515	0.482562266
0.36	0.541659835	0.44366281
0.39	0.586798154	0.406619126
0.42	0.631936474	0.371486103
0.45	0.677074794	0.338300649
0.5	0.752305326	0.28736502
0.51	0.767351433	0.277833801
0.57	0.857628072	0.225179967
0.6	0.902766391	0.201706696
0.63	0.947904711	0.18007004
0.66	0.993043031	0.1602073
0.69	1.03818135	0.142047197
0.72	1.08331967	0.125511277
0.78	1.173596309	0.096971664
0.81	1.218734628	0.084788949
0.84	1.263872948	0.073875093
0.87	1.309011268	0.064137709
0.9	1.354149587	0.055485279
0.93	1.399287907	0.047828183
0.96	1.444426226	0.041079459
0.99	1.489564546	0.035155536
1.02	1.534702865	0.029976741

$$\beta = \frac{z}{2\sqrt{D^* \times t}}$$

Where:

z: Depth (m) t: time (s)

D*: Effective diffusion coefficient (m^2/s)

$$\frac{C_{(z,t)}}{C_0} = \text{ERFC}(\beta)[1]$$

Where:

C(z, t): Solute concentration at depth z and time t.

C_0: Source concentration of the solute.

Table C-4: Outputs of $\delta^{18}O$ one-dimensional diffusion model D*= $3.5*10^{-10}$

$D^*(m^2/s)$ =	3.5E-10	
T (years)=	1.917	(23 months)
Dpeth (mbgl)	β	erfc (β)= C/C_0
0	0	1
0.003	0.010312896	0.988363556
0.006	0.020625792	0.976729586
0.008	0.027501056	0.968976203
0.01	0.03437632	0.961225751
0.03	0.10312896	0.884042666
0.06	0.20625792	0.770521555
0.08	0.27501056	0.697332616
0.09	0.30938688	0.66172041
0.1	0.3437632	0.626857572
0.12	0.41251584	0.55963382
0.15	0.5156448	0.465859842
0.18	0.61877376	0.381531336
0.21	0.72190272	0.30729044
0.25	0.859408001	0.224218882
0.27	0.928160641	0.189312003
0.3	1.031289601	0.144712817
0.33	1.134418561	0.108645741
0.36	1.237547521	0.080091334
0.39	1.340676481	0.057959675
0.42	1.443805441	0.041166493
0.45	1.546934401	0.028691785
0.48	1.650063361	0.019619719
0.5	1.718816001	0.015066656
0.54	1.856321281	0.008658925
0.57	1.959450241	0.005587051
0.6	2.062579201	0.00353498
0.63	2.165708161	0.002192957
0.66	2.268837121	0.001333735
0.69	2.371966082	0.000795182
0.72	2.475095042	0.000464712
0.75	2.578224002	0.000266189
0.77	2.646976642	0.000181554
0.81	2.784481922	8.22142E-05
0.84	2.887610882	4.43245E-05
0.87	2.990739842	2.34165E-05
0.9	3.093868802	1.21215E-05
0.93	3.196997762	6.14791E-06
0.95	3.265750402	3.86583E-06
0.99	3.403255682	1.48733E-06
1.02	3.506384642	7.09384E-07

$$\beta = \frac{z}{2\sqrt{D^* \times t}}$$

Where:

z: Depth (m) t: time (s)

D*: Effective diffusion coefficient (m^2/s)

$$\frac{C_{(z,t)}}{C_0} = \text{ERFC}(\beta)[1]$$

Where:

C(z, t): Solute concentration at depth z and time t.

C_0: Source concentration of the solute.

Table C-5: Outputs of $\delta^{18}O$ one-dimensional diffusion model D*= $7*10^{-10}$

$D^*(m^2/s)$ =	7.0E-10	
T (years)=	1.917	(23 months)
Dpeth (mbgl)	β	erfc (β)= C/C_0
0	0	1
0.003	0.007292319	0.991771645
0.006	0.014584637	0.983544166
0.008	0.019446183	0.978060098
0.01	0.024307729	0.972577066
0.03	0.072923187	0.917860621
0.06	0.145846374	0.836589447
0.08	0.194461832	0.783308125
0.09	0.218769561	0.757027249
0.1	0.24307729	0.731024378
0.12	0.291692748	0.679961373
0.15	0.364615935	0.606102515
0.18	0.437539122	0.536065411
0.21	0.510462309	0.470354291
0.25	0.607693225	0.390115459
0.27	0.656308683	0.353324252
0.3	0.72923187	0.302405277
0.33	0.802155057	0.256619184
0.36	0.875078244	0.215883993
0.39	0.948001431	0.180025607
0.42	1.020924618	0.148793776
0.45	1.093847805	0.121879096
0.48	1.166770992	0.098930008
0.5	1.21538645	0.085647895
0.54	1.312617366	0.06340779
0.57	1.385540553	0.050060092
0.6	1.45846374	0.039152629
0.63	1.531386927	0.030333498
0.66	1.604310114	0.023278236
0.69	1.677233301	0.017693716
0.72	1.750156488	0.013320074
0.75	1.823079675	0.00993096
0.77	1.871695133	0.008121497
0.81	1.968926049	0.005361331
0.84	2.041849236	0.003881798
0.87	2.114772423	0.002783025
0.9	2.18769561	0.001975648
0.93	2.260618797	0.00138866
0.95	2.309234255	0.001091744
0.99	2.406465171	0.000665879
1.02	2.479388358	0.000454238

$$\beta = \frac{z}{2\sqrt{D^* \times t}}$$

Where:

z: Depth (m) t: time (s)

D*: Effective diffusion coefficient (m^2/s)

$$\frac{C_{(z,t)}}{C_0} = \text{ERFC}\ (\beta)[1]$$

Where:

C(z, t): Solute concentration at depth z and time t.

C_0: Source concentration of the solute.

Table C-6: Outputs of $\delta^{18}O$ one-dimensional diffusion model D*= $1.05*10^{-9}$

$D^*(m^2/s)$ =	1.05E-09	
T (years)=	1.917	(23 months)
Dpeth (mbgl)	β	erfc (β)= C/C_0
0	0	1
0.003	0.005954153	0.993281537
0.006	0.011908307	0.98656355
0.008	0.015877742	0.982085392
0.01	0.019847178	0.977607798
0.03	0.059541533	0.932893886
0.06	0.119083066	0.866261618
0.08	0.158777421	0.822333114
0.09	0.178624599	0.800567028
0.1	0.198471776	0.778954717
0.12	0.238166131	0.736254275
0.15	0.297707664	0.673738859
0.18	0.357249197	0.613399648
0.21	0.41679073	0.555572117
0.25	0.49617944	0.48286397
0.27	0.535873796	0.448546784
0.3	0.595415329	0.399763084
0.33	0.654956861	0.354316662
0.36	0.714498394	0.312278412
0.39	0.774039927	0.273666818
0.42	0.83358146	0.238453221
0.45	0.893122993	0.206565342
0.48	0.952664526	0.177893024
0.5	0.992358881	0.160495457
0.54	1.071747591	0.129600338
0.57	1.131289124	0.109624256
0.6	1.190830657	0.092164517
0.63	1.25037219	0.077011898
0.66	1.309913723	0.063954393
0.69	1.369455256	0.05278177
0.72	1.428996789	0.043289436
0.75	1.488538321	0.035281645
0.77	1.528232677	0.030676239
0.81	1.607621387	0.022994867
0.84	1.66716292	0.018387339
0.87	1.726704453	0.014609026
0.9	1.786245986	0.011532572
0.93	1.845787519	0.009045288
0.95	1.885481874	0.007665153
0.99	1.964870584	0.005456907
1.02	2.024412117	0.004197154

$$\beta = \frac{z}{2\sqrt{D^* \times t}}$$

Where:

z: Depth (m) t: time (s)

D*: Effective diffusion coefficient (m^2/s)

$$\frac{C_{(z,t)}}{C_0} = \text{ERFC}(\beta)[1]$$

Where:

C(z, t): Solute concentration at depth z and time t.

C_0: Source concentration of the solute.

Appendix C References

(1) Fetter CW. Contaminant hydrogeology. New York : Macmillan Pub. Co.; Toronto; New York: Maxwell Macmillan Canada; Maxwell Macmillan International; 1993.